
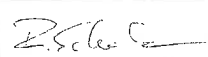




D2: Data Acquisition Report of SSM Experiment

SARSimHT-NG – Simulation of Hydroterra SAR System Performance in the Mediterranean and the Alps Based on Experimental Airborne SAR Data
(ESA Contract No. 4000134680/21/NL/FF/an)


Reference: DLR-HR-TR-SARSimHT-NG-02

	Name	Signature
Prepared by	Horn, Ralf	 <small>Digitally signed by Ralf Horn DN: O=Deutsches Zentrum fuer Luft- und Raumfahrt e.V. (DLR), CN=Ralf Horn, E=ralf.horn@dlr.de Reason: I am the author of this document Location: Weesling Date: 2023.09.06 17:15:49+02:00 Foxit PDF Editor Version: 12.1.3</small>
	Scheiber, Rolf	 <small>Digitally signed by Rolf Scheiber DN: C=de, OU=DLR, O=DLR, CN=Rolf Scheiber, E=rolf.scheiber@dlr.de Grund: Ich bin der Verfasser dieses Dokuments Ort: Oberpfaffenhofen Datum: 2023.09.07 09:50:12+02:00 Foxit PDF Reader Version: 12.1.3</small>
	Balenzano, Anna	
Released by	Reigber, Andreas	 <small>Digitally signed by Dr. Andreas Reigber DN: C=DE, S=Nordrhein-Westfalen, L=Köln, O=Deutsches Zentrum fuer Luft- und Raumfahrt e.V. (DLR), SN=Reigber, G=Andreas, CN=Dr. Andreas Reigber Grund: Ich genehmige dieses Dokument Ort: Oberpfaffenhofen Datum: 2023.09.11 16:57:09+02:00 Foxit PDF Editor Version: 12.1.3</small>

Approval and release information:

This document has been approved either by manual signatures or via electronic workflow.



	SARSimHT-NG – Simulation of Hydroterra SAR System Performance in the Mediterranean and the Alps Based on Experimental Airborne SAR Data D2: Data Acquisition Report of SSM Experiment	Doc.: DLR-HR-TR-SARSimHT-NG-02 Issue: 1.7 (final) Date: 06.09.2023
---	--	--

Document Preparation

The document on hand was prepared with contributions from the personnel listed below:

Name	Organization
Horn, Ralf	DLR-HR
Fischer, Jens	DLR-HR
Scheiber, Rolf	DLR-HR
Balenzano, Anna	CNR-IREA

Distribution List

Name	Organization	Type
Alberto Moreira	DLR-HR	PDF
Andreas Reigber	DLR-HR	PDF
Anna Balenzano	CNR-IREA	DOCX, PDF
Julia Kubanek	ESA	DOCX, PDF


Document Change Details

Latest changes to the document are listed first.


Issue	Date	Modified Pages/Sections	Changes
1.7	06.09.2023	all	Final issue
1.6	25.06.2023	all	Draft
1.5	23.06.2023	Sect. 4, 5 and 6	Added, updated
1.3	08.06.2023	Sect. 3 and 7	Updated, added
1.2	06.05.2023	Sect. 1, 2 & 3	Added, updated
0.1	06.12.2022	all	Template

Table of Contents

Table of Contents.....	3
List of Acronyms and Abbreviations.....	5
Documents.....	6
Applicable Documents.....	6
Reference Documents	6
1 Introduction and Purpose of the Document	7
2 Airborne SAR Measurements for SSM.....	8
2.1 The F-SAR System – Description and Measurement Settings.....	8
2.2 Flight Planning and Radar Geometry	9
2.3 22HTERRA SSM Campaign Execution	11
2.3.1 Acquisition Procedure for Hydroterra Simulation	12
3 Field Measurements.....	13
3.1 Description of the test site	13
3.2 Permanent hydrologic network.....	15
3.3 Field measurements.....	16
3.3.1 Soil and vegetation sampling and temporary ground stations	16
3.4 Field campaign 28. - 29.04.2022	18
3.4.1 Temporary stations.....	21
3.4.2 Soil moisture and vegetation grid samplings	23
3.5 Field campaign 15. - 16.06.2022	27
3.5.1 Temporary stations.....	29
3.5.2 Soil moisture and vegetation grid samplings	31
3.6 Database description	34
4 Processing Strategy and Inventory.....	36
4.1 Preparations.....	36
4.1.1 Digital Elevation Model	36
4.1.2 Radar Image Geometries	37
4.1.3 Squint Angle Analysis.....	38
4.1.4 Processing Strategy	40
4.2 Processing Results	42
4.2.1 Radar Geometry Image (RGI) Product Generation.....	42
4.2.2 Geocoded and Terrain Corrected (GTC) Product Generation.....	44
4.2.3 Interferometric Image Product (INF) Product Generation	44
4.3 Inventory of Delivered Data Products	48
4.3.1 Radar Geometry Image (RGI) Products	48
4.3.2 Geocoded and Terrain Corrected (GTC) Products	48
4.3.3 Interferometric (INF) Products	48
4.3.4 Summary of RGI, GTC and INF products delivered	53
5 Simulation of Hydroterra Products.....	54
5.1 Overview.....	54
5.2 Simulation Procedure	54


	<p>SARSimHT-NG – Simulation of Hydroterra SAR System Performance in the Mediterranean and the Alps Based on Experimental Airborne SAR Data</p> <p>D2: Data Acquisition Report of SSM Experiment</p>	<p>Doc.: DLR-HR-TR-SARSimHT-NG-02</p> <p>Issue: 1.7 (final)</p> <p>Date: 06.09.2023</p>
---	---	---

5.3	Simulation Results	55
5.3.1	Integration Times	55
5.3.2	Geosynchronous SAR Products (GEO)	56
5.3.3	Hydroterra SAR Products (HT)	57
5.4	Simulation Product Data Formats and Data Set Structure	60
5.4.1	Geosynchronous SAR Product (GEO) Compilation	60
5.4.2	Hydroterra SAR Product (HT) Compilation	62
5.5	Inventory of Delivered Simulation Products	65
6	Summary	66
7	Appendix A: Portable Sensor Calibration.....	67

	SARSimHT-NG – Simulation of Hydroterra SAR System Performance in the Mediterranean and the Alps Based on Experimental Airborne SAR Data D2: Data Acquisition Report of SSM Experiment	Doc.: DLR-HR-TR-SARSimHT-NG-02 Issue: 1.7 (final) Date: 06.09.2023
---	--	--

List of Acronyms and Abbreviations

CNR-IREA	National Research Council of Italy - Institute for Electromagnetic Sensing of the Environment
CREA-CI	Consiglio per la Ricerca in agricoltura e l'analisi dell'Economia Agraria – Centro di ricerca per le Colture Industriali
DAR	Data Acquisition Report
DLR	Deutsches Zentrum für Luft- und Raumfahrt e.V., German Aerospace Center
DLR-HR	German Aerospace Center, Microwaves and Radar Institute
ENVEO IT	Environmental Earth Observation Information Technology GmbH
ESA	European Space Agency
InSAR	Interferometric SAR
NESZ	Noise Equivalent Sigma Zero
PRF	Pulse Repetition Frequency
ROSE-L	L-Band Radar Observation System for Europe
SAR	Synthetic Aperture Radar
Sentinel-1 NG	Sentinel-1 Next Generation
SLC	Single-Look Complex
SNR	Signal-to-Noise Ratio
SSM	Surface Soil Moisture
SWE	Snow Water Equivalent
WCA	Wind Correction Angle
WP	Work Package

	SARSimHT-NG – Simulation of Hydroterra SAR System Performance in the Mediterranean and the Alps Based on Experimental Airborne SAR Data D2: Data Acquisition Report of SSM Experiment	Doc.: DLR-HR-TR-SARSimHT-NG-02 Issue: 1.7 (final) Date: 06.09.2023
---	--	--


Documents

Applicable Documents

- [A1] Statement of Work. SARSimHT-NG – Simulation of Hydroterra SAR System Performance in the Mediterranean and the Alps Based on Experimental Airborne SAR Data. ESA-EOPSM-CAMP-SOW-3812, Issue 1, Revision 6, 04/02/2021.

Reference Documents

- [1] SARSimHT 2019: "Final Report", Technical Report: DLR-HR-TR-SARSimHT-2019-003, Oct. 2020.
- [2] Ralf Horn, Marc Jaeger, Martin Keller, Markus Limbach, Anton Nottensteiner, Matteo Pardini, Andreas Reigber, Rolf Scheiber (2017), "F-SAR – Recent Upgrades and Campaign Activities". In: 13th International Radar Symposium (IRS), 2017-06-28 - 2017-06-30, Prague, Czechia. CUVILLIER VERLAG. ISBN 978-3-7369-9542-0.)
- [3] Fierz, C., Armstrong, R.L., Durand, Y., Etchevers, P., Greene, E., McClung, D.M., Nishimura, K., Satyawali, P.K. and Sokratov, S.A. 2009. The International Classification for Seasonal Snow on the Ground. IHP-VII Technical Documents in Hydrology No. 83, UNESCO-IHP, Paris. 90 pp.
- [4] R. Scheiber, S.-K. Lee, K. P. Papathanassiou, N. Floury, "Extrapolation of Airborne Polarimetry and Interferometric SAR Data for Validation of Bio-Geo-Retrieval Algorithms for Future Spaceborne SAR Missions", Proc. IGARSS, Cape Town, 2009.
- [5] Description of Simulated Amplitude Results for Hydroterra (Technical Report: DLR-HR-TR-SARSimHT-2019-002).
- [6] Curlander, J. C., and R. N. McDonough, "Synthetic Aperture Radar: Systems and Signal Processing", 647 pp., John Wiley, New York, 1991.
- [7] Hydroterra Earth Explorer 10 Mission Candidate Mission Assumptions and Preliminary Technical Requirements (MATER).
- [8] DLR's Airborne SAR System F-SAR PRODUCT DESCRIPTION, Version: 3.2.
- [9] Valeria Gracheva, Pau Prats, Rolf Scheiber, Ralf Horn, Martin Keller, Jens Fischer, Andreas Reigber, Alberto Moreira, "Simulation of Geosynchronous Hydroterra Image Products with Airborne SAR Data", Proceedings of the European Conference on Synthetic Aperture Radar (EUSAR), March 2021, pp.581-586.
- [10] Valeria Gracheva, Rolf Scheiber, Pau Prats, Ralf Horn, Martin Keller, Jens Fischer, Alberto Moreira, Julia Kubanek, Roger Haagmans, "Airborne SAR Experiment to Simulate Geosynchronous Hydro-Terra Data and Investigate the Detection of Diurnal Changes", Proceedings of the IEEE International Geoscience and Remote Sensing Symposium (IGARSS), July 2021, pp. 3285-3288.

	SARSimHT-NG – Simulation of Hydroterra SAR System Performance in the Mediterranean and the Alps Based on Experimental Airborne SAR Data D2: Data Acquisition Report of SSM Experiment	Doc.: DLR-HR-TR-SARSimHT-NG-02 Issue: 1.7 (final) Date: 06.09.2023
---	--	--

1 Introduction and Purpose of the Document

This document provides an overview of the airborne L- and C-band SAR campaign conducted in Spring 2022 at the test site 'Apulian Tavoliere' located west of the City of Foggia in Italy, the simultaneously collected ground measurements, processed radar data and simulated Hydroterra products. This data will be used to analyse the potential of geo-synchronous SAR to measure and monitor surface soil moisture (SSM) from space. Another retrieval will be performed from conventional L- and C-band SAR data to support the development of the ROSE-L and Sentinel-1 NG missions.

The data described in this document will be used as basis for the SARSimHT-NG study requested by ESA. The main goal of this study is to perform an assessment of the potential to retrieve snow water equivalent (SWE) and surface soil moisture (SSM) from future SAR systems in geosynchronous orbits. For this analysis the results from the SARSimHT 2019 study [1] will be used. In 2019 airborne radar data of the F-SAR system of DLR were used for the first time to simulate geosynchronous SAR products of the system Hydroterra. Hydroterra was considered as one of three candidates for ESA's Earth Explorer 10 mission. Its mission concept consists in placing a C-band SAR system into a geosynchronous orbit.

This document focusses on the data acquisition for an assessment of SSM retrieval. This document is structured as follows: Chapter 2 describes the airborne campaign. The ground-truth measurements are documented in Chapter 3. The processing of the airborne data is described in Chapter 4 and an inventory is provided. The simulation procedure of Hydroterra products is outlined in Chapter 5.

2 Airborne SAR Measurements for SSM

This chapter summarises the airborne SAR measurements which were performed with DLR's airborne radar system F-SAR over the 'Apulian Tavoliere' test site in Italy to investigate capabilities of spaceborne SAR instruments of deriving measures on Surface Soil Moisture (SSM) in the Mediterranean region. The measurements were carried out in C- and L-bands in regard to Sentinel-1 and upcoming Hydroterra, ROSE-L and Sentinel-1 Next Generation (NG) space systems.

2.1 The F-SAR System – Description and Measurement Settings

F-SAR is a fully polarimetric and interferometric airborne radar system, which can operate in X-, C-, S-, L- and P-bands. See [2] for more details. It was developed to define the "state-of-the-art" in SAR technology and perform scientific flight campaigns for the preparation of new satellite missions.

F-SAR is certified airworthy on-board the DLR DO 228-212 aircraft. The DO 228 is a twin-engine short take-off and landing turbo-prop aircraft without pressurised cabin. Figure 2-1 shows the DO 228 aircraft equipped with the F-SAR system. All antennas are pointing to the right-hand side of the aircraft. The antenna footprints on ground overlap from 20° to 65° off-nadir.



Figure 2-1: The F-SAR instrument on-board a DLR Dornier DO 228 aircraft. Antennas are mounted behind the wing (X-C-S-L) and under the cockpit (P).

Data collection took place in late April and mid of June 2022 as part of the 22HTERRA campaign in cooperation with CNR-IREA and CREA-CI. F-SAR was operated in a 4-channel, dual-frequency, C- and L-band, fully polarimetric mode to match the new Hydroterra and ROSE-L space missions. Relevant system settings are listed in Table 2-1 below. In each radar band F-SAR operates with a single TX and two parallel RX chains. It requires two pulses for a fully polarimetric measurement. Polarisation is switched on transmit. Here in particular an L-band pulse is transmitted simultaneously with every second C-band pulse.

Table 2-1: F-SAR system parameters used in the course of the 22HTERRA measurement flights.

F-SAR system parameters	C-band	L-band
RF centre frequency	5300 MHz	1325 MHz
Signal bandwidth	384 MHz	150 MHz
Type of signal	FM modulated pulse ('Down-Chirp')	
Pulse duration	10 μ s	
Pulse repetition frequency per channel	1811 Hz	905.5 Hz
System range delay	25.7 μ s	
Receive gate duration	28 μ s	

2.2 Flight Planning and Radar Geometry

The 'Apulian Tavoliere' test site (see Figure 2-2) is located on the western outskirts of the City of Foggia in the Italian province Apulia. The 9km x 3.5km large agricultural site is oriented North-South. It is characterized by an almost flat topography.

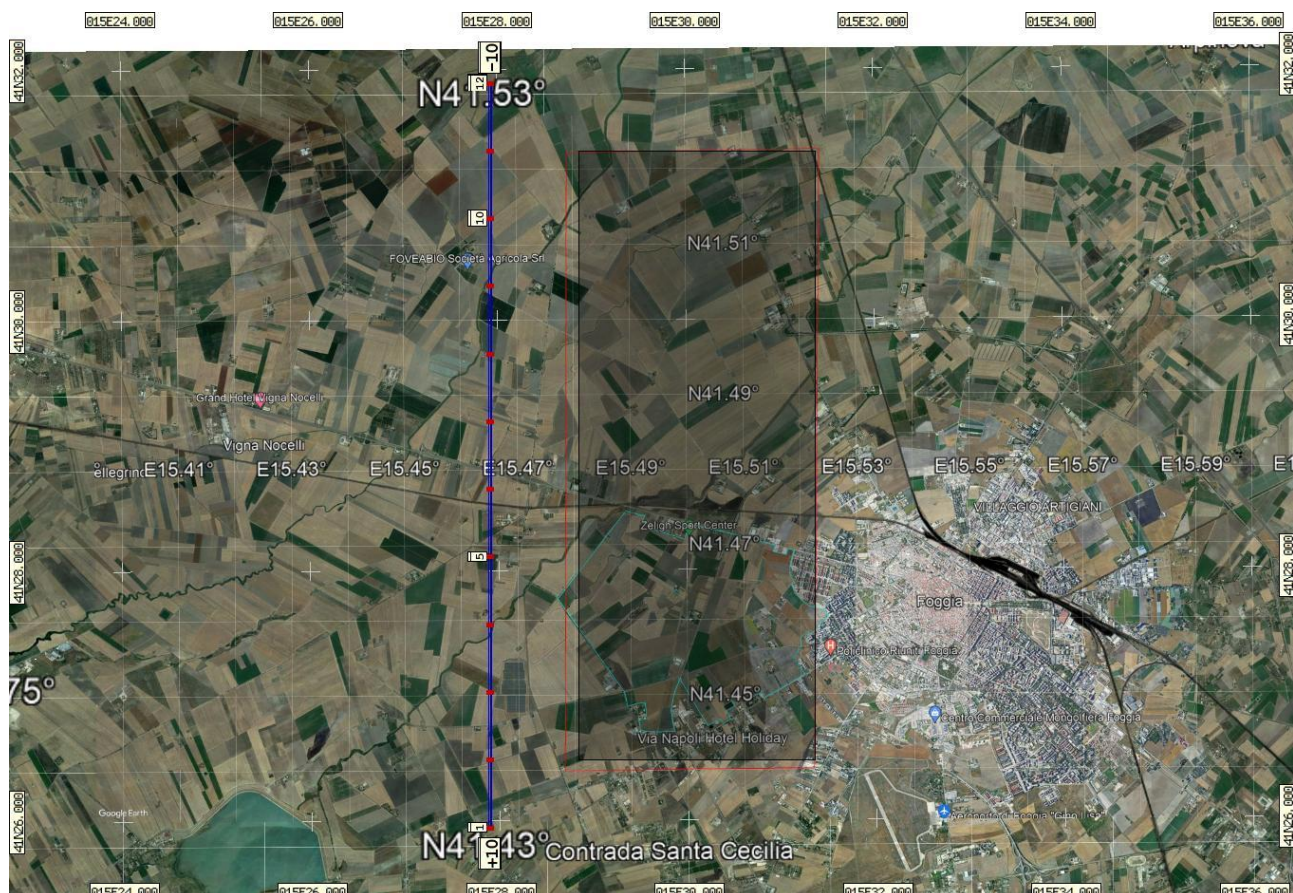


Figure 2-2: The 'Apulian Tavoliere' test site situated on the western outskirts of the City of Foggia (Italy). The dark shaded rectangle indicates the area to be imaged by F-SAR. The measurement flight track #10 is shown in blue.

CNR-IREA, in coordination with DLR, specified the test site such that ground measurements and irrigation could be performed on two locations in the same imaged area. Actually, there are two farms in the scene, the CREA-CI experimental farm in the south and the Caione private farm in the north. Radar

illumination was agreed to be from the west. The flight track #10 is offset to the west by approx. 1.3km from the near range edge. The off-nadir angle range is approx. 23° (NR) to 58° (FR).

Flight planning is done in the WGS84 system in general. Hence, all altitudes are referenced to the WGS84 ellipsoid. The map base is Google Earth (GE). GE represents geographical coordinates in WGS84 and topographic heights are referenced to sea level. Therefore, in F-SAR flight planning we consider the local geoid height (from EGM96 or EGM2008) to obtain ellipsoidal terrain heights.

It is current practice to define F-SAR flight altitudes above ‘flat terrain’. This is basically a plane which cuts through the local topography at an average height above the WGS84 ellipsoid (see Figure 2-3).

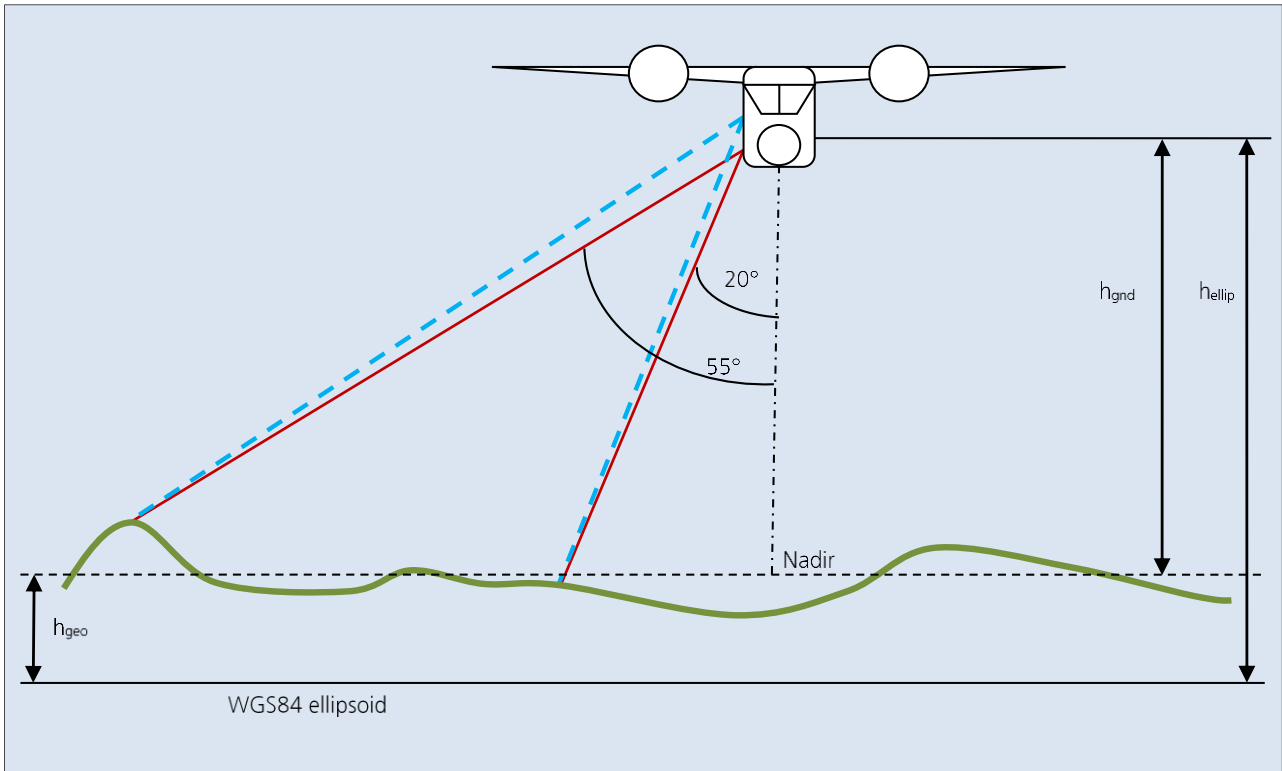


Figure 2-3: F-SAR standard flight geometry referenced to the WGS84 ellipsoid (GPS). Antennas are pointing to the right-hand side of the aircraft.

For the SSM measurement flights the geometry settings listed in Table 2-2 below were chosen.

Table 2-2: F-SAR flight geometry parameters used during 22HTERRA measurement flights.

Geometry parameters	Track #10
Geoid height (EGM96)	47.5 m
Average ‘terrain’ height above WGS84 ellipsoid (h_{geo})	150 m
Height above average ‘terrain’ (h_{gnd})	3050 m
Flight altitude above WGS84 ellipsoid (h_{ellip})	3200 m or 10500 ft
Approximate distance from near range edge	1.3 km (23° off-nadir)

The specifications in WGS84 for the flight track #10 are listed in Table 2-3.

Table 2-3: F-SAR flight track specification used during 22HTERRA measurement flights.

Track #	Start point coordinates		End point coordinates		Heading	Length
10	41N25.9458	015E27.8965	41N31.8905	015E27.9390	360°	11 km

2.3 22HTERRA SSM Campaign Execution

The 22HTERRA SSM campaign was executed following a standard routine. F-SAR with its X-C-S-L instrument configuration was installed in DLR's DO228 research aeroplane in March 2022. The pre-campaign calibration flight over DLR's calibration test site Kaufbeuren took place on Friday, April 22, 2022.

In two missions, the first on April 28 and 29, the second on June 15 and 16, 2022, a total of eight measurement flights were performed over the 'Apulian Tavoliere' test site. Details are listed in Table 2-4. An additional calibration flight was performed on return from Foggia, on April 17, 2022.

Table 2-4: Listing of F-SAR measurement flights and passes executed during the 22HTERRA campaign.

Flight #	Date	Time of departure	Flight time	# of passes T10	Drift T10	Weather observations at flight level
1	28.04.2022	08:50 CEST	3.2 h	12	+0° to +2°	Wind 300°/18kt, dry
2	28.04.2022	14:00 CEST	3.4 h	12	-1°	Wind 010°/10kt, dry
3	29.04.2022	08:55 CEST	3.2 h	12	-1°	Wind 350°/6kt, dry
4	29.04.2022	14:10 CEST	2 h	4	0° to +1°	Wind 010°/8kt, dry
5	15.06.2022	09:10 CEST	3 h	11	-2° to -3°	Wind 010°/17kt, dry
6	15.06.2022	14:10 CEST	3.3 h	12	0°	Wind 360°/20kt, dry
7	16.06.2022	08:55 CEST	3.3 h	12	-2°	Wind 020°/20kt, dry
8	16.06.2022	14:10 CEST	2 h	4	0°	Wind 340°/8kt, dry

As listed in Table 2-4 we have had dry conditions during both missions. The weather history in April and June 2022, obtained from Meteoblue, is shown in Figure 2-4 and Figure 2-5, respectively.

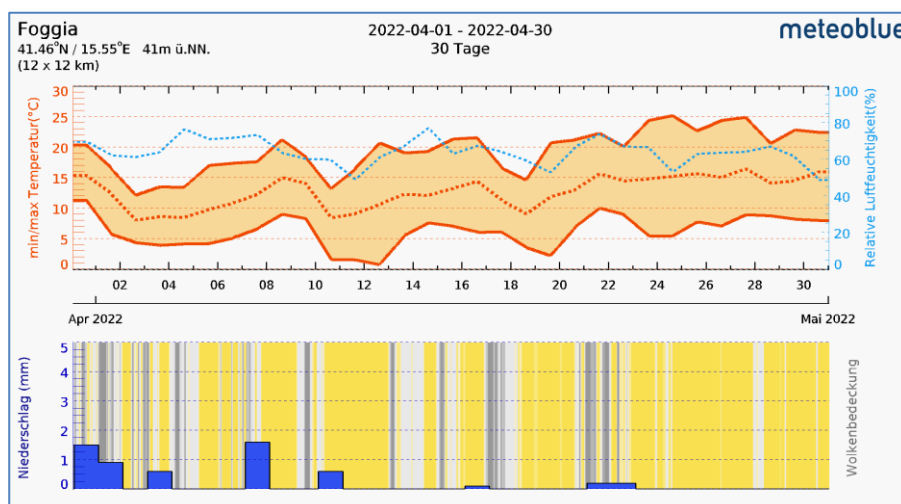


Figure 2-4: Weather history for April 2022 obtained from meteoblue.com.

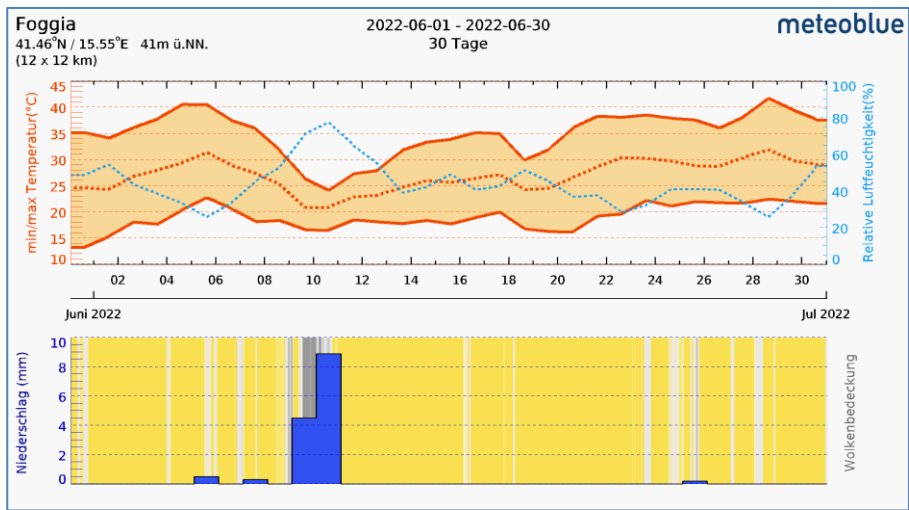


Figure 2-5: Weather history for June 2022 obtained from meteoblue.com.

2.3.1 Acquisition Procedure for Hydroterra Simulation

In order to simulate the long integration time of Hydroterra DLR has used the same procedure as for the first experiment carried out in July 2019 [1]. Track #10 has been flown pass-by-pass as many times as possible during a measurement flight. Per flight a stack of up to 12 strip-map SAR data sets was acquired with zero-meter spatial baseline and an approx. 10-minute temporal baseline. During the second mission in June we encountered hardware dropouts of the data recorder. Every 12th recording on SSD failed with an error resulting in a 20-minute time gap in the stacks of flights #5, #6 and #7. Further, for flight #5 only 11 passes are available in the stack. In Figure 2-6 the principle of the HT acquisition procedure is visualized.

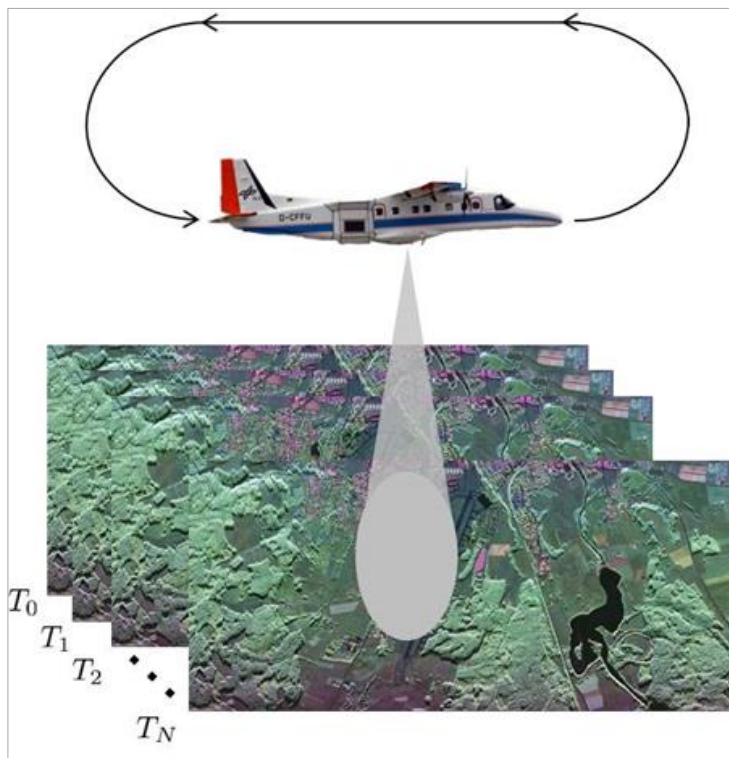


Figure 2-6: Typical acquisition procedure of a Hydroterra airborne experiment.

This procedure was applied to flights #1, #2 and #3 in April 2022, and to #5, #6 and #7 in June 2022 (refer to Table 2-4). In total six data sets were obtained covering integration times up to 24h.

The temporal distance between flights #1 and #2 is approx. 5h. Between #1 and #3 it is 24h, and 19h between #2 and #3.

This pattern was repeated in the second mission in June.

3 Field Measurements

For supporting the C- and L-band SAR acquisitions executed by DLR and the scientific analysis of the data set, two experimental campaigns on April, 28-29, and June, 15-16, were organized and performed by CNR-IREA in collaboration with CREA-CI.

The test area is an agricultural area at the Apulian Tavoliere in the Apulian Region (southern Italy).

3.1 Description of the test site

The Apulian Tavoliere is the second largest plain in Italy. It stretches on ~4000 km² in the province of Foggia, in the Apulian region (Figure 3-1). The plain is bounded in the North by Gargano and in the West by the Daunia mountains and is located in a steppe (Bsk) climate zone according to the Köppen-Geiger 2018 classification (<https://www.gloh2o.org/koppen>). Winter seasons enjoy mild temperatures rarely dropping below 0°C, while summer temperatures can exceed 40°C. Annual rainfall is approximately 530 mm and mainly concentrated in the autumn months. The rainiest months are October and November, while the dry period is from May to September. In general, soil suffers from the scarcity of precipitation. Main seasonal crops are durum wheat and tomato. Durum wheat is rain-fed while tomato is irrigated. Other irrigated crops are asparagus, artichoke, alfalfa and maize while horse bean and chick-peas when necessary. A large part of the area is served by an irrigation consortium (Consorzio per la Bonifica della Capitanata) which satisfies the water needs of spring-summer crops. Over the plain, there are also permanent crops, such as olives, vines, and fruit trees (mainly peach trees).

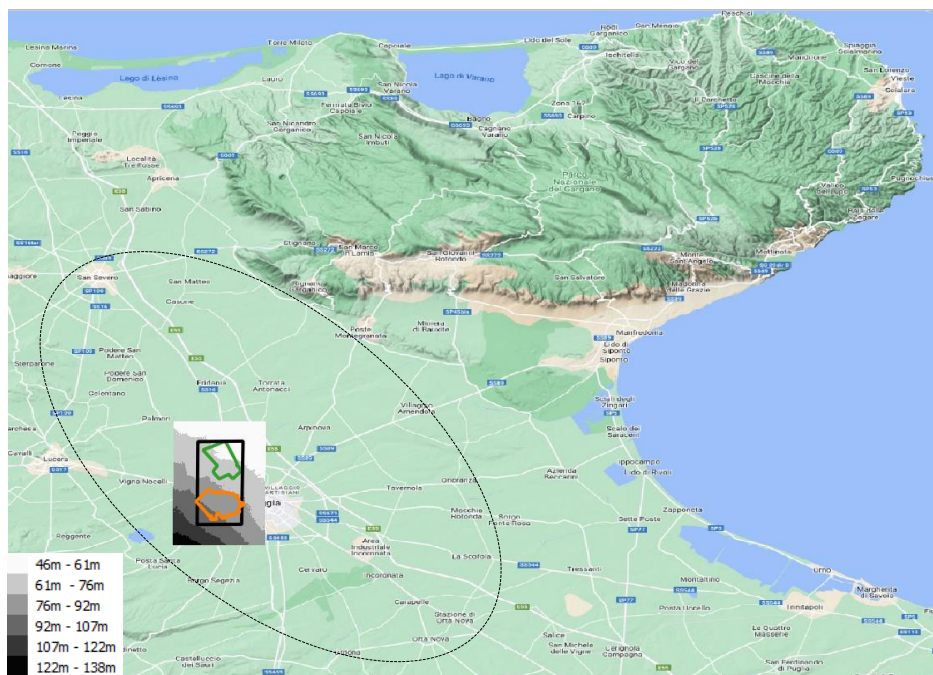


Figure 3-1: Map of the Apulian Tavoliere plain (black dashed contour) with the area of interest (AOI) (black rectangle) and the Caione private farm (green contour) and the CREA-CI experimental farm (orange contour). DEM (UTM 33 N, WGS84, 8m spatial resolution) of the AOI in grey colour is over imposed.

Two experimental sites were selected over the area. Figure 3-1 shows the area of interest (AOI) and the experimental sites, which are the private agricultural farm (Az. F.lli Caione) marked by the green contour and the CREA experimental farm (Manfredini-Menichella farm) marked by the orange contour, both located near the city of Foggia. Both farms are equipped with irrigation infrastructures. The AOI is almost flat, with a mean altitude of $75.2\text{m} \pm 12.5\text{m}$. At the farms, soils have clay loam texture (sand = 24.5%, clay = 38.2% on average at Caione farm and sand = 26.8%, clay = 32.4% on average at CREA farm). In preparation of the experiment, three surveys of the AOI were planned and carried out for collecting crop information and providing updated land use maps in April and June. A total of 193 fields were

identified and a GIS of April land use was first built and then updated in June. Land use maps include attributes of crop type and extent (ha) per each field (polygon) and crop height (cm), where available. Figure 3-2 illustrates the polygons pinpointed during the surveys and coloured according to a crop code. It is noted that the majority of fields are in yellow, indicating that those fields were durum wheat fields. The second most populated class is tomato in June. Durum wheat is a winter crop usually sown in December and harvested at mid-June. Spring-summer crops, i.e. tomato, maize, sunflower, quinoa, are generally sown between April and May and harvested in August.

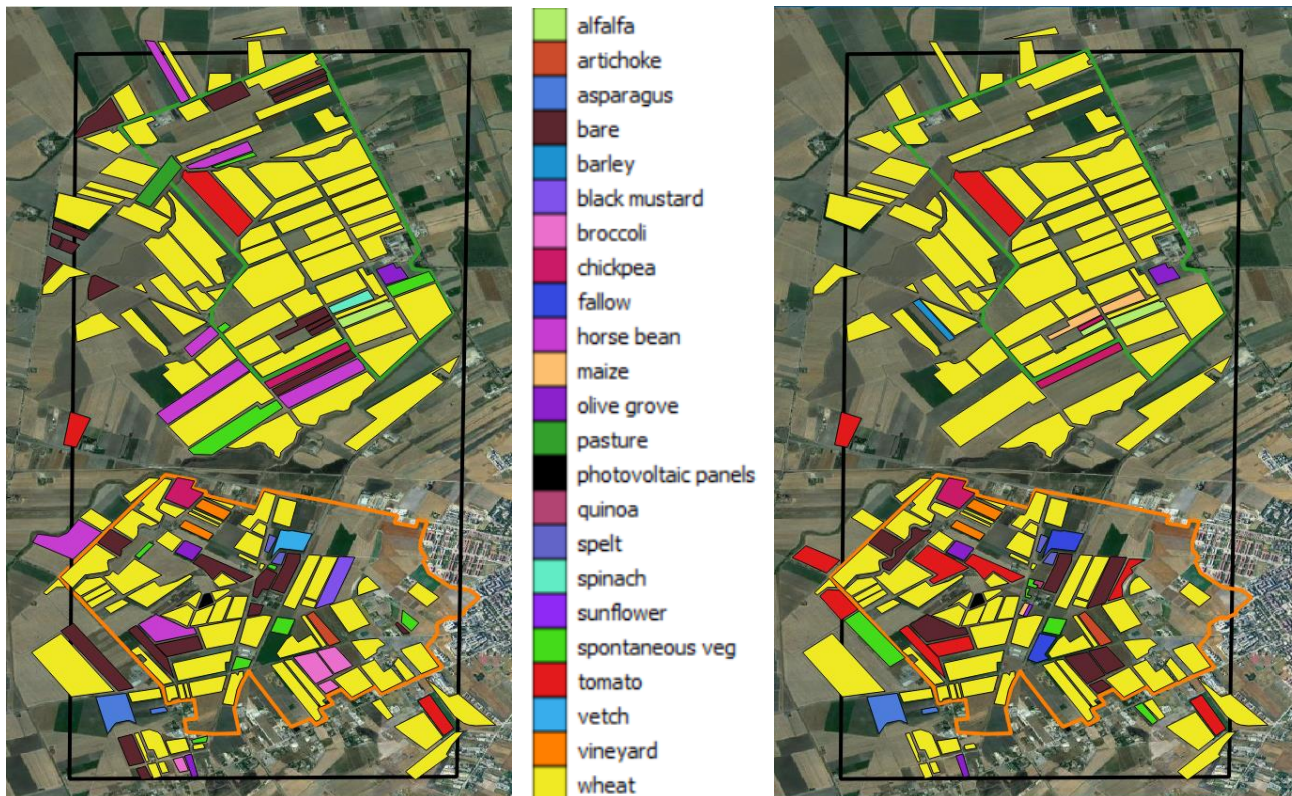


Figure 3-2: Land use map of April (left) and June (right) 2022 compiled by ground surveys (coloured full polygons). The legend in the middle reports the colours of the identified crop types at the Caione (green contour) and CREA (orange contour) farms.

3.2 Permanent hydrologic network

At the CREA farm, CNR-IREA deployed a hydrologic network in July 2017. The network consists of 10 ground stations. Each station measures soil moisture content at 4 depths (i.e., 2.5-10 cm and 20-40 cm) every 20 minutes by Decagon's 5TM and 10HS capacitance sensors. Red points in Figure 3-3 show the location of the ground stations, while the white point identifies the CREA meteorological station. In 2022, most of the fields were cultivated with durum wheat. However, Fg01, Fg02, Fg03, and Fg09 were located in horse bean, vetch, spelt, and broccoli fields, respectively. The horse bean field was harvested by the middle of April and, then, tomatoes were planted and irrigated by drip irrigation in June. The broccoli field was irrigated by drip irrigation in April - May and harvested at the beginning of June. The vetch field was harvested in May. Figure 3-4 shows the temporal behaviour of the surface soil moisture at 2.5 cm from April to June as well as the hourly precipitation measured by the meteo station. The higher soil moisture level of the irrigated broccoli field can be observed between the end of April and the beginning of May. Stations Fg04, Fg05 and Fg08 suffered from malfunctioning, as well as sensors at the deeper depths.



Figure 3-3: Location of the permanent hydrologic network (red points) and of the CREA meteorological station (white point).

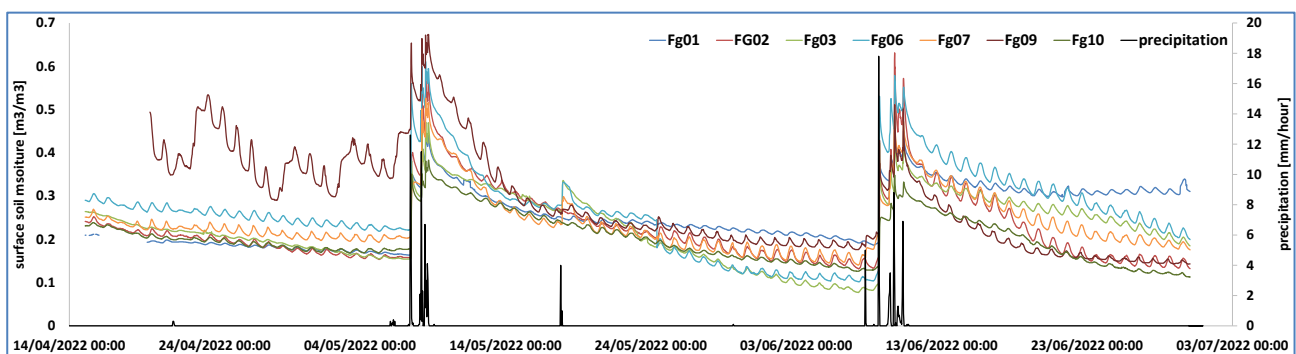


Figure 3-4: Temporal behaviour of surface soil moisture (2.5cm) measured by permanent ground stations every 20 minutes. Hourly precipitation is in black. Time scale: April 14, 0:00h CEST – July 3, 0:00h CEST.

3.3 Field measurements

During the intensive ground campaigns, two fields at the Caione farm and two (three) fields at CREA farm were selected in April (and June) for intensive monitoring during the F-SAR flights. A large number of soil and vegetation samples were measured, both from temporary ground stations and at gridded sample points. Additional information about the phenological stage was also gathered.

Part of the selected fields was equipped with irrigation systems, i.e., mobile boom or drip irrigation. They were irrigated on different dates to produce a sufficient soil moisture contrast between irrigated and non-irrigated areas during the F-SAR overflights. The amount of water supplied and starting and end times of the irrigation were also recorded.

3.3.1 Soil and vegetation sampling and temporary ground stations

Soil moisture measurements were collected over the selected agricultural fields in coincidence with the F-SAR overpasses. Four crews were equipped with portable instruments, i.e. three Stephen's HydraGO and one Spectrum's Field Scout TDR 300 sensors (Figure 3-5). The Field Scout TDR 300 uses the principle of time-domain reflectometry, measuring the travel time of an electromagnetic wave along a waveguide. Electronics in the TDR 300 generate and sense the return of a high energy signal that travels down and back, through the soil, along the waveguide composed of the two rods. Thereafter, the high-frequency signal information is then converted to volumetric water content. The Stephen's HydraGO is a coaxial impedance dielectric sensor, measuring both components of the complex dielectric permittivity, allowing simultaneously measuring soil moisture and soil electrical conductivity. HydraGO and Field Scout TDR 300 were inserted vertically into the soil and provided soil water content measurements integrated over the top 5.7 cm and 3.8 cm, respectively. The measurements were collected on sample grids and recorded digitally. The records consist of geographic coordinates, date and time and soil moisture measurements for each grid point.



Figure 3-5: Stephen's HydraGO (on the left) and Spectrum's Field Scout TDR 300 (on the right).

Additionally, in April, three ground stations were temporally installed and kept in the fields from April to May at the CREA farm over the monitored fields and three ground stations at the Caione farm. Then, the stations were moved to the experimental fields selected in June. Each station (see Figure 3-6) measured soil moisture content at two depths (i.e. 5cm and 20cm) every 15 minutes by Decagon's TEROS 11 or 10HS capacitance sensors. TEROS 11 measured soil temperature, as well. Besides, Decagon's Phytos 31 Dielectric Leaf Wetness sensors were tightened to the leaves of two wheat fields in April and of the

sunflower field in June. Phytos 31 uses capacitance technology to determine the leaf surface water by measuring the dielectric constant of the sensor's upper surface.

Site-specific calibration (see Appendix A) of both portable and temporary soil moisture sensors was carried out by thermos-gravimetric method, using standardized 100 cm³ Kopecky rings (Figure 3-7). Samples were collected and brought immediately after in the lab, weighted and re-weighted after oven-drying at 105°C for 48h.

Fresh vegetation biomass was also collected via destructive sampling at selected grid points as shown in Figure 3-7. Biomass samples were weighted in the lab immediately after. The dry weight was measured after oven-drying the plants at 70°C for 48h.

In the following sections, the SARSimHT-NG ground data collection in April and June is detailed.

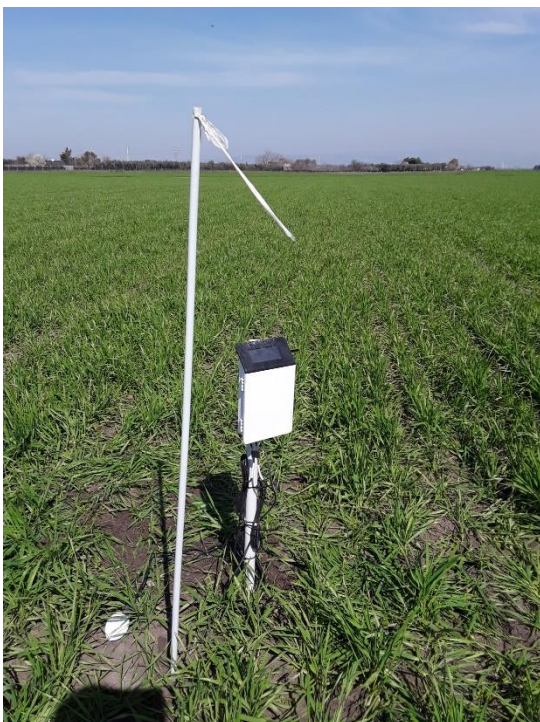


Figure 3-6: Example of temporary station set-up, equipped with soil moisture and temperature sensors at 5cm and 20cm and dielectric leaf wetness sensor.



Figure 3-7: Kopecky rings (on the left) and fresh biomass sampling (on the right).

3.4 Field campaign 28. - 29.04.2022

Three fields cultivated with durum wheat (CA01_DW, CA02_DW, and CREA_DW) and one bare soil (CREA_BS) were selected in April. Field locations are shown in Figure 3-8, left panel. Figure 3-9 and Figure 3-10 give an overview of the monitored fields and Table 3-1 reports the plant phenological stages. Ground measurements were collected between approximately 9:00 and 16:00 local time (CEST) on April 28 and 29, during sunny and windy (wind speed approximately 9 m/s in average on each day) days.

CA01_DW, CA02_DW, and CREA_DW were irrigated by mobile boom systems while CREA_BS was irrigated by drip irrigation. Each wheat field was divided into four stripes (Figure 3-8, right panel) and irrigated on different dates. Table 3-2 and Table 3-3 report the irrigation scheduling, the water supplied, the length and width of the irrigated area and the irrigation system. The irrigation started from the inner part of the fields toward the streets, as indicated by the black arrows. It is noted that the CREA mobile boom system covered a length of 120 m, which is shorter than the entire CREA_DW stripes.

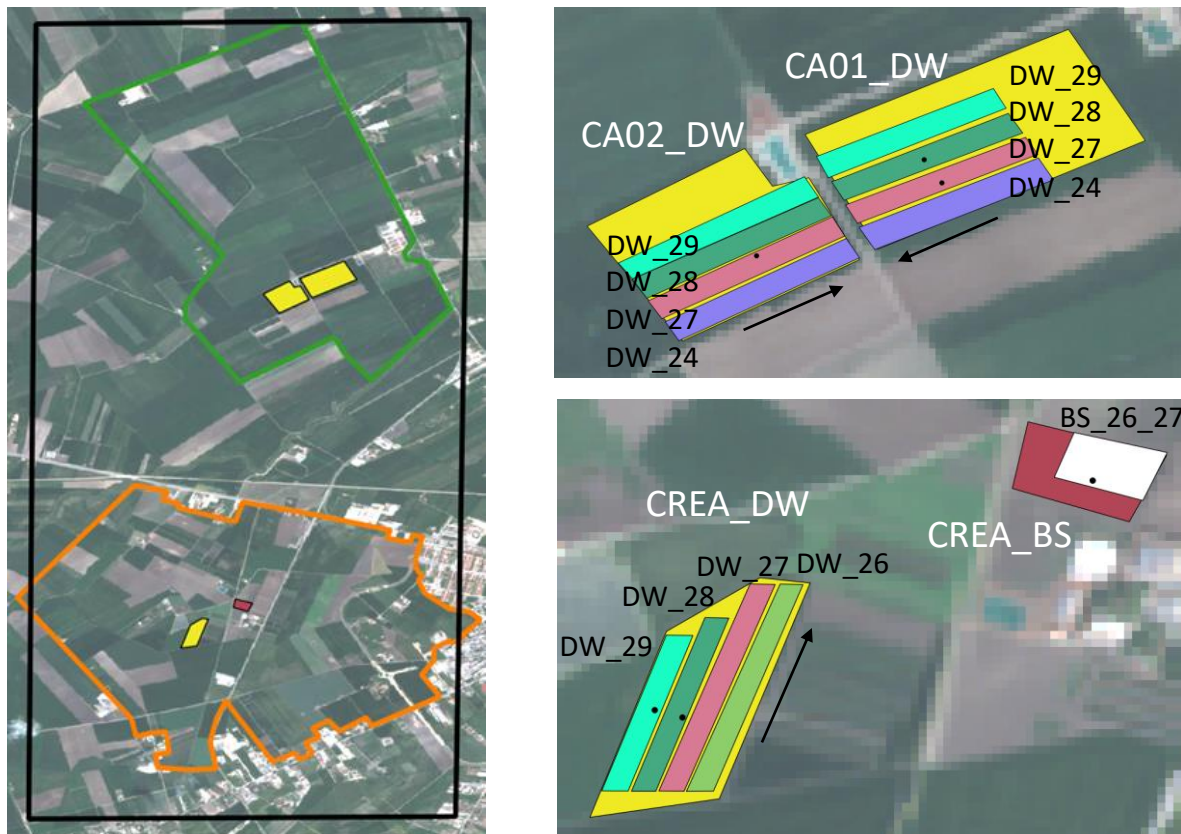


Figure 3-8: Monitored durum wheat (DW) and bare (BS) fields at Caione (green contour) and CREA (orange contour) farms (left panel). Areas irrigated on different dates at each durum wheat and bare fields (right panel). Temporary ground stations in black points. Black arrows: moving direction of the mobile boom irrigation systems. The image in the background is the Sentinel-2 RGB image on April 27, 2022.



Figure 3-9: Durum wheat (left) and bare (right) fields at CREA farm and irrigation systems.



Figure 3-10: Durum wheat, CA01 (left) and CA02 (right) fields at Caione farm and irrigation system.

Table 3-1: Phenological stages of durum wheat plants.

Field ID	Principal growth stage	Phenological stage	BBCH code
CREA_DW	booting	Mid boot stage: flag leaf sheath just visibly swollen	43
CA01_DW	booting	Mid boot stage: flag leaf sheath just visibly swollen	43
CA02_DW	booting	Mid boot stage: flag leaf sheath just visibly swollen	43


	SARSimHT-NG – Simulation of Hydroterra SAR System Performance in the Mediterranean and the Alps Based on Experimental Airborne SAR Data D2: Data Acquisition Report of SSM Experiment	Doc.: DLR-HR-TR-SARSimHT-NG-02 Issue: 1.7 (final) Date: 06.09.2023
---	--	--

Table 3-2: Irrigation scheduling, water supplied, length and width of the irrigated area and irrigation system at CREA farm. Times are given in local time (CEST).

Field ID	Start time	End time	Irrigation volume [m ³ /ha]	length [m]	width [m]	Irrigation System
CREA_DW_26	26/04/2022, 09:00:00	26/04/2022, 14:00:00	378.7	120	25	mobile boom system
CREA_DW_27	27/04/2022, 09:00:00	27/04/2022, 15:00:00	361.3	120	25	
CREA_DW_28	28/04/2022, 09:00:00	28/04/2022, 15:00:00	549.8	120	25	
CREA_DW_29	29/04/2022, 09:00:00	29/04/2022, 15:00:00	486.7	120	25	
CREA_BS_26_27	26/04/2022, 14:00:00	26/04/2022, 22:00:00	512.4	90	60	drip
CREA_BS_26_27	27/04/2022, 15:00:00	27/04/2022, 19:00:00	456.8	90	60	

Table 3-3: Irrigation scheduling, water supplied, length and width of the irrigated area and irrigation system at Caione farm. Times are given in local time (CEST).

Field ID	Start time	End time	Irrigation volume [m ³ /ha]	length [m]	width [m]	Irrigation system
CA01_DW_24 CA02_DW_24	23/04/2022, 10:00:00	24/04/2022, 08:00:00	600	450	40	mobile boom system
CA01_DW_27 CA02_DW_27	26/04/2022, 10:00:00	27/04/2022, 08:00:00	600	450	40	
CA01_DW_28 CA02_DW_28	27/04/2022, 09:00:00	28/04/2022, 07:00:00	600	450	40	
CA01_DW_29 CA02_DW_29	28/04/2022, 09:00:00	29/04/2022, 07:00:00	600	450	40	

3.4.1 Temporary stations

Figure 3-11 and Figure 3-12 illustrate the temporal behaviour of the soil moisture and temperature measured by the temporary stations from April to May at CREA and Caione farms, respectively. Figure 3-11 shows the abrupt increase of soil moisture due to the irrigation events on April 26 and April 27 over the CREA bare soil and on April 28 and 29 over the CREA wheat fields, while Figure 3-12 shows the increase of soil moisture due to the irrigation events on April 27-28 and April 28-29 over the Caione wheat fields. Increase of soil moisture due to precipitation on May 7 and 8 was recorded by all stations.

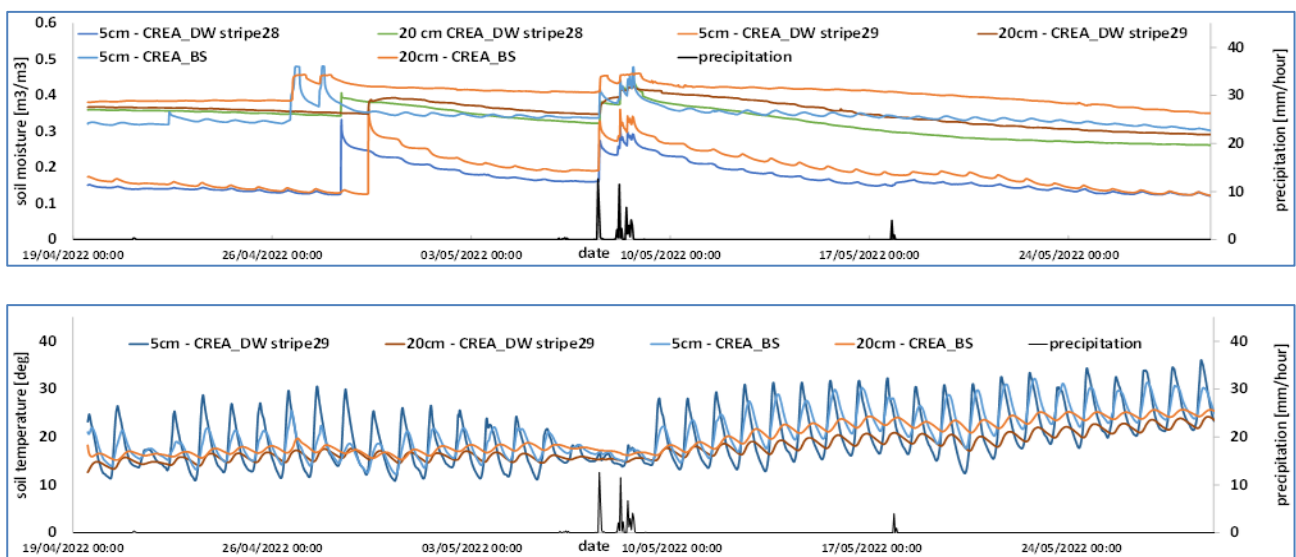


Figure 3-11: Soil moisture (upper panel) and temperature (lower panel) at 5cm and 20cm measured by the temporary stations at CREA durum wheat and bare fields. Time scale: April 19, 0:00h CEST – May 29, 0:00h CEST.

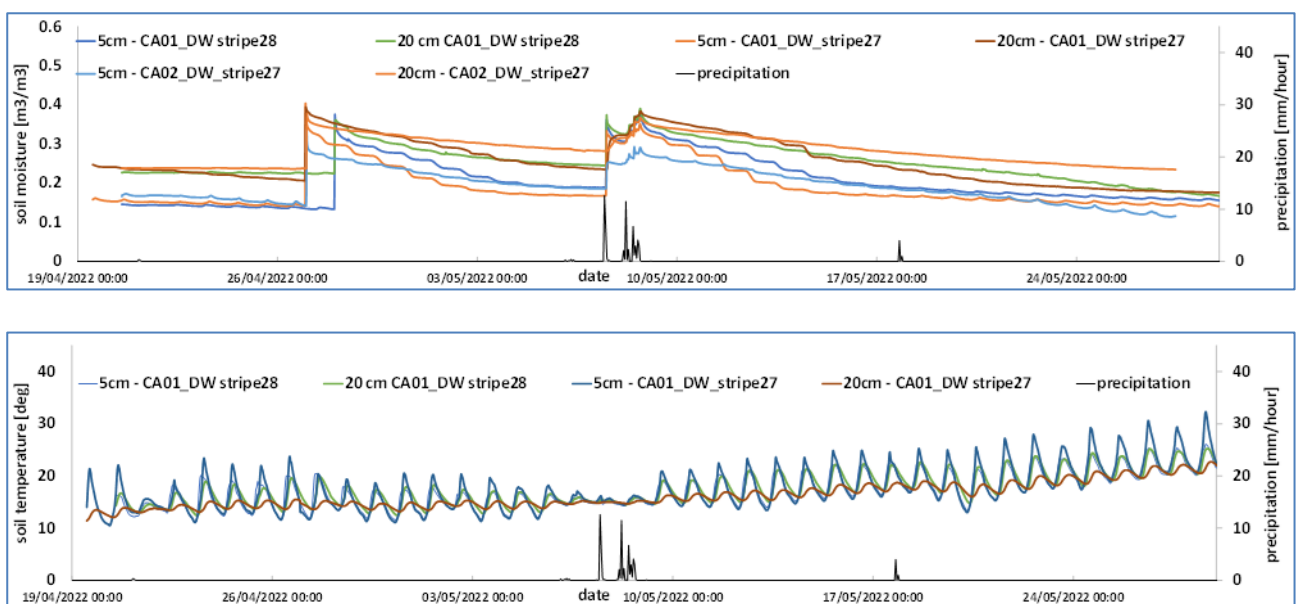


Figure 3-12: Soil moisture (upper panel) and temperature (lower panel) at 5cm and 20cm measured by the temporary stations at Caione durum wheat fields. Time scale: April 19, 0:00h CEST – May 29, 0:00h CEST.

As expected, the soil moisture values of the top soil surface (5 cm) are lower than soil moisture of the deeper depth. Diurnal soil temperature cycle is also observed for both soil layers.

Figure 3-13 shows the leaf wetness measured at the CREA_DW_29 and CA01_DW_28 wheat fields. Soil moisture and temperature at 5cm depth and precipitation are also reported. Leaf interception is observed during irrigation on April 29 and 28 and during precipitation on May 7 and 8. Increases of leaf wetness at CREA_DW_29 during early mornings of the first two weeks of May are suspected dew.

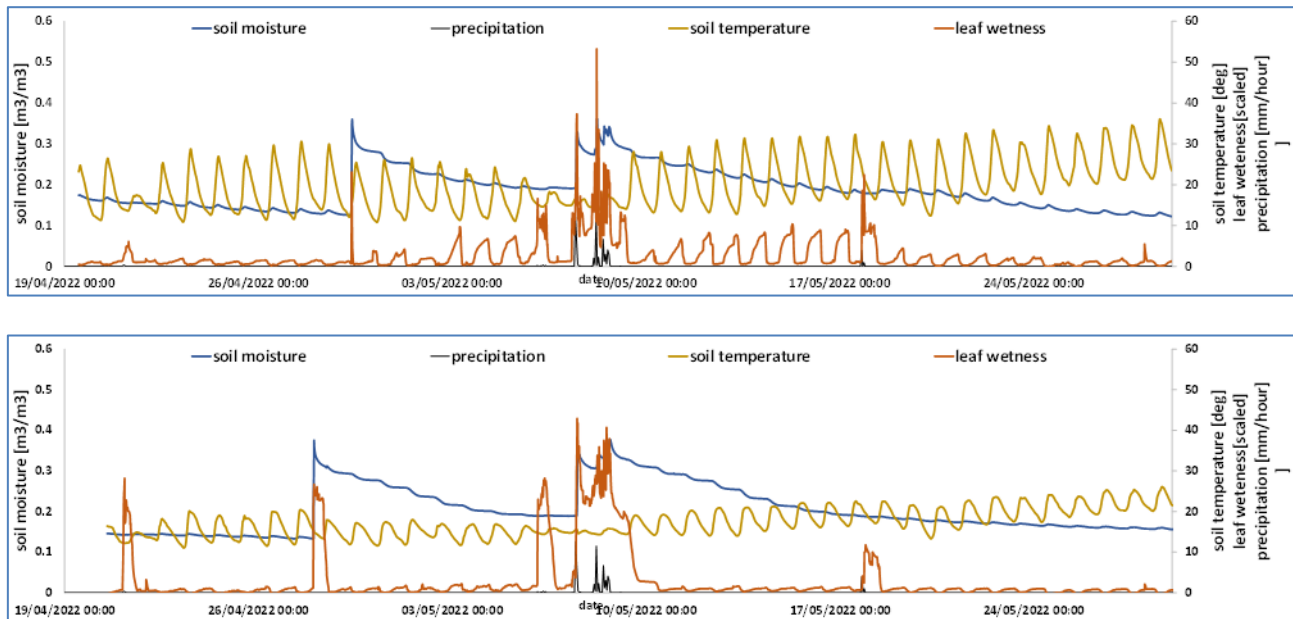


Figure 3-13: Soil moisture (blue line) and temperature (yellow line) at 5cm and scaled (i.e. divided by 10) leaf wetness (orange line) measured by the temporary station at CREA _DW_29 (upper panel) and CA01_DW_28 (lower panel) durum wheat fields. Precipitation also reported in black line. Time scale: April 19, 0:00h CEST – May 29, 0:00h CEST.

3.4.2 Soil moisture and vegetation grid samplings

Figure 3-14 shows the sampling points of soil moisture, measured by the portable probes, and of fresh biomass measurements. Distance between points along a stripe is approximately 15m. Table 3-4 summarizes the number of soil moisture and vegetation samples collected during the campaign in April. Stripes _26 and _27 of CREA_DW and _24 and _27 of CA01_DW and CA02_DW and CREA_BS_26 and _27 were monitored on April 28 and 29 in the morning and in the afternoon. Stripes _28 and _29 of CREA_DW and of CA01_DW and CA02_DW were monitored either on April 29 or April 28 in the morning and in the afternoon, i.e. when no irrigation was being provided. The total number of soil moisture samples is 756 in CREA fields and 696 in Caione fields. Figure 3-15 gives an example of the soil moisture distribution in Caione wheat fields on the mornings of 28 and 29 April.

Table 3-4: Number of soil moisture and fresh biomass samples per stripe and date/time.

Field ID	Stripe ID	Date/time of samplings	Probe type	Number of soil moisture samples per sampling	Number of biomass samples in total
CREA_DW	_26	April 28-29, morning & afternoon	Hydra-GO	40	3
	_27	April 28-29, morning & afternoon		40	3
CREA_DW	_28	April 29, morning & afternoon	Hydra-GO	34	3
	_29	April 28, morning & afternoon		30	3
CREA_BS	_26_27	April 29, morning & afternoon	Hydra-GO	77	
		April 28, morning & afternoon			
CA01_DW	_24	April 28-29, morning & afternoon	Field Scout	29	3
	_27	April 28-29, morning & afternoon		29	3
CA01_DW	_28	April 29, morning & afternoon	Field Scout	29	3
	_29	April 28, morning & afternoon		29	3
CA02_DW	_24	April 28-29, morning & afternoon	Field Scout	29	3
	_27	April 28-29, morning & afternoon		29	3
CA02_DW	_28	April 29, morning & afternoon	Field Scout	29	3
	_29	April 28, morning & afternoon		29	3

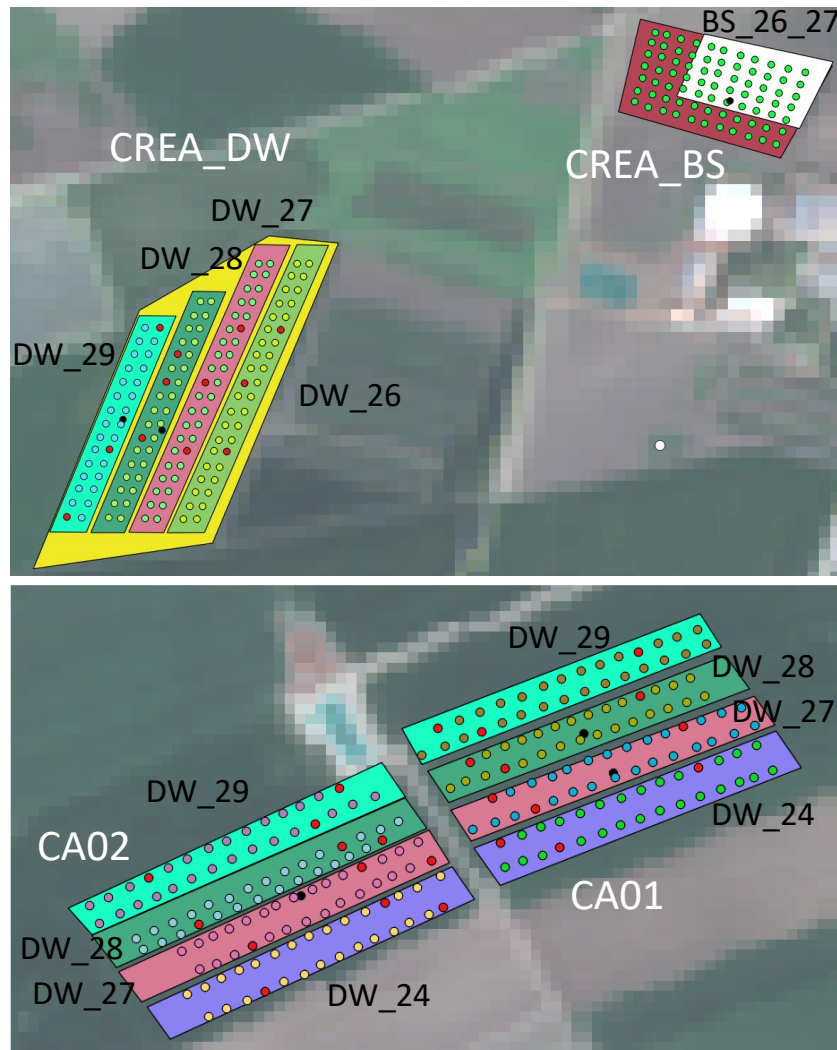


Figure 3-14: Soil moisture sampling with portable probes at CREA durum wheat and bare fields (upper panel) and Caione durum wheat fields (lower panel). Red points indicate the vegetation sample locations. Temporary ground stations were located at black points. The image in the background is the Sentinel-2 RGB image on April 27.

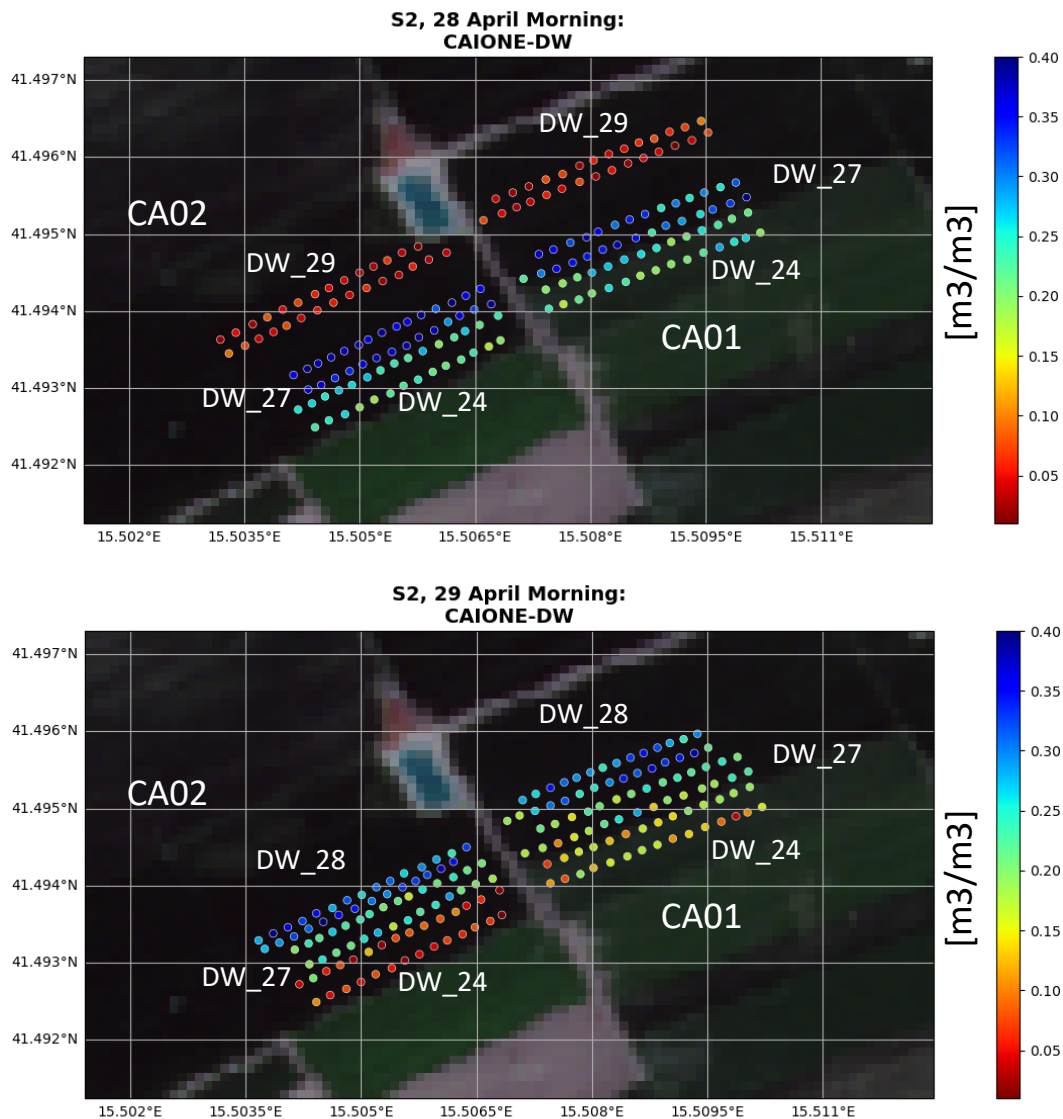


Figure 3-15: Example of soil moisture distribution on the mornings of April 28 (upper panel) and of April 29 (lower panel) in Caione durum wheat fields. The image in the background is the Sentinel-2 RGB image on April 27.

Additionally, three vegetation samples per stripe were collected. The total number of vegetation samples is 36. Figure 3-16 reports the measured fresh (green circles) and dry (orange circles) biomass at the various CREA and Caione field stripes. The black dashed line represents the mean fresh biomass per stripe and the related standard deviation is also reported. Fresh biomass was quite homogeneous per stripe apart from the stripes CREA_DW_27 and Caione_DW_28, where the values of fresh biomass are $638.5 \pm 337.3 \text{ g/m}^2$ and $843.0 \pm 270.9 \text{ g/m}^2$, respectively. An example of inhomogeneity of plants at the centre part (point 30 of the sampling) of the CREA wheat field's stripe 27 with respect to the remaining part is shown in Figure 3-16, upper right panel.

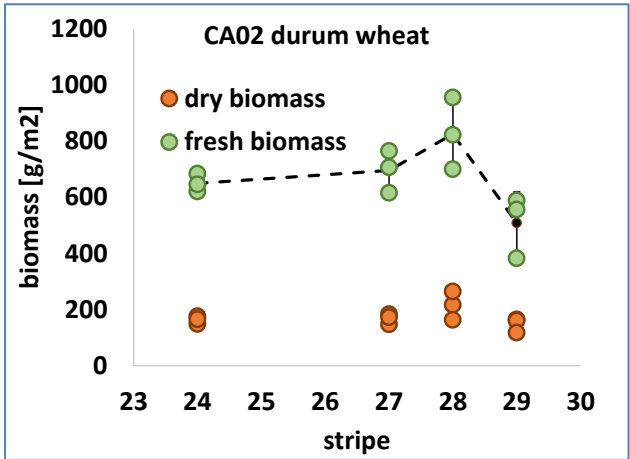
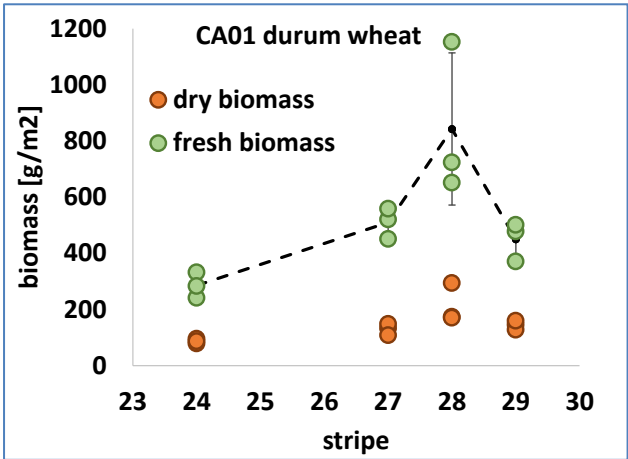
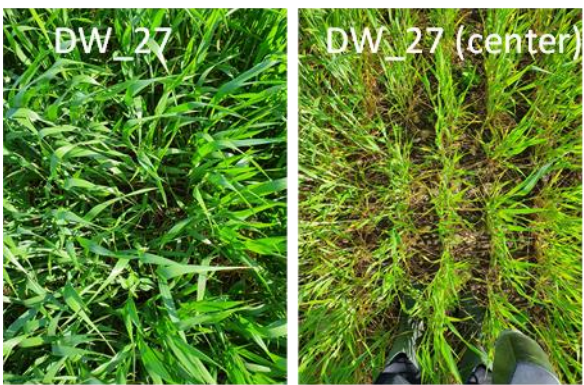
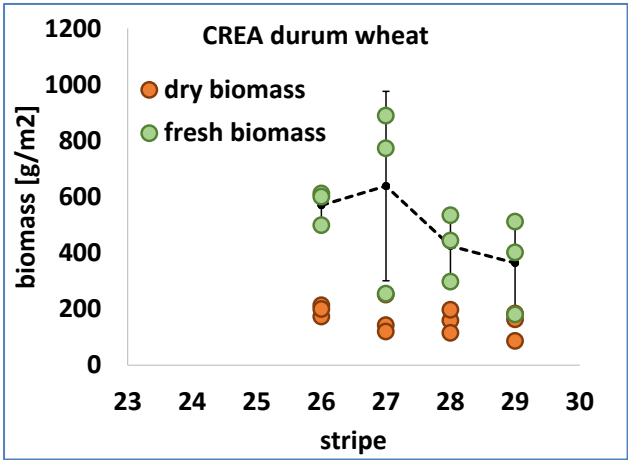


Figure 3-16: Fresh (green circles) and dry (orange circles) biomass at four stripes of CREA (upper left panel) and Caione (lower panels) wheat plants. Black dashed lines represent the mean fresh biomass. The related standard deviation is also reported in black. Upper right panel: Example of inhomogeneity of plants at the centre part (point 30 of the sampling) of the CREA wheat field’s stripe 27 with respect to the remaining part.

3.5 Field campaign 15. - 16.06.2022

In June, maize and alfalfa fields (CA_MA and CA_AA) were monitored at the Caione farm. At CREA farm, maize, sunflower and quinoa fields (CREA_MA, CREA_SF and CREA_QU) were selected (Figure 3-17, left panel). It is worth noting that CREA_QU was the CREA bare soil selected in April. In May, the field was partly cultivated with quinoa, which was irrigated, and partly covered by spontaneous vegetation. Table 3-5 reports the phenological stages of the plants. Ground measurements were collected between approximately 9:00 and 16:00 CEST on June 15 and 16, during sunny and light wind (wind speeds of approximately 3-5 m/s on average) days.

CREA_SF was irrigated by mobile boom system while CA_MA and CREA_QU by drip irrigation. CA_MA was divided in two parts, MA_13 and MA_14, and irrigated on two subsequent dates (Figure 3-17, right panel). Table 3-6 and Table 3-7 report the irrigation scheduling, the water supplied, the length and width of the irrigated area and the irrigation system.

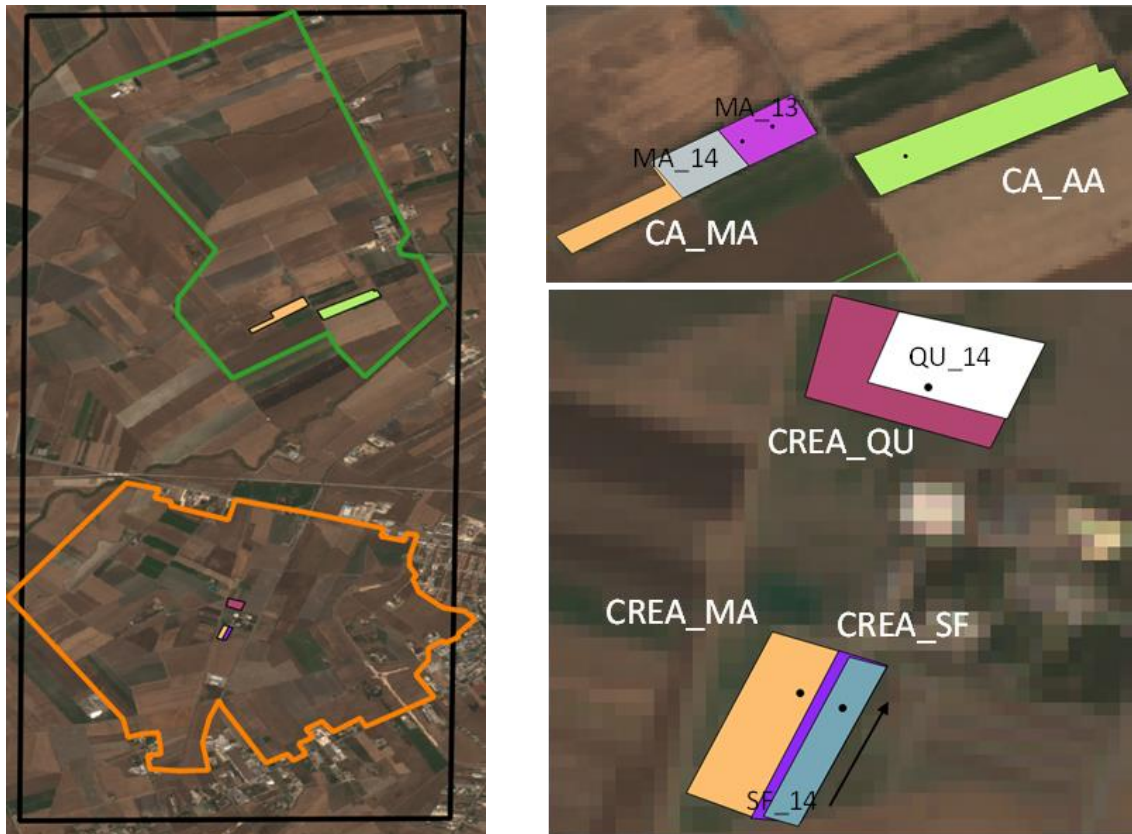


Figure 3-17: Monitored maize (MA) and alfalfa (AA) fields at Caione farm and maize, sunflower and quinoa fields at CREA farm (left panel). Areas irrigated at each maize (MA_13, MA_14), sunflower (SF_14), and quinoa (QU_14) field (right panel). Temporary ground stations marked by black points. Black arrows: moving direction of the boom irrigation system. The image in the background is the Sentinel-2 RGB image on June 16, 2022.



Figure 3-18: Maize (upper left panel) and sunflower (upper right panel), and quinoa (lower panel) fields at CREA farm.



Figure 3-19: Maize (left panel) and alfalfa (right panel) fields at Caione farm.


	SARSimHT-NG – Simulation of Hydroterra SAR System Performance in the Mediterranean and the Alps Based on Experimental Airborne SAR Data D2: Data Acquisition Report of SSM Experiment	Doc.: DLR-HR-TR-SARSimHT-NG-02 Issue: 1.7 (final) Date: 06.09.2023
---	--	--

Table 3-5: Phenological stages of maize, sunflower, quinoa and alfalfa plants.

Field ID	Principal growth stage	Phenological stage	BBCH code
CREA_MA	stem elongation	3 nodes detectable	33
CREA_SF	stem elongation	2 visibly extended internodes	32
CREA_QU	Inflorescence emergence	Individual flower buds (secondary inflorescences visible but still closed)	57
CA_MA	stem elongation	4 nodes detectable	34
CA_AA	flowering	40% of flowers on main raceme open	64

Table 3-6: Irrigation scheduling, water supplied, length and width of the irrigated area and irrigation system at CREA farm. Times are given in local time (CEST).

Field ID	Start time	End time	Irrigation volume [m ³ /ha]	length [m]	width [m]	Irrigation System
CREA_QUINOA	14/06/2022, 13:00:00	14/06/2022, 19:00:00	413.93	90	60	drip
CREA_SF	14/06/2022, 08:30:00	14/06/2022, 12:30:00	310.27	120	25	mobile boom system

Table 3-7: Irrigation scheduling, water supplied and irrigation system at Caione farm. Times are given in local time (CEST).

Field ID	Start time	End time	Irrigation volume [m ³ /ha]	Irrigation System
CA_MA_13	13/06/2022, 08:00:00	13/06/2022, 20:00:00	600	drip
CA_MA_14	14/06/2022, 08:00:00	14/06/2022, 20:00:00	600	drip

3.5.1 Temporary stations

Figure 3-20 and Figure 3-21 illustrate the temporal behaviour of the soil moisture and temperature measured by the temporary stations in June at CREA and Caione farms, respectively. Increase of soil moisture due to precipitation on June 8 was observed by the CREA station only, while all stations recorded the soil moisture increase due to the precipitation on June 9-10. Figure 3-20 shows the abrupt increase of soil moisture due to the irrigation events on June 14 over the CREA quinoa and sunflower fields. CREA maize and sunflower fields were also irrigated on June 23 and 24, respectively. Besides, Figure 3-21 shows the increase of soil moisture due to the irrigation events on June 13 and 14 over the Caione maize field. Other irrigation events after the campaign can be observed. Soil moisture values of the top soil surface (5 cm) are always lower than soil moisture of the deeper depth. Diurnal soil temperature cycle is observed for both soil layers.

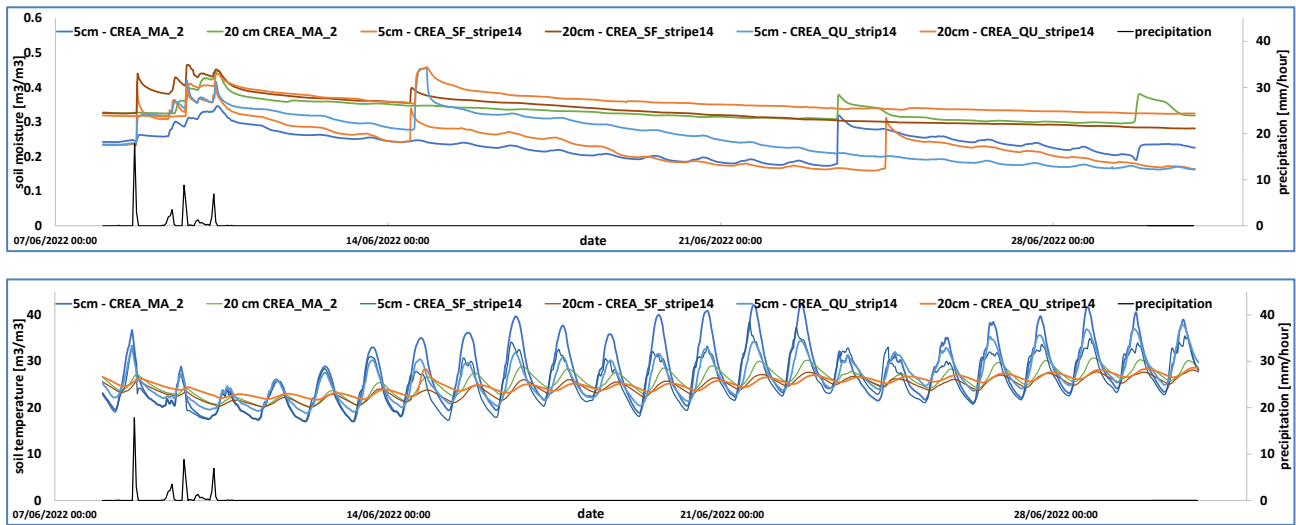


Figure 3-20: Soil moisture (upper panel) and temperature (lower panel) at 5cm and 20cm measured by the temporary stations at CREA maize, sunflower and quinoa fields. Time scale: June 7, 0:00h CEST – July 1, 0:00h CEST.

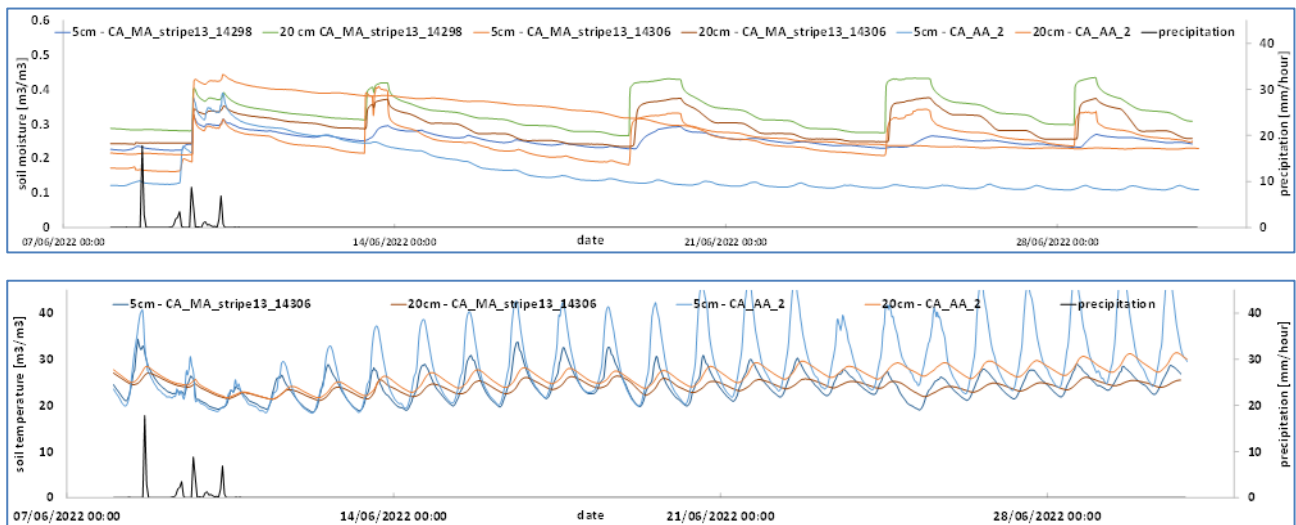


Figure 3-21: Soil moisture (upper panel) and temperature (lower panel) at 5cm and 20cm measured by the temporary stations at Caione maize and alfalfa fields. Time scale: June 7, 0:00h CEST – July 1, 0:00h CEST.

Figure 3-22 shows the leaf wetness measured at the CREA sunflower field. Soil moisture and temperature at 5cm depth and precipitation are also reported. Leaf interception is observed during irrigation on June 14 and 24 and during precipitation between June 8 and 10.

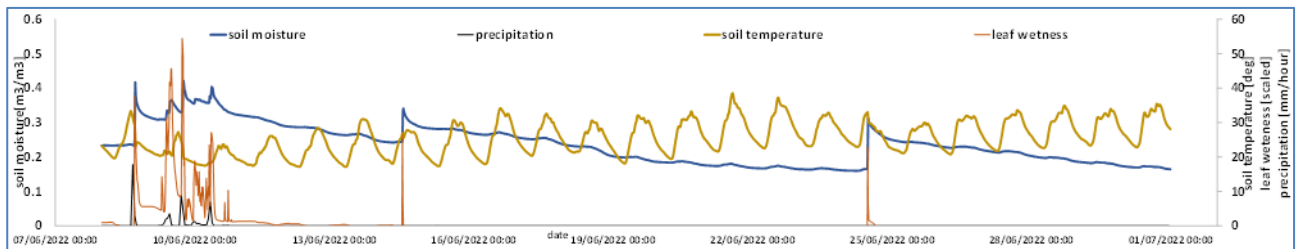


Figure 3-22: Soil moisture (blue line) and temperature (yellow line) at 5cm and scaled (i.e. divided by 10) leaf wetness (orange line) measured by the temporary station at CREA sunflower field. Precipitation is also reported in black line. Time scale: June 7, 0:00h CEST – July 1, 0:00h CEST.

3.5.2 Soil moisture and vegetation grid samplings

Figure 3-23 shows the sampling points of soil moisture measured by the portable probes and of fresh biomass measurements. Distance between points along a stripe is approximately 15m. Table 3-8 summarizes the number of soil moisture and vegetation samples collected during the campaign in June.

Table 3-8: Number of soil moisture and fresh biomass samples per stripe and date/time.

Field ID	Stripe ID	Date/time of samplings	Probe type	Number of soil moisture samples per sampling	Number of biomass samples in total
CREA_MA	_1	June 15-16, morning & afternoon	HydraGO	22	3
	_2	June 15-16, morning & afternoon		22	3
CREA_SF	_14	June 15-16, morning & afternoon	HydraGO	20	3
CREA_QU	_14	June 15-16, morning & afternoon	HydraGO	77	3
CA_MA	_1	June 15-16, morning & afternoon	HydraGO	52	3
	_2	June 15-16, morning & afternoon		52	3
	_3	June 15-16, morning & afternoon		52	3
CA_MA	_4	June 15-16, morning & afternoon	Field Scout	26	3
CA_AA	_1	June, 15-16 morning & afternoon	Field Scout	26	3
	_2	June, 15-16 morning & afternoon		26	3
	_3	June, 15-16 morning & afternoon		26	3

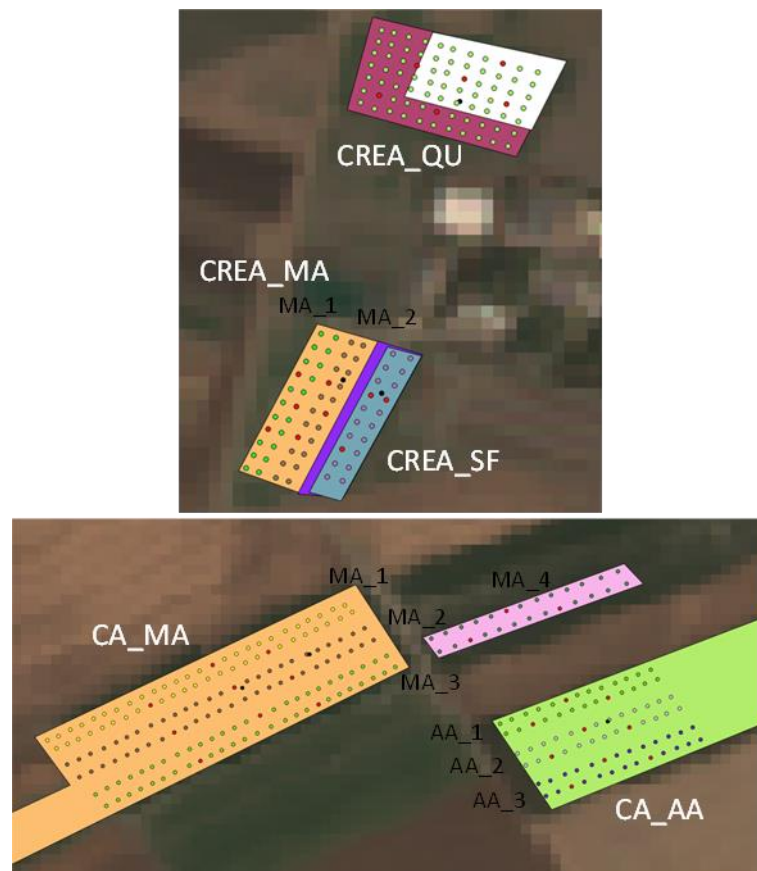


Figure 3-23: Soil moisture sampling with portable probes at CREA maize, sunflower and quinoa fields (upper panel) and Caione maize and alfalfa fields (lower panel). Red points indicate the vegetation samples locations. Temporary ground stations were located in the black points. The image in the background is the Sentinel-2 RGB image on June 16, 2022.

The CREA maize field was divided in two stripes for sampling, i.e. MA_1 and MA_2 whereas, Caione maize and alfalfa were divided in three stripes, i.e. MA_1, MA_2, MA_3, and AA_1, AA_2, AA_3. Besides, an additional stripe (MA_4) in the maize field opposite to CA_MA was also included in the sampling. All stripes were monitored on June 15 and 16 in the morning and in the afternoon. The total number of soil moisture samples is 564 at CREA fields and 1040 at Caione fields. Figure 3-24 gives an example of the soil moisture distribution at CREA maize and sunflower fields on the mornings of June 15 and 16.

Again, like in April, three vegetation samples were collected per stripe. The total number of vegetation samples is 33. Figure 3-25 reports the measured fresh and dry biomass at the CREA and Caione fields. Biomass was homogeneous within the stripes and the fields. A slight difference in the fresh biomass was observed between the stripe 1 and 2 of the CREA maize field.

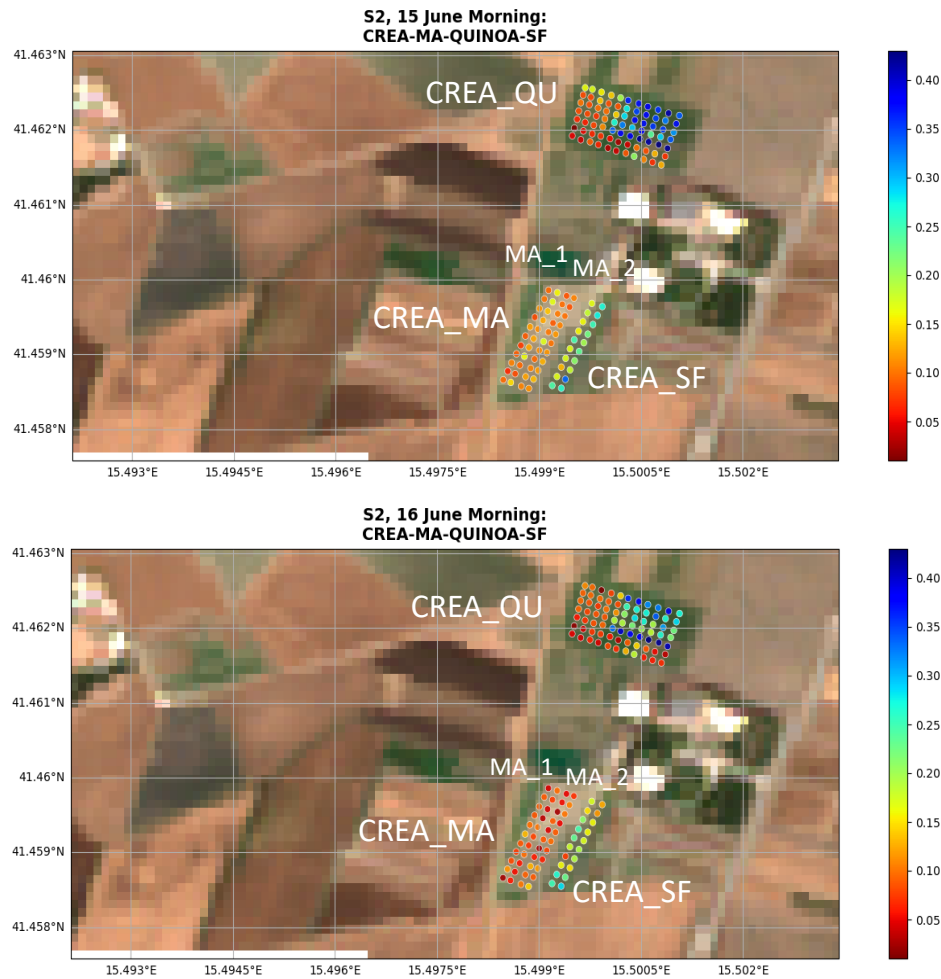


Figure 3-24: Example of soil moisture distribution on the mornings of June 15 (upper panel) and June 16 (lower panel) at the CREA maize, sunflower and quinoa fields. The image in the background is the Sentinel-2 RGB image on June 16, 2022.

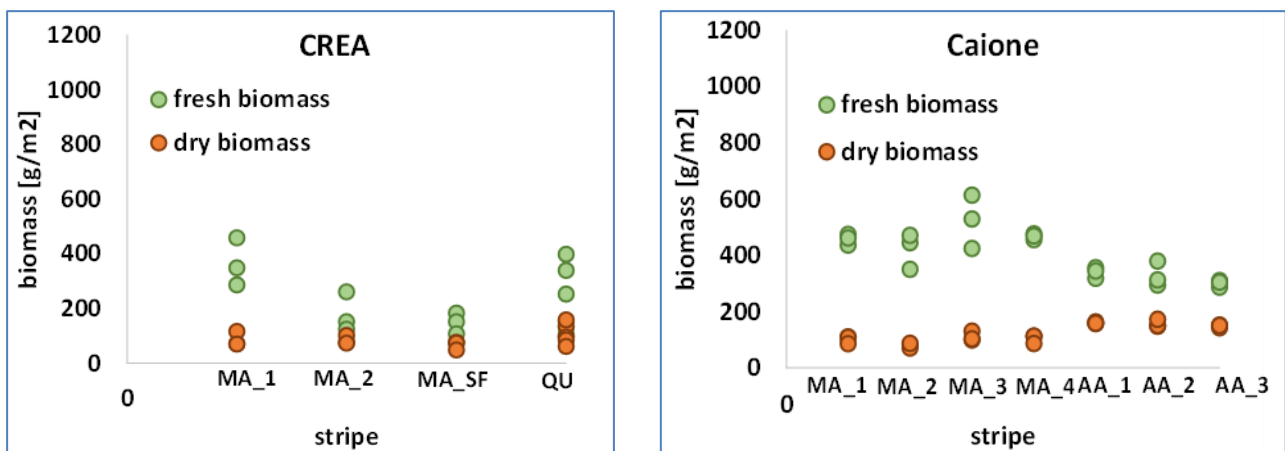



Figure 3-25: Fresh (green circles) and dry (orange circles) biomass at CREA maize, sunflower and quinoa (left panel) and Caione (right panel) maize and alfalfa plants.

	SARSimHT-NG – Simulation of Hydroterra SAR System Performance in the Mediterranean and the Alps Based on Experimental Airborne SAR Data D2: Data Acquisition Report of SSM Experiment	Doc.: DLR-HR-TR-SARSimHT-NG-02 Issue: 1.7 (final) Date: 06.09.2023
---	--	--

3.6 Database description

The collected dataset is organized according to the folder structure shown in Figure 3-26. Under the root directory the content is:

- **April22:** data collected during the April campaign
- **June22:** data collected during the June campaign
- **permanent_stations:** soil moisture values [m^3/m^3] from April to June measured by the permanent stations every 20 minutes (sm_permanent_stations.xlsx) and locations of the ground stations (permanent_stations.shp)
- **precipitation:** hourly precipitation [mm/hour] from the CREA meteo station (precipitation_Apr_June.xlsx) and location of the meteo station (CREA_meteo_station.shp)
- **shp:** shapefiles of the AOI (AOI_ApulianTavoliere.shp), the Caione (Caione_farm.shp) and CREA (CREA_farm.shp) farms
- **soil_texture:** soil texture [%] at CREA and Caione temporary stations, and at each permanent station (soil_texture.xlsx)

April22 and **June22** folders contain the ground data collected during the campaigns:

- **crop map:** land use in April (2022_APRIL_cropmap.shp) and June (2022_JUNE_cropmap.shp). Crop types and field extent [ha] are included and crop height [cm] when available.
- **irrigation:** start time and end time of irrigation events, irrigation volumes [m^3/ha] and irrigation systems in April (irrigation_scheduling_April.xlsx) and in June (irrigation_scheduling_June.xlsx)
- **leaf_wetness:** Phytos 31 measurements at CREA_DW_29 and CA01_DW_28 in April (leaf_wetness_APRIL.xlsx) and at CREA_SF in June (leaf_wetness_JUNE.xlsx)
- **monitored_fields_shp:** shape files of the monitored fields in April and June
- **phenology:** phenological stages (BBCH scale) in April (phenology_April.xlsx) and June (phenology_June.xlsx)
- **photos:** photos collected during the campaigns
- **soil_moisture_sensors:** .csv-files of date/time, locations [lon/lat; EPSG: 4326] and values of the gridded soil moisture [m^3/m^3] measurements collected by HydraGO and Field Scout TDR 300 over the monitored fields in April (CA1_DW_24.csv, CA1_DW_27.csv, CA1_DW_28.csv, CA1_DW_29.csv, CA2_DW_24.csv, CA2_DW_27.csv, CA2_DW_28.csv, CA2_DW_29.csv, CREA_BS_APRIL.csv, CREA_DW26.csv, CREA_DW27.csv, CREA_DW28.csv, CREA_DW29.csv) and June (CA_AA_1.csv, CA_AA_2.csv, CA_AA_3.csv, CA_MA_1.csv, CA_MA_2.csv, CA_MA_3.csv, CA_MA_4.csv, CREA_MA_1.csv, CREA_MA_2.csv, CREA_SF.csv and CREA_QUINOVA.csv)
- **soil_moisture_stations:** soil moisture [m^3/m^3] at 5cm and 20cm and soil temperature [deg] measured every 15 minutes by the temporary stations in April (sm_temporary_stations_April.xlsx) and June (sm_temporary_stations_June.xlsx) and their locations in April (temporary_stations_April.shp) and June (temporary_stations_June.shp)
- **vegetation_biomass:** .csv-files of date and locations [lon/lat; EPSG: 4326] of fresh and dry biomass (g/m^2) samples in April (CREA_BIOMASS_APRIL.csv and CAIONE_BIOMASS_APRIL.csv) and June (CREA_BIOMASS_JUNE.csv and CAIONE_BIOMASS_JUNE.csv)
- **wind:** hourly wind speed [m/s] and direction [deg] during the April (wind_April.xlsx) and June campaigns (wind_June.xlsx)

The time reported in the files is local time (CEST = UTC+2).

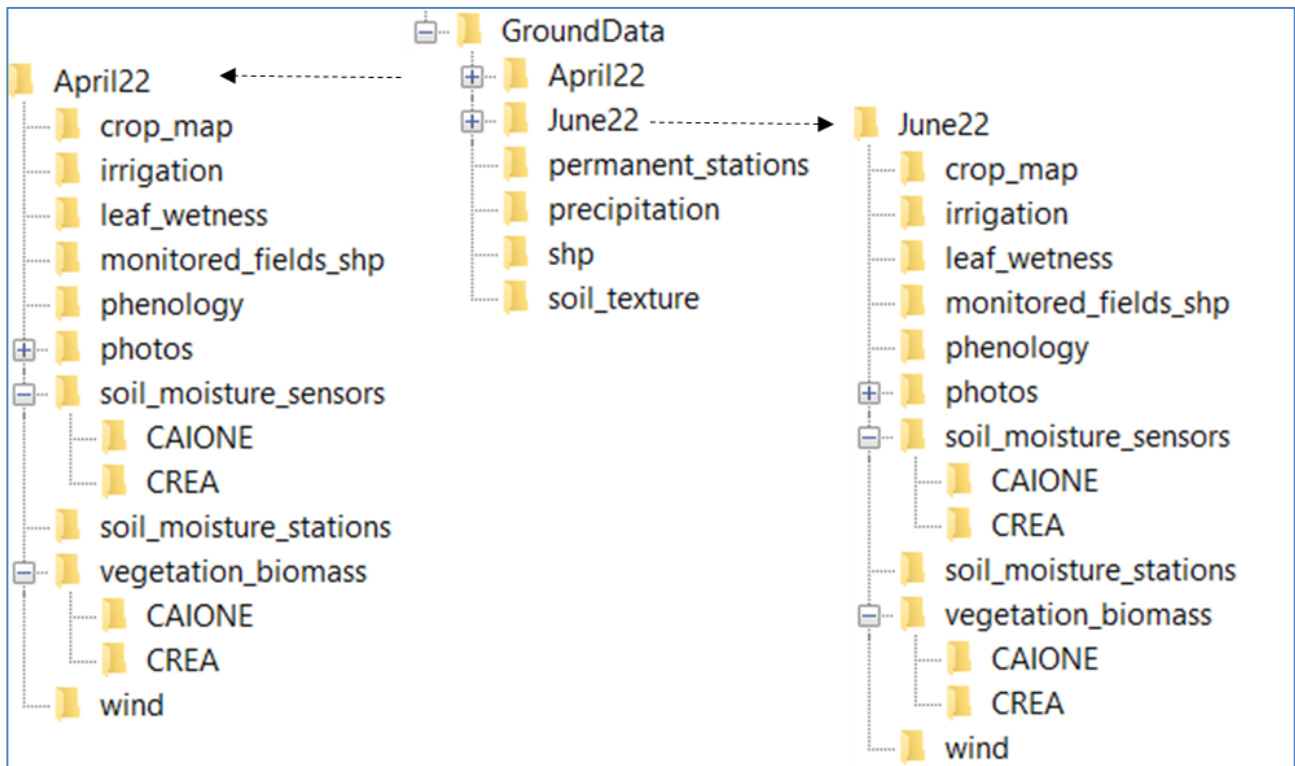


Figure 3-26: Structure of the SARSimHT-NG soil moisture database.

4 Processing Strategy and Inventory

4.1 Preparations

In addition to the radar data, several other auxiliary data need to be prepared for the processing of acquired synthetic aperture radar (SAR) data. These include a Digital Elevation Model (DEM) as a reference plane for SAR processing and, if available, corner reflectors as ground control points (GCP) to check the calibration of the radar system. Aircraft motion is measured in flight to allow later compensation for deviations of the aircraft from the intended straight line during off-line SAR processing. Information on antenna mounting on the aircraft and respective antenna characteristics is required. SAR signal replicas recorded before and after SAR measurements are used to equalise radar receiver nonidealities. Mission planning information is required, additionally, to set up the SAR processor.

At the ‘Apulian Tavoliere’ test site near Foggia, Italy, no GCPs were in place. The F-SAR radar has been calibrated before and after each mission in April and June 2022. The evaluation of these data showed no noticeable problems with the radar instrument.

In the following, the DEM preparation and the determination of ideal flight tracks for interferometric processing is being described in more detail.

4.1.1 Digital Elevation Model

A laser-scanned Digital Elevation Model (DEM) “dtm-8mPosting+45.rat” has been provided in-kind by CNR-IREA. It serves as reference plane for precision SAR processing. The DEM is depicted in Figure 4-1.



Figure 4-1: Quicklook of the DEM used for SAR processing. Ellipsoidal heights are ranging from 91.5 m to 183.1 m.

The DEM was routinely checked for errors. The key parameters of this model are listed in Table 4-1. The coordinate reference system is the WGS84 ellipsoid (EPSG 3857) and its projection is Universal Transverse Mercator (UTM), zone 33N.


	SARSimHT-NG – Simulation of Hydroterra SAR System Performance in the Mediterranean and the Alps Based on Experimental Airborne SAR Data D2: Data Acquisition Report of SSM Experiment	Doc.: DLR-HR-TR-SARSimHT-NG-02 Issue: 1.7 (final) Date: 06.09.2023
---	--	--

Table 4-1: Digital Elevation Model (DEM) key parameters.

Coordinate Reference System (CRS)	EPSG:32633 - WGS 84 / UTM zone 33N
Extension	538000.0 / 4585488.0 : 545504.0 / 4598992.0
Unit	Meter
X-Dimension	838
Y-Dimension	1688
Data	Float32 - 32-Bit floating-point number
Format	ENVI (data *.rat and header *.rat.hdr)
File Name / File Size	dtm-8mPosting+45.rat / 6.04 MB
Region	Foggia, Italy
Area or Point	Area
Dimensions	X: 7504; Y: 13504; Channels: 1
Origin	N 538000 / E 4598992
Pixel Size [m]	+8, -8
Undulation [m]	45.67

Next, we need to determine ideal flight tracks for the scenes to be processed. These flight tracks determine the resulting image geometry, that is, the number of pixels in x and y direction (azimuth and range) in slant range geometry of the scenery. For reasons of comparison it is important to have the same image geometry for all images – but this depends on the prevailing wind conditions.

4.1.2 Radar Image Geometries

We distinguish three different kinds of geometries in radar imaging: (1) the *slant range geometry*, (2) the *ground range geometry* (projected either onto a virtual flat terrain or the real terrain given by a DEM) and (3) the *geocoded and terrain corrected image geometry*. In this project we deliver two kinds of products RGI (Radar Geometry Image) products which is geometry (1) and GTC (Geocoded and Terrain Corrected) image products which is geometry (3).

In RGI products, the resulting radar image geometry (number of pixels in x and y direction in slant range geometry) depends on the real track flown. This track and the actual airplane attitude depend on wind conditions present at flight level. To counteract the effect of wind and to fly the desired course over ground it is necessary to point the aircraft's nose towards the wind by the so-called wind correction angle (WCA). With respect to the line-of-sight (LOS) direction the WCA is transferred into the resulting squint angle. Squint angle zero means the aircraft nose points exactly into flight direction (no wind), slant range images will be trapezoid (or regular) shaped in this case. Otherwise shearing arises and the radar images become more parallelogram shaped, tilted in the one or the other direction (see Figure 4-2).

For the 22HTERRA campaign, the wind conditions at flight level have been very advantageous (see the next section) such that merely two image geometries exist (Table 4-2), one for C-band and one for L-band. However, due to the large time gap of nearly two months between mission 01 (April 2022) and mission 02 (June 2022) we decided to process the two missions separately in individual interferometric groups. Due to the changes on the ground the decorrelation between images acquired in mission 01 and mission 02 would turn out to be too large. Therefore, four interferometric groups were obtained in total.

Table 4-2: Image geometries and interferometric groups, $x = n_{\text{pixel}}$ in azimuth, $y = n_{\text{pixels}}$ in slant range.

Geometry	Mission	Band	Flight Direction	Illumination	x	y	Group
1	01 (April)	C-band	towards north	towards east	54016	9072	C1
2	02 (June)	C-band	towards north	towards east	54016	9072	C2
3	01 (April)	L-band	towards north	towards east	27136	4536	L1
4	02 (June)	L-band	towards north	towards east	27136	4536	L2

In the next section the way the two geometries (C-band, L-band) are determined is described in detail.

4.1.3 Squint Angle Analysis

A parameter that influences the final image geometry is the squint angle resulting from wind conditions during SAR data acquisition. Image geometry examples are shown in Figure 4-2.

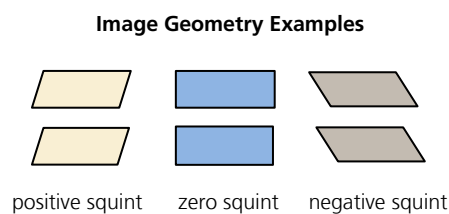


Figure 4-2: Image geometries due to wind conditions.

SAR processing can compensate different squinted geometry conditions to some degree, depending on the width of the antenna main lobe in flight direction. It is, however, recommended to select the processed Doppler centroid (DC) as close as possible to the real Doppler centroid present in the data because forcing another DC means to misalign the processed azimuth bandwidth from the optimum high-gain main lobe area of the antenna. As a result, the image noise level increases the farther the scene is processed from its real squint angle.

In the pre-processing of the SAR data of the 22HTERRA campaign we have analysed the Doppler history of all passes. The variation of the Doppler Centroid over time for all passes acquired in April and June 2022 is shown in Figure 4-3 for C-band and in Figure 4-4 for L-band. We note that we have been very lucky with the weather situation in both missions. Squint angles vary from pass to pass and from flight to flight only very little in comparison with the antenna's azimuth 3dB-beamwidth in the respective frequency band. We have half-power beamwidths of 12° for C-band and 18° for L-band one-way. After some averaging across all data sets we note that the deviations from the respective optimum DC found in the data are within tolerances for both frequencies, C- and L-band.

Based on this analysis, we decided to have two common image geometries, one for C-band with an average squint angle of -1.54° , and one for L-band with an average squint angle of -1.85° (see the summary in Table 4-3). It should be noted that a common squint angle for both C- and L-band is not required.

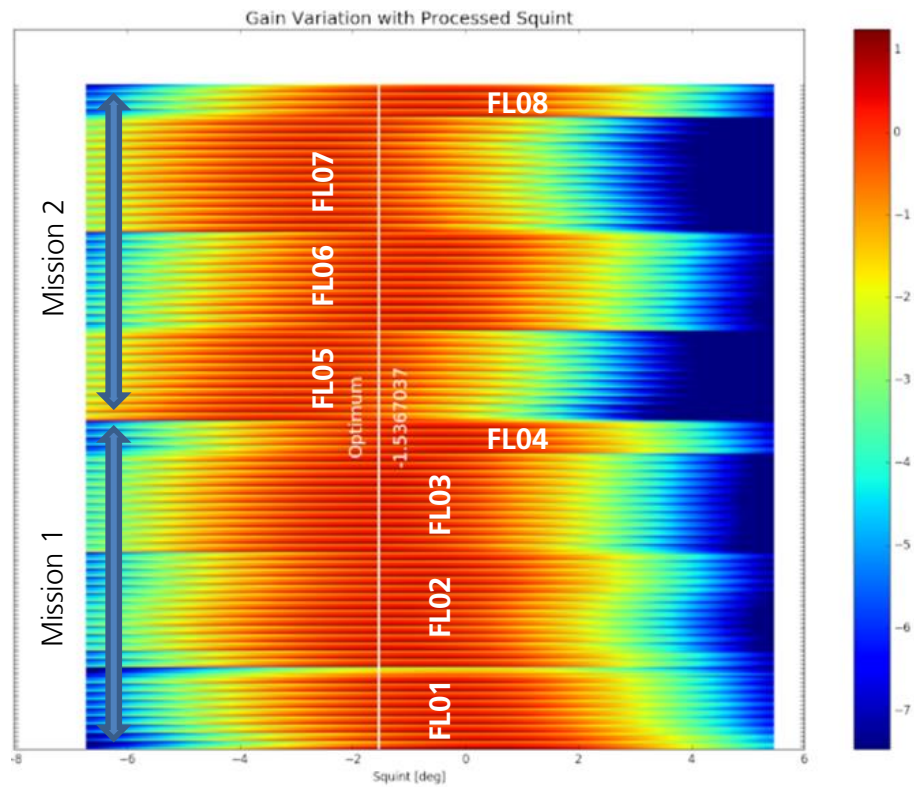


Figure 4-3: Squint angle determination (white line) for C-band through all acquired passes of two missions.

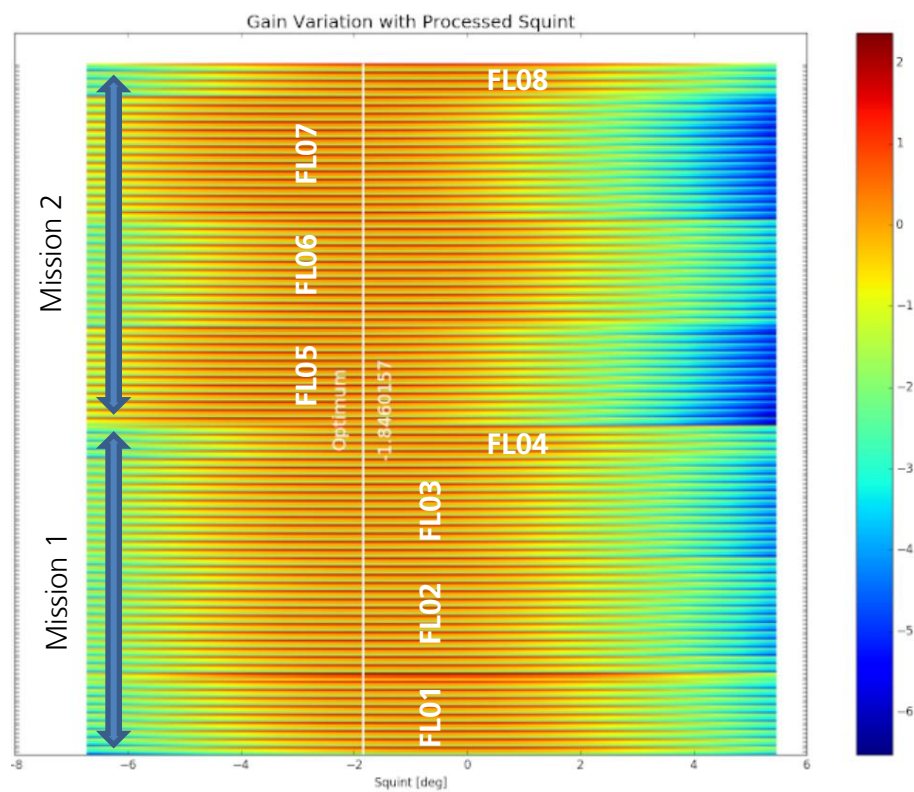


Figure 4-4: Squint angle determination (white line) for L-band through all acquired passes of two missions.


	SARSimHT-NG – Simulation of Hydroterra SAR System Performance in the Mediterranean and the Alps Based on Experimental Airborne SAR Data D2: Data Acquisition Report of SSM Experiment	Doc.: DLR-HR-TR-SARSimHT-NG-02 Issue: 1.7 (final) Date: 06.09.2023
---	--	--

Table 4-3: Average squint angles in acquired data, bold values are used for processing all data.

Frequency	Geometry	Mission 01	Mission 02	Both missions
C-band	Master	-0.98825996°	-2.0499522°	-1.5367037°
L-band	Master	-1.2696233°	-2.1387676°	-1.8460157°

Taking this result and considering the site coverage defined in the flight planning (see Figure 2-2), we have tailored the SLC slant range image data sets (RGI) in azimuth and range to 54016 x 9072 pixels in C-band and 27136 x 4536 pixels in L-band. Values are listed in Table 4-2.

The next step, after squint angle analysis, is the project setup which includes the calculation of an ideal (straight) track from all real flight tracks.

4.1.4 Processing Strategy

The processing steps include (i) project initialization, (ii) SAR processing (F-SAR RGI product generation), (iii) geocoding (F-SAR GTC product generation), (iv) interferometric processing (F-SAR INF product generation) and (v) satellite simulation product generation (1 = High resolution Geosynchronous SAR product generation and 2 = Low resolution Hydroterra SAR product generation).

i. Project Initialization

The project has been setup using the keyword “/same_reftr”, which means that all passes in this project have exactly the same ideal reference track and, hence, the same image geometry.

ii. RGI Processing

The processing in C-band has been started using the keyword “squint=-1.54” to force the required squint angle. Processing in L band has been started using keywords “squint=-1.85” and “rfi=4”. The latter allows to mitigate radio frequency interference (RFI) which we noticed during test processing. We have assigned the try number T01 to C-band and the try number T02 to L-band. Try numbers describe the set of fixed parameters which are used to convert radar raw data into radar image data (Table 4-8). Different try numbers mean different parameter sets and thus different products.

iii. GTC Processing

Since all images have the same geometry, we have geocoded the master passes only, that is, Pass 0204 in the group of (FL01, FL02, FL03, FL04), which is Mission 01, and Pass 0604 in the group of (FL05, FL06, FL07, FL08), which is Mission 02. In C- and L-band, this yields four geocoded products. The geocoding of all other scenes can be done using the lookup tables which are part of the GTC product file set of the respective master pass.

iv. INF Processing

We have processed two interferometric groups (one for Mission 01 and one for Mission 02) per frequency band (C and L). In total four interferometric groups (“C1”, “C2”, “L1”, “L2”) were formed. As the possible amount of interferometric combinations is enormous, we have deliberately limited the combinations to those listed as sub-groups in Table 4-4 to Table 4-7. Note, that the master tracks are the same as in GTC processing: Pass 0204 for Mission 01 and Pass 0604 for Mission 02.

Table 4-4: Interferometric Subgroups in Group “C1” – Flights FL01, FL02, FL03, FL04, C-band, Mission 01

Mission 01	Master	Slave1	Slave2	Slave3	Slave4	Slave5	Slave6	Slave7	Slave8	Slave9	Slave10	Slave11	Slave12
hterra01C	2-4	1-4	1-5	1-6	1-7	1-8	1-9	1-10	1-11	1-12	1-13	1-14	1-15
hterra02C	2-4		2-5	2-6	2-7	2-8	2-9	2-10	2-11	2-12	2-13	2-14	2-15
hterra03C	2-4	3-4	3-5	3-6	3-7	3-8	3-9	3-10	3-11	3-12	3-13	3-14	3-15
hterra04C	2-4	(4-2)	4-3	4-4	4-7	4-8							

Table 4-5: Interferometric Subgroups in Group “C2” – Flights FL05, FL06, FL07, FL08, C-band, Mission 02

Mission 02	Master	Slave1	Slave2	Slave3	Slave4	Slave5	Slave6	Slave7	Slave8	Slave9	Slave10	Slave11	Slave12
hterra05C	6-4	5-4	5-5	5-6	5-7	5-8	5-9	5-10	5-11	5-13	5-14	5-15	
hterra06C	6-4		6-5	6-6	6-7	6-8	6-9	6-10	6-11	6-13	6-14	6-15	6-16
hterra07C	6-4	7-4	7-5	7-6	7-7	7-8	7-9	7-10	7-11	7-13	7-14	7-15	7-16
hterra08C	6-4	8-4	8-5	8-6	8-9								

Table 4-6: Interferometric Subgroups in Group “L1” – Flights FL01, FL02, FL03, FL04, L-band, Mission 01

Mission 01	Master	Slave1	Slave2	Slave3	Slave4	Slave5	Slave6	Slave7	Slave8	Slave9	Slave10	Slave11	Slave12
hterra01L	2-4	1-4	1-5	1-6	1-7	1-8	1-9	1-10	1-11	1-12	1-13	1-14	1-15
hterra02L	2-4		2-5	2-6	2-7	2-8	2-9	2-10	2-11	2-12	2-13	2-14	2-15
hterra03L	2-4	3-4	3-5	3-6	3-7	3-8	3-9	3-10	3-11	3-12	3-13	3-14	3-15
hterra04L	2-4	(4-2)	4-3	4-4	4-7	4-8							

Table 4-7: Interferometric Subgroups in Group “L2” – Flights FL05, FL06, FL07, FL08, L-band, Mission 02

Mission 02	Master	Slave1	Slave2	Slave3	Slave4	Slave5	Slave6	Slave7	Slave8	Slave9	Slave10	Slave11	Slave12
hterra05L	6-4	5-4	5-5	5-6	5-7	5-8	5-9	5-10	5-11	5-13	5-14	5-15	
hterra06L	6-4		6-5	6-6	6-7	6-8	6-9	6-10	6-11	6-13	6-14	6-15	6-16
hterra07L	6-4	7-4	7-5	7-6	7-7	7-8	7-9	7-10	7-11	7-13	7-14	7-15	7-16
hterra08L	6-4	8-4	8-5	8-6	8-9								

Please note, passes 5-12, 6-12, 7-12 of mission 02 in C- and L-band do not exist due to a hardware dropout as explained in Sect. 2.3.1. Slave 12 for flight FL05 is missing. Only 11 passes are in the stack. Note also the interferometric pair 4-2 in Table 4-4 and Table 4-6 put in brackets. It represents a 30m spatial baseline and has been accidentally added and delivered as part of the particular stack. However, the presence of this pass in this interferometric group can be ignored, it does not harm the overall processing quality in any way, see Figure 4-7.

The red frames in Table 4-4 and in Table 4-5 indicate the Hydroterra project. Two C-band Hydroterra simulation products (hi-res and low-res) have been generated per flight.

Flights FL04 and FL08 are merely add-ons. They are additionally packed into the groups (“C1”, “C2”, “L1”, “L2”) in order to allow an individual comparison between passes within their group. They do not serve the Hydroterra product formation.

The master pass of each interferometric group is indicated by a black frame. The master scene determines the image geometry and, hence, the interferogram geometry of each group and is used as master for the computation of coherence and interferometric phase for all slaves.

For the interferometric processing in L-band we have set an additional key-word “be_res=100” in order to have no more than 100 iterations for residual baseline error estimation.

4.2 Processing Results

4.2.1 Radar Geometry Image (RGI) Product Generation

The 22HTERRA campaign data is processed with the DLR Microwaves and Radar Institute, STE department's Processor (STEP) using standard processing parameters. These are summarized in Table 4-8.

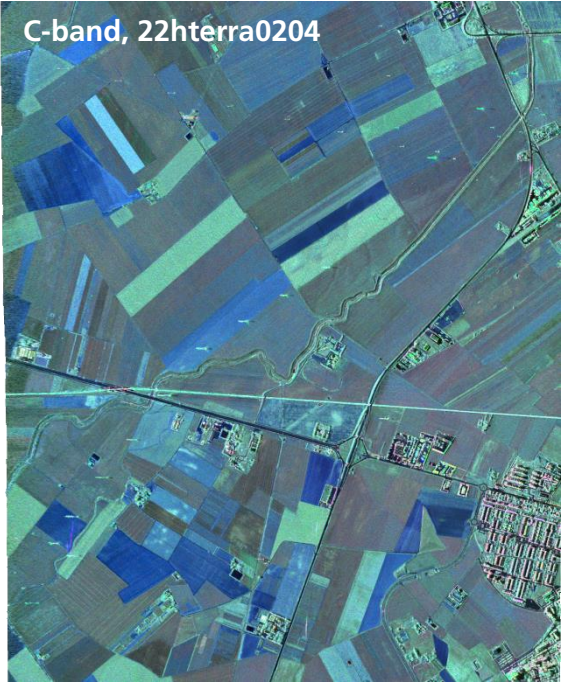
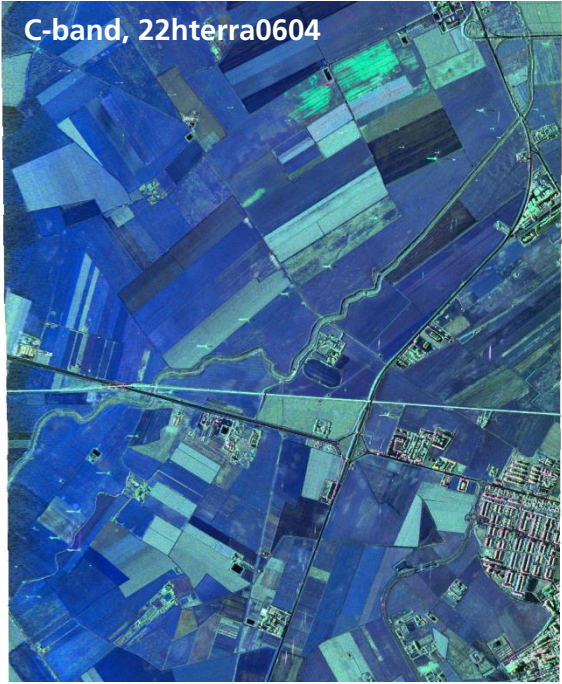


Table 4-8: Processing parameters used for SAR processing.


Processing Parameters	T01	T02
Processor	STEP	STEP
Kernel Type	Extended Omega-K	Extended Omega-K
Software Version	6307	6307
Band	C	L
Centre Frequency [GHz]	5.3	1.325
PRF [Hz]	1811.59	905.79
Chirp Duration (μ s)	10.016	10.016
Range Delay (μ s)	21.728	21.728
Range Sampling [MHz]	500	250
Platform velocity [m/s]	94.8	94.8
Wavelength [cm]	5.65	22.62
Sensor Altitude [m]	3198	3198
Average Terrain Height [m]	100	100
Chirp Bandwidth [MHz]	384	150
Processed Azimuth Bandwidth [Hz]	243	202
Weighting Factor Azimuth	0.54	0.54
Weighting Factor Range	0.54	0.54
Resolution Azimuth [cm]	50	60
Resolution Slant Range [cm]	50	130
Pixel Size Azimuth [cm]	20	40
Pixel Size Slant Range [cm]	30	60

With regard to the pixel sizes in both C- and L-bands we can conclude that any C-band image has about four times the number of pixels as any L-band image. This is, however, not completely true because of the different mean squint angles present in both frequency bands (see Table 4-2 and Table 4-3).

The images in Table 4-9 display a remarkable change in polarimetric scattering from season to season in both C-band (top row) and L-band (bottom row).

Table 4-9: Geocoded C- and L- band master images of flights 2 and 6 (Pauli-decomposition). Colour code: double bounce (red), diffuse (green) and single bounce (blue) scattering.

Mission 01: April 2022	Mission 02: June 2022
<p>C-band, 22hterra0204</p> 	<p>C-band, 22hterra0604</p> 
<p>L-band, 22hterra0204</p> 	<p>L-band, 22hterra0604</p> 

	<p>SARSimHT-NG – Simulation of Hydroterra SAR System Performance in the Mediterranean and the Alps Based on Experimental Airborne SAR Data</p> <p>D2: Data Acquisition Report of SSM Experiment</p>	<p>Doc.: DLR-HR-TR-SARSimHT-NG-02</p> <p>Issue: 1.7 (final)</p> <p>Date: 06.09.2023</p>
---	---	---

4.2.2 Geocoded and Terrain Corrected (GTC) Product Generation

The C- and L-band master products (0204 and 0604) only have been geocoded, because there are only two different image geometries, one for all C-band and one for all L-band images.

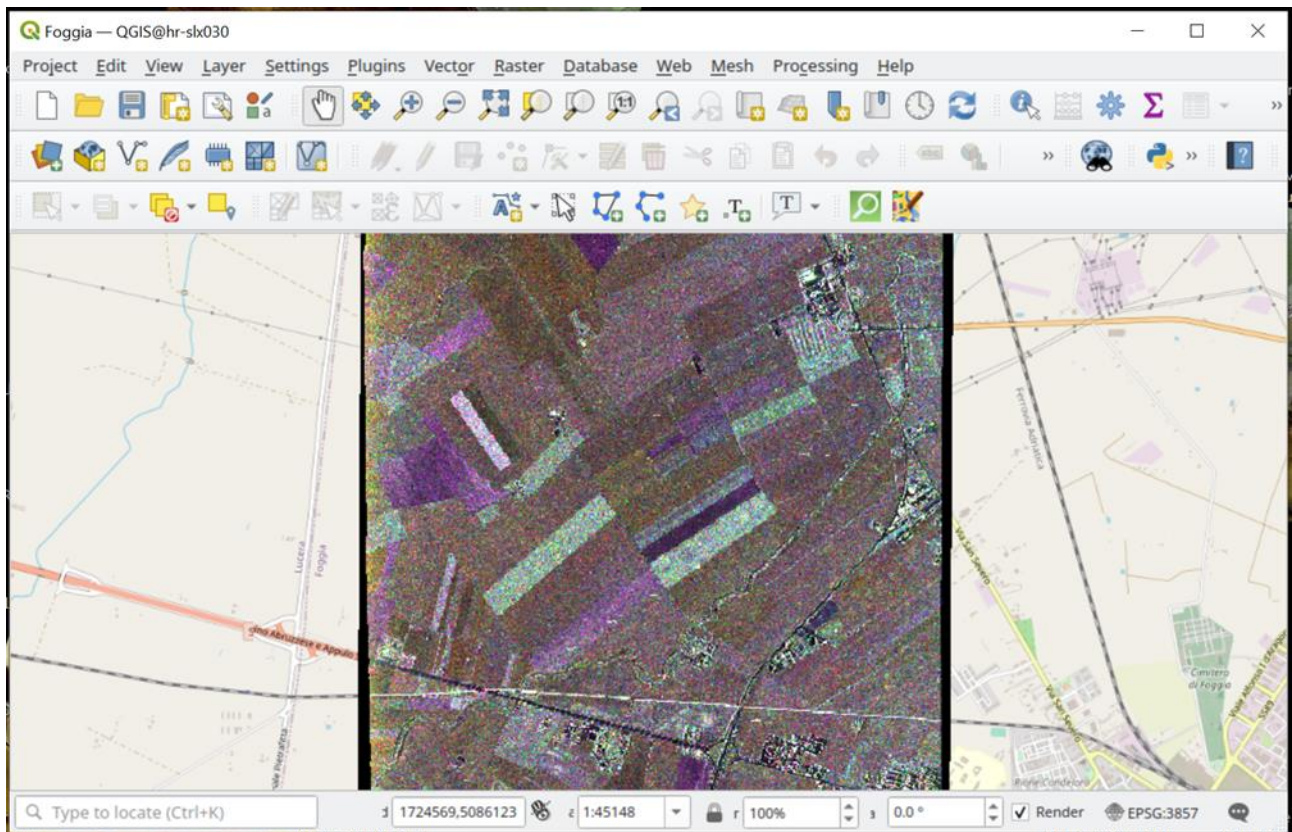


Figure 4-5: The 'ampgeo'-images C-HH (red), C-HV (green) and C-VV (blue) composed as RGB image of master 0204 in QGIS.

All other (slave) image products can be geocoded using the lookup tables which are part of the master image geocoded product (GTC-LUT). In Figure 4-5, we show an example in QGIS. This RGB colour composite is created using the Virtual Raster layer functionality in QGIS by composing 'ampgeo'-images of master scene 0204 in C-band. It can be seen that the geocoding fits well because all roads and the railway line have continuous transitions to the OpenStreetMap layer in the background.

4.2.3 Interferometric Image Product (INF) Product Generation

In contrast to RGI and GTC product generation, which is, firstly, the focusing of radar raw data to images (in slant range geometry, every image is created in its own geometry) and, secondly, their mapping to a geographic coordinate system, the interferometric product generation is necessary in order to compute and compensate residual baseline errors for all slave images to map them to the same geometry as the master pass – which is pass 0204 in mission 01 and pass 0604 in mission 02. This processing step is commonly known as pixel-coregistration.

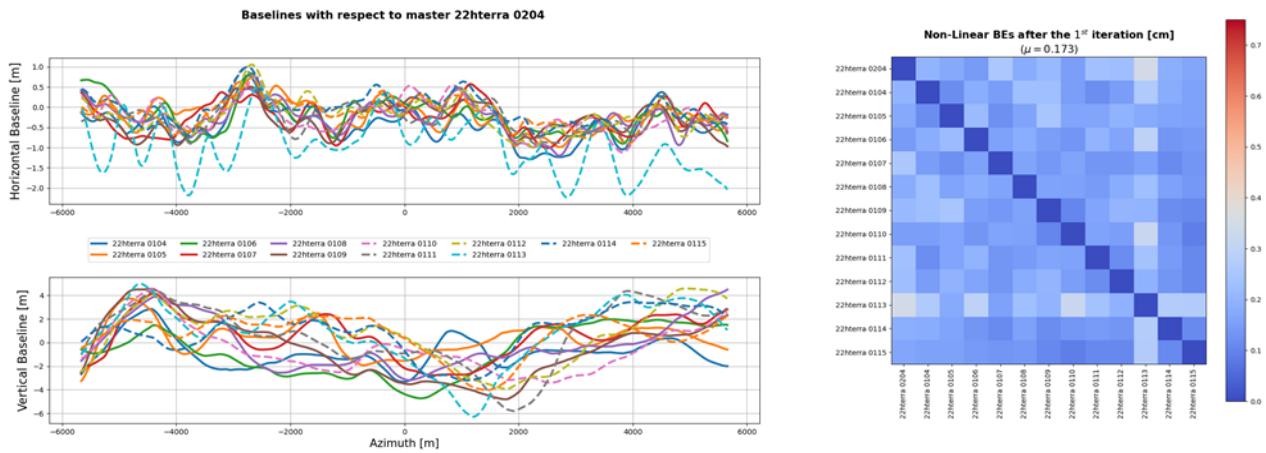


Figure 4-6: Baselines (left) and baseline error convergence (right), master 0204 with 12 slaves of flight 01.

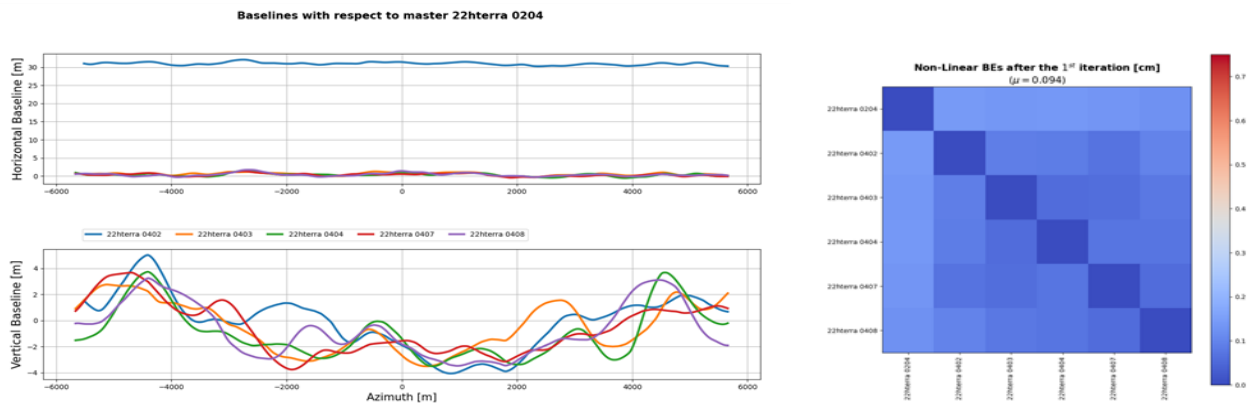


Figure 4-7: Baselines (left) and baseline error convergence (right), master 0204 with 5 slaves of flight 04. A 30m baseline, pass 0402, has been included accidentally.

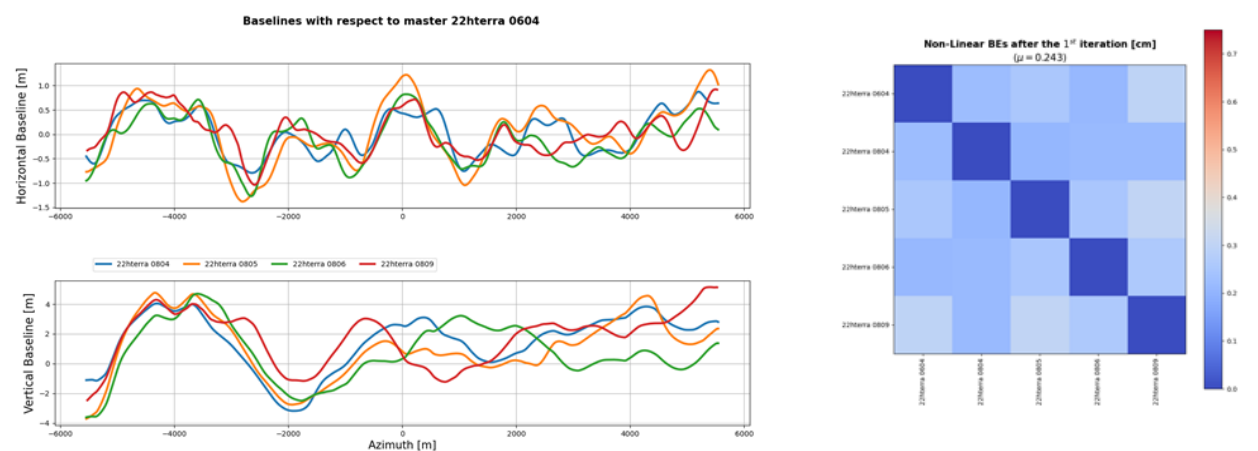


Figure 4-8: Baselines (left) and baseline error convergence (right), master 0204 with 4 slaves of flight 08.

In Figure 4-6, we note that the horizontal baseline of pass 0113 (dashed blue line) deviates a little from the average of all the other passes of FL01. This is reflected by a minor drop in coherency or minor convergence, respectively, indicated by light blue colour in the baseline convergence diagram.

In general, the very small baseline differences between master and slave tracks, as shown above, can be regarded as evidence for excellent flight conditions. These diagrams for FL01, ..., FL08 can be found in the **INF product** (quicklook INF-QL) of the respective delivered master passes (0204 in mission 01 and 0604 in mission 02). The dark blue colour in the matrix diagram on the right indicates excellent convergence of the baseline error estimation process.

As there is no need to convert master passes (0204 and 0604) into master geometry, their **INF product** should be empty. However, we use it as a container to store information about the residual motion error estimation process of the entire image stacks (e.g. baseline error estimation convergences).

As slave images in master geometry only are needed for further data analysis work, we skip delivering their individual RGI products. We deliver the slave images as co-registered products only which we call **INF product**. Images of this type feature slant range geometry. They can be converted into geocoded geometry using the lookup tables in the respective master **GTC product**. See the component GTC-LUT, where LUT stands for Look-Up-Table.

An overview of all baseline error convergences (mission 01 and mission 02 in C- and L-band), only those which are used for satellite product simulations (FL01, FL02, FL03 and FL05, FL06, FL07) are summarized in Figure 4-9. The blue colour indicates excellent baseline error estimation convergence.

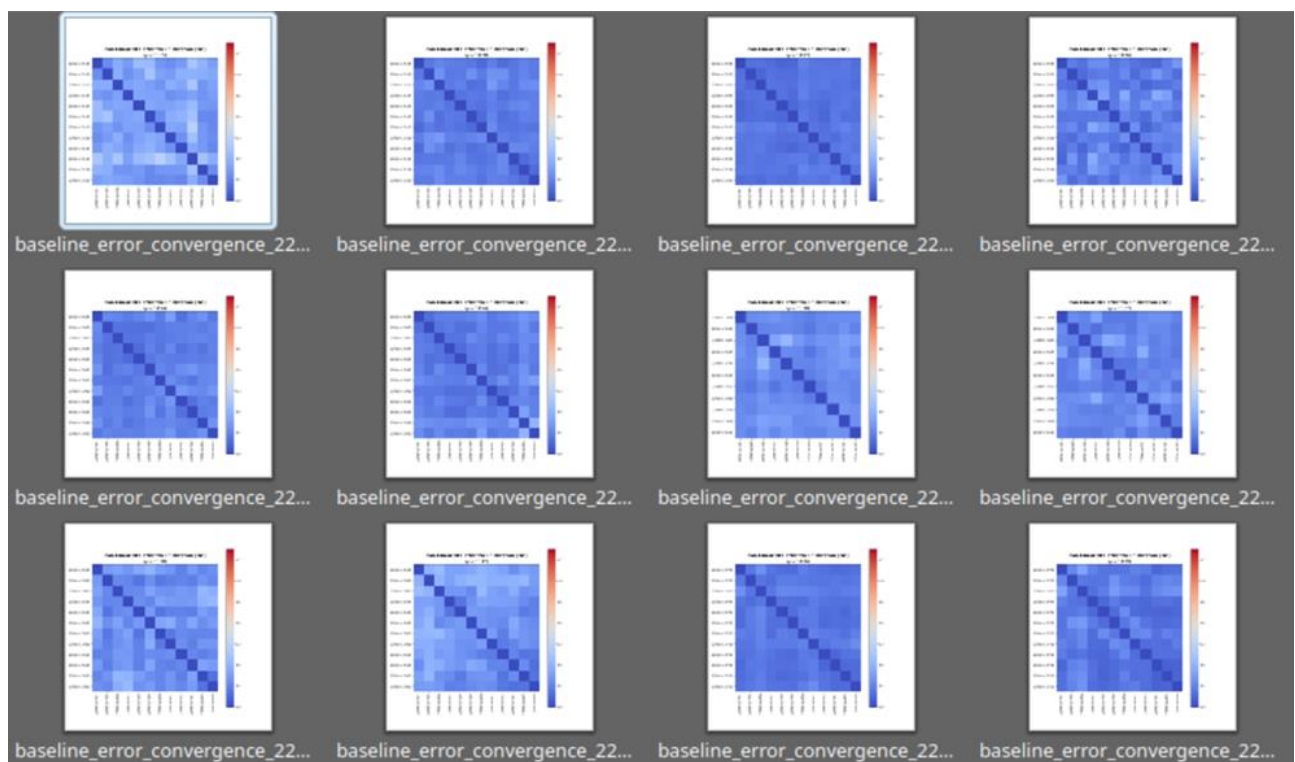


Figure 4-9: Baseline error convergence diagrams for all interferometric groups (FL01-FL03, FL05-FL07 in C- and L-band).


One result of interferometric processing is that all images of the same frequency band obtain the same image dimensions in slant range image geometry. It is indicated in Figure 4-10 and Figure 4-11. The window headers ("38001x9072" and "19105x4536") show slant-range image size after conversion to squared pixel geometry including squint angle distortion. A non-zero squint angle introduces a shift in azimuth direction which increases from near range to far range (black margins).



Figure 4-10: All C-band images are sized 38001 x 9072 pixels.



Figure 4-11: All L-band images are sized 19105 x 4536 pixels.

	SARSimHT-NG – Simulation of Hydroterra SAR System Performance in the Mediterranean and the Alps Based on Experimental Airborne SAR Data D2: Data Acquisition Report of SSM Experiment	Doc.: DLR-HR-TR-SARSimHT-NG-02 Issue: 1.7 (final) Date: 06.09.2023
---	--	--

4.3 Inventory of Delivered Data Products

In this section all RGI, GTC and INF products, delivered on hard disc to CNR-IREA and ESA-ESTEC on January 27, 2023, are listed.

The following rules apply:

- **RGI** products and **GTC** products are delivered for master passes only;
- **INF** products are delivered for slave passes only (in master geometry);
- **Pseudo-INF** products for master passes exist, they merely contain meta data.

4.3.1 Radar Geometry Image (RGI) Products

The following RGI products (master passes) have been delivered.

Table 4-10: RGI products delivered.

No.	Product	Size	Location	Remark
1	RGI	25G	/mnt/esa/22HTERRA/F-SAR/RGI/FL02/PS04/T01/RGI	Mission01-C
2	RGI	6.3G	/mnt/esa/22HTERRA/F-SAR/RGI/FL02/PS04/T02/RGI	Mission01-L
3	RGI	25G	/mnt/esa/22HTERRA/F-SAR/RGI/FL06/PS04/T01/RGI	Mission02-C
4	RGI	6.3G	/mnt/esa/22HTERRA/F-SAR/RGI/FL06/PS04/T02/RGI	Mission02-L

4.3.2 Geocoded and Terrain Corrected (GTC) Products

The following GTC products have been delivered.

Table 4-11: GTC products delivered.

No.	Product	Size	Location	Remark
1	GTC	5.2G	/mnt/esa/22HTERRA/F-SAR/GTC/FL02/PS04/T01/GTC	Mission01-C
2	GTC	3.4G	/mnt/esa/22HTERRA/F-SAR/GTC/FL02/PS04/T02/GTC	Mission01-L
3	GTC	3.4G	/mnt/esa/22HTERRA/F-SAR/GTC/FL06/PS04/T01/GTC	Mission02-C
4	GTC	3.4G	/mnt/esa/22HTERRA/F-SAR/GTC/FL06/PS04/T02/GTC	Mission02-L

GTC products of master passes include a GTC-LUT component. Look-Up-Tables (LUT) may be used to convert slave passes into geocoded geometry or, vice versa, to convert geocoded ground truth data into slant range geometry.

4.3.3 Interferometric (INF) Products

The following INF products have been delivered (Table 4-12). These products are listed within their interferometric group (indicated in red frames) called "hterra01C", ..., "hterra08C" and "hterra01L", ..., "hterra08L", respectively. The master in each group is merely containing information about the INF processing in each group, it is not a proper INF product.

Please note, the inclusion of pass 0402 in group "hterra04C" is a data compilation error. The data product is available on disk, and may be used with some caution.


	SARSimHT-NG – Simulation of Hydroterra SAR System Performance in the Mediterranean and the Alps Based on Experimental Airborne SAR Data D2: Data Acquisition Report of SSM Experiment	Doc.: DLR-HR-TR-SARSimHT-NG-02 Issue: 1.7 (final) Date: 06.09.2023
---	--	--

Table 4-12: INF products delivered.

No.	Product	Size	Location	Remark
1	INF	326M	/mnt/esa/22HTERRA/F-SAR/INF/C-BAND/FL02/PS04/T01/INF_hterra01C	master
2	INF	41G	/mnt/esa/22HTERRA/F-SAR/INF/C-BAND/FL01/PS04/T01/INF_hterra01C	
3	INF	41G	/mnt/esa/22HTERRA/F-SAR/INF/C-BAND/FL01/PS05/T01/INF_hterra01C	
4	INF	41G	/mnt/esa/22HTERRA/F-SAR/INF/C-BAND/FL01/PS06/T01/INF_hterra01C	
5	INF	41G	/mnt/esa/22HTERRA/F-SAR/INF/C-BAND/FL01/PS07/T01/INF_hterra01C	
6	INF	41G	/mnt/esa/22HTERRA/F-SAR/INF/C-BAND/FL01/PS08/T01/INF_hterra01C	
7	INF	41G	/mnt/esa/22HTERRA/F-SAR/INF/C-BAND/FL01/PS09/T01/INF_hterra01C	
8	INF	41G	/mnt/esa/22HTERRA/F-SAR/INF/C-BAND/FL01/PS10/T01/INF_hterra01C	
9	INF	41G	/mnt/esa/22HTERRA/F-SAR/INF/C-BAND/FL01/PS11/T01/INF_hterra01C	
10	INF	41G	/mnt/esa/22HTERRA/F-SAR/INF/C-BAND/FL01/PS12/T01/INF_hterra01C	
11	INF	41G	/mnt/esa/22HTERRA/F-SAR/INF/C-BAND/FL01/PS13/T01/INF_hterra01C	
12	INF	41G	/mnt/esa/22HTERRA/F-SAR/INF/C-BAND/FL01/PS14/T01/INF_hterra01C	
13	INF	41G	/mnt/esa/22HTERRA/F-SAR/INF/C-BAND/FL01/PS15/T01/INF_hterra01C	
14	INF	326M	/mnt/esa/22HTERRA/F-SAR/INF/C-BAND/FL02/PS04/T01/INF_hterra02C	master
15	INF	41G	/mnt/esa/22HTERRA/F-SAR/INF/C-BAND/FL02/PS05/T01/INF_hterra02C	
16	INF	41G	/mnt/esa/22HTERRA/F-SAR/INF/C-BAND/FL02/PS06/T01/INF_hterra02C	
17	INF	41G	/mnt/esa/22HTERRA/F-SAR/INF/C-BAND/FL02/PS07/T01/INF_hterra02C	
18	INF	41G	/mnt/esa/22HTERRA/F-SAR/INF/C-BAND/FL02/PS08/T01/INF_hterra02C	
19	INF	41G	/mnt/esa/22HTERRA/F-SAR/INF/C-BAND/FL02/PS09/T01/INF_hterra02C	
20	INF	41G	/mnt/esa/22HTERRA/F-SAR/INF/C-BAND/FL02/PS10/T01/INF_hterra02C	
21	INF	41G	/mnt/esa/22HTERRA/F-SAR/INF/C-BAND/FL02/PS11/T01/INF_hterra02C	
22	INF	41G	/mnt/esa/22HTERRA/F-SAR/INF/C-BAND/FL02/PS12/T01/INF_hterra02C	
23	INF	41G	/mnt/esa/22HTERRA/F-SAR/INF/C-BAND/FL02/PS13/T01/INF_hterra02C	
24	INF	41G	/mnt/esa/22HTERRA/F-SAR/INF/C-BAND/FL02/PS14/T01/INF_hterra02C	
25	INF	41G	/mnt/esa/22HTERRA/F-SAR/INF/C-BAND/FL02/PS15/T01/INF_hterra02C	
26	INF	326M	/mnt/esa/22HTERRA/F-SAR/INF/C-BAND/FL02/PS04/T01/INF_hterra03C	master
27	INF	41G	/mnt/esa/22HTERRA/F-SAR/INF/C-BAND/FL03/PS04/T01/INF_hterra03C	
28	INF	41G	/mnt/esa/22HTERRA/F-SAR/INF/C-BAND/FL03/PS05/T01/INF_hterra03C	
29	INF	41G	/mnt/esa/22HTERRA/F-SAR/INF/C-BAND/FL03/PS06/T01/INF_hterra03C	
30	INF	41G	/mnt/esa/22HTERRA/F-SAR/INF/C-BAND/FL03/PS07/T01/INF_hterra03C	
31	INF	41G	/mnt/esa/22HTERRA/F-SAR/INF/C-BAND/FL03/PS08/T01/INF_hterra03C	
32	INF	41G	/mnt/esa/22HTERRA/F-SAR/INF/C-BAND/FL03/PS09/T01/INF_hterra03C	
33	INF	41G	/mnt/esa/22HTERRA/F-SAR/INF/C-BAND/FL03/PS10/T01/INF_hterra03C	
34	INF	41G	/mnt/esa/22HTERRA/F-SAR/INF/C-BAND/FL03/PS11/T01/INF_hterra03C	
35	INF	41G	/mnt/esa/22HTERRA/F-SAR/INF/C-BAND/FL03/PS12/T01/INF_hterra03C	
36	INF	41G	/mnt/esa/22HTERRA/F-SAR/INF/C-BAND/FL03/PS13/T01/INF_hterra03C	
37	INF	41G	/mnt/esa/22HTERRA/F-SAR/INF/C-BAND/FL03/PS14/T01/INF_hterra03C	
38	INF	41G	/mnt/esa/22HTERRA/F-SAR/INF/C-BAND/FL03/PS15/T01/INF_hterra03C	
39	INF	324M	/mnt/esa/22HTERRA/F-SAR/INF/C-BAND/FL02/PS04/T01/INF_hterra04C	master



40	INF	41G	/mnt/esa/22HTERRA/F-SAR/INF/C-BAND/FL04/PS02/T01/INF_hterra04C	(error)
41	INF	41G	/mnt/esa/22HTERRA/F-SAR/INF/C-BAND/FL04/PS03/T01/INF_hterra04C	
42	INF	41G	/mnt/esa/22HTERRA/F-SAR/INF/C-BAND/FL04/PS04/T01/INF_hterra04C	
43	INF	41G	/mnt/esa/22HTERRA/F-SAR/INF/C-BAND/FL04/PS07/T01/INF_hterra04C	
44	INF	41G	/mnt/esa/22HTERRA/F-SAR/INF/C-BAND/FL04/PS08/T01/INF_hterra04C	

No.	Product	Size	Location	Remark
1	INF	324M	/mnt/esa/22HTERRA/F-SAR/INF/C-BAND/FL06/PS04/T01/INF_hterra05C	master
2	INF	41G	/mnt/esa/22HTERRA/F-SAR/INF/C-BAND/FL05/PS04/T01/INF_hterra05C	
3	INF	41G	/mnt/esa/22HTERRA/F-SAR/INF/C-BAND/FL05/PS05/T01/INF_hterra05C	
4	INF	41G	/mnt/esa/22HTERRA/F-SAR/INF/C-BAND/FL05/PS06/T01/INF_hterra05C	
5	INF	41G	/mnt/esa/22HTERRA/F-SAR/INF/C-BAND/FL05/PS07/T01/INF_hterra05C	
6	INF	41G	/mnt/esa/22HTERRA/F-SAR/INF/C-BAND/FL05/PS08/T01/INF_hterra05C	
7	INF	41G	/mnt/esa/22HTERRA/F-SAR/INF/C-BAND/FL05/PS09/T01/INF_hterra05C	
8	INF	41G	/mnt/esa/22HTERRA/F-SAR/INF/C-BAND/FL05/PS10/T01/INF_hterra05C	
9	INF	41G	/mnt/esa/22HTERRA/F-SAR/INF/C-BAND/FL05/PS11/T01/INF_hterra05C	
10	INF	41G	/mnt/esa/22HTERRA/F-SAR/INF/C-BAND/FL05/PS13/T01/INF_hterra05C	
11	INF	41G	/mnt/esa/22HTERRA/F-SAR/INF/C-BAND/FL05/PS14/T01/INF_hterra05C	
12	INF	41G	/mnt/esa/22HTERRA/F-SAR/INF/C-BAND/FL05/PS15/T01/INF_hterra05C	
13	INF	323M	/mnt/esa/22HTERRA/F-SAR/INF/C-BAND/FL06/PS04/T01/INF_hterra06C	master
14	INF	41G	/mnt/esa/22HTERRA/F-SAR/INF/C-BAND/FL06/PS05/T01/INF_hterra06C	
15	INF	41G	/mnt/esa/22HTERRA/F-SAR/INF/C-BAND/FL06/PS06/T01/INF_hterra06C	
16	INF	41G	/mnt/esa/22HTERRA/F-SAR/INF/C-BAND/FL06/PS07/T01/INF_hterra06C	
17	INF	41G	/mnt/esa/22HTERRA/F-SAR/INF/C-BAND/FL06/PS08/T01/INF_hterra06C	
18	INF	41G	/mnt/esa/22HTERRA/F-SAR/INF/C-BAND/FL06/PS09/T01/INF_hterra06C	
19	INF	41G	/mnt/esa/22HTERRA/F-SAR/INF/C-BAND/FL06/PS10/T01/INF_hterra06C	
20	INF	41G	/mnt/esa/22HTERRA/F-SAR/INF/C-BAND/FL06/PS11/T01/INF_hterra06C	
21	INF	41G	/mnt/esa/22HTERRA/F-SAR/INF/C-BAND/FL06/PS13/T01/INF_hterra06C	
22	INF	41G	/mnt/esa/22HTERRA/F-SAR/INF/C-BAND/FL06/PS14/T01/INF_hterra06C	
23	INF	41G	/mnt/esa/22HTERRA/F-SAR/INF/C-BAND/FL06/PS15/T01/INF_hterra06C	
24	INF	41G	/mnt/esa/22HTERRA/F-SAR/INF/C-BAND/FL06/PS16/T01/INF_hterra06C	
25	INF	323M	/mnt/esa/22HTERRA/F-SAR/INF/C-BAND/FL06/PS04/T01/INF_hterra07C	master
26	INF	41G	/mnt/esa/22HTERRA/F-SAR/INF/C-BAND/FL07/PS04/T01/INF_hterra07C	
27	INF	41G	/mnt/esa/22HTERRA/F-SAR/INF/C-BAND/FL07/PS05/T01/INF_hterra07C	
28	INF	41G	/mnt/esa/22HTERRA/F-SAR/INF/C-BAND/FL07/PS06/T01/INF_hterra07C	
29	INF	41G	/mnt/esa/22HTERRA/F-SAR/INF/C-BAND/FL07/PS07/T01/INF_hterra07C	
30	INF	41G	/mnt/esa/22HTERRA/F-SAR/INF/C-BAND/FL07/PS08/T01/INF_hterra07C	
31	INF	41G	/mnt/esa/22HTERRA/F-SAR/INF/C-BAND/FL07/PS09/T01/INF_hterra07C	
32	INF	41G	/mnt/esa/22HTERRA/F-SAR/INF/C-BAND/FL07/PS10/T01/INF_hterra07C	
33	INF	41G	/mnt/esa/22HTERRA/F-SAR/INF/C-BAND/FL07/PS11/T01/INF_hterra07C	
34	INF	41G	/mnt/esa/22HTERRA/F-SAR/INF/C-BAND/FL07/PS13/T01/INF_hterra07C	



35	INF	41G	/mnt/esa/22HTERRA/F-SAR/INF/C-BAND/FL07/PS14/T01/INF_hterra07C	
36	INF	41G	/mnt/esa/22HTERRA/F-SAR/INF/C-BAND/FL07/PS15/T01/INF_hterra07C	
37	INF	41G	/mnt/esa/22HTERRA/F-SAR/INF/C-BAND/FL07/PS16/T01/INF_hterra07C	
38	INF	323M	/mnt/esa/22HTERRA/F-SAR/INF/C-BAND/FL06/PS04/T01/INF_hterra08C	master
39	INF	41G	/mnt/esa/22HTERRA/F-SAR/INF/C-BAND/FL08/PS04/T01/INF_hterra08C	
40	INF	41G	/mnt/esa/22HTERRA/F-SAR/INF/C-BAND/FL08/PS05/T01/INF_hterra08C	
41	INF	41G	/mnt/esa/22HTERRA/F-SAR/INF/C-BAND/FL08/PS06/T01/INF_hterra08C	
42	INF	41G	/mnt/esa/22HTERRA/F-SAR/INF/C-BAND/FL08/PS09/T01/INF_hterra08C	

No.	Product	Size	Location	Remark
1	INF	158M	/mnt/esa/22HTERRA/F-SAR/INF/L-BAND/FL02/PS04/T02/INF_hterra01L	master
2	INF	11G	/mnt/esa/22HTERRA/F-SAR/INF/L-BAND/FL01/PS04/T02/INF_hterra01L	
3	INF	21G	/mnt/esa/22HTERRA/F-SAR/INF/L-BAND/FL01/PS05/T02/INF_hterra01L	
4	INF	21G	/mnt/esa/22HTERRA/F-SAR/INF/L-BAND/FL01/PS06/T02/INF_hterra01L	
5	INF	21G	/mnt/esa/22HTERRA/F-SAR/INF/L-BAND/FL01/PS07/T02/INF_hterra01L	
6	INF	21G	/mnt/esa/22HTERRA/F-SAR/INF/L-BAND/FL01/PS08/T02/INF_hterra01L	
7	INF	21G	/mnt/esa/22HTERRA/F-SAR/INF/L-BAND/FL01/PS09/T02/INF_hterra01L	
8	INF	21G	/mnt/esa/22HTERRA/F-SAR/INF/L-BAND/FL01/PS10/T02/INF_hterra01L	
9	INF	21G	/mnt/esa/22HTERRA/F-SAR/INF/L-BAND/FL01/PS11/T02/INF_hterra01L	
10	INF	21G	/mnt/esa/22HTERRA/F-SAR/INF/L-BAND/FL01/PS12/T02/INF_hterra01L	
11	INF	21G	/mnt/esa/22HTERRA/F-SAR/INF/L-BAND/FL01/PS13/T02/INF_hterra01L	
12	INF	21G	/mnt/esa/22HTERRA/F-SAR/INF/L-BAND/FL01/PS14/T02/INF_hterra01L	
13	INF	21G	/mnt/esa/22HTERRA/F-SAR/INF/L-BAND/FL01/PS15/T02/INF_hterra01L	
14	INF	157M	/mnt/esa/22HTERRA/F-SAR/INF/L-BAND/FL02/PS04/T02/INF_hterra02L	master
15	INF	11G	/mnt/esa/22HTERRA/F-SAR/INF/L-BAND/FL02/PS05/T02/INF_hterra02L	
16	INF	11G	/mnt/esa/22HTERRA/F-SAR/INF/L-BAND/FL02/PS06/T02/INF_hterra02L	
17	INF	11G	/mnt/esa/22HTERRA/F-SAR/INF/L-BAND/FL02/PS07/T02/INF_hterra02L	
18	INF	11G	/mnt/esa/22HTERRA/F-SAR/INF/L-BAND/FL02/PS08/T02/INF_hterra02L	
19	INF	11G	/mnt/esa/22HTERRA/F-SAR/INF/L-BAND/FL02/PS09/T02/INF_hterra02L	
20	INF	11G	/mnt/esa/22HTERRA/F-SAR/INF/L-BAND/FL02/PS10/T02/INF_hterra02L	
21	INF	11G	/mnt/esa/22HTERRA/F-SAR/INF/L-BAND/FL02/PS11/T02/INF_hterra02L	
22	INF	11G	/mnt/esa/22HTERRA/F-SAR/INF/L-BAND/FL02/PS12/T02/INF_hterra02L	
23	INF	11G	/mnt/esa/22HTERRA/F-SAR/INF/L-BAND/FL02/PS13/T02/INF_hterra02L	
24	INF	11G	/mnt/esa/22HTERRA/F-SAR/INF/L-BAND/FL02/PS14/T02/INF_hterra02L	
25	INF	11G	/mnt/esa/22HTERRA/F-SAR/INF/L-BAND/FL02/PS15/T02/INF_hterra02L	
26	INF	157M	/mnt/esa/22HTERRA/F-SAR/INF/L-BAND/FL02/PS04/T02/INF_hterra03L	master
27	INF	11G	/mnt/esa/22HTERRA/F-SAR/INF/L-BAND/FL03/PS04/T02/INF_hterra03L	
28	INF	21G	/mnt/esa/22HTERRA/F-SAR/INF/L-BAND/FL03/PS05/T02/INF_hterra03L	
29	INF	21G	/mnt/esa/22HTERRA/F-SAR/INF/L-BAND/FL03/PS06/T02/INF_hterra03L	
30	INF	21G	/mnt/esa/22HTERRA/F-SAR/INF/L-BAND/FL03/PS07/T02/INF_hterra03L	
31	INF	21G	/mnt/esa/22HTERRA/F-SAR/INF/L-BAND/FL03/PS08/T02/INF_hterra03L	



32	INF	21G	/mnt/esa/22HTERRA/F-SAR/INF/L-BAND/FL03/PS09/T02/INF_hterra03L	
33	INF	21G	/mnt/esa/22HTERRA/F-SAR/INF/L-BAND/FL03/PS10/T02/INF_hterra03L	
34	INF	21G	/mnt/esa/22HTERRA/F-SAR/INF/L-BAND/FL03/PS11/T02/INF_hterra03L	
35	INF	21G	/mnt/esa/22HTERRA/F-SAR/INF/L-BAND/FL03/PS12/T02/INF_hterra03L	
36	INF	21G	/mnt/esa/22HTERRA/F-SAR/INF/L-BAND/FL03/PS13/T02/INF_hterra03L	
37	INF	21G	/mnt/esa/22HTERRA/F-SAR/INF/L-BAND/FL03/PS14/T02/INF_hterra03L	
38	INF	21G	/mnt/esa/22HTERRA/F-SAR/INF/L-BAND/FL03/PS15/T02/INF_hterra03L	
39	INF	157M	/mnt/esa/22HTERRA/F-SAR/INF/L-BAND/FL02/PS04/T02/INF_hterra04L	master
40	INF	11G	/mnt/esa/22HTERRA/F-SAR/INF/L-BAND/FL04/PS02/T02/INF_hterra04L	(error)
41	INF	21G	/mnt/esa/22HTERRA/F-SAR/INF/L-BAND/FL04/PS03/T02/INF_hterra04L	
42	INF	11G	/mnt/esa/22HTERRA/F-SAR/INF/L-BAND/FL04/PS04/T02/INF_hterra04L	
43	INF	21G	/mnt/esa/22HTERRA/F-SAR/INF/L-BAND/FL04/PS07/T02/INF_hterra04L	
44	INF	21G	/mnt/esa/22HTERRA/F-SAR/INF/L-BAND/FL04/PS08/T02/INF_hterra04L	

No.	Product	Size	Location	Remark
1	INF	157M	/mnt/esa/22HTERRA/F-SAR/INF/L-BAND/FL06/PS04/T02/INF_hterra05L	master
2	INF	11G	/mnt/esa/22HTERRA/F-SAR/INF/L-BAND/FL05/PS04/T02/INF_hterra05L	
3	INF	21G	/mnt/esa/22HTERRA/F-SAR/INF/L-BAND/FL05/PS05/T02/INF_hterra05L	
4	INF	21G	/mnt/esa/22HTERRA/F-SAR/INF/L-BAND/FL05/PS06/T02/INF_hterra05L	
5	INF	21G	/mnt/esa/22HTERRA/F-SAR/INF/L-BAND/FL05/PS07/T02/INF_hterra05L	
6	INF	21G	/mnt/esa/22HTERRA/F-SAR/INF/L-BAND/FL05/PS08/T02/INF_hterra05L	
7	INF	21G	/mnt/esa/22HTERRA/F-SAR/INF/L-BAND/FL05/PS09/T02/INF_hterra05L	
8	INF	21G	/mnt/esa/22HTERRA/F-SAR/INF/L-BAND/FL05/PS10/T02/INF_hterra05L	
9	INF	21G	/mnt/esa/22HTERRA/F-SAR/INF/L-BAND/FL05/PS11/T02/INF_hterra05L	
10	INF	21G	/mnt/esa/22HTERRA/F-SAR/INF/L-BAND/FL05/PS13/T02/INF_hterra05L	
11	INF	21G	/mnt/esa/22HTERRA/F-SAR/INF/L-BAND/FL05/PS14/T02/INF_hterra05L	
12	INF	21G	/mnt/esa/22HTERRA/F-SAR/INF/L-BAND/FL05/PS15/T02/INF_hterra05L	
13	INF	157M	/mnt/esa/22HTERRA/F-SAR/INF/L-BAND/FL06/PS04/T02/INF_hterra06L	master
14	INF	11G	/mnt/esa/22HTERRA/F-SAR/INF/L-BAND/FL06/PS05/T02/INF_hterra06L	
15	INF	11G	/mnt/esa/22HTERRA/F-SAR/INF/L-BAND/FL06/PS06/T02/INF_hterra06L	
16	INF	11G	/mnt/esa/22HTERRA/F-SAR/INF/L-BAND/FL06/PS07/T02/INF_hterra06L	
17	INF	11G	/mnt/esa/22HTERRA/F-SAR/INF/L-BAND/FL06/PS08/T02/INF_hterra06L	
18	INF	11G	/mnt/esa/22HTERRA/F-SAR/INF/L-BAND/FL06/PS09/T02/INF_hterra06L	
19	INF	11G	/mnt/esa/22HTERRA/F-SAR/INF/L-BAND/FL06/PS10/T02/INF_hterra06L	
20	INF	11G	/mnt/esa/22HTERRA/F-SAR/INF/L-BAND/FL06/PS11/T02/INF_hterra06L	
21	INF	11G	/mnt/esa/22HTERRA/F-SAR/INF/L-BAND/FL06/PS13/T02/INF_hterra06L	
22	INF	11G	/mnt/esa/22HTERRA/F-SAR/INF/L-BAND/FL06/PS14/T02/INF_hterra06L	
23	INF	11G	/mnt/esa/22HTERRA/F-SAR/INF/L-BAND/FL06/PS15/T02/INF_hterra06L	
24	INF	11G	/mnt/esa/22HTERRA/F-SAR/INF/L-BAND/FL06/PS16/T02/INF_hterra06L	
25	INF	156M	/mnt/esa/22HTERRA/F-SAR/INF/L-BAND/FL06/PS04/T02/INF_hterra07L	master
26	INF	11G	/mnt/esa/22HTERRA/F-SAR/INF/L-BAND/FL07/PS04/T02/INF_hterra07L	

27	INF	21G	/mnt/esa/22HTERRA/F-SAR/INF/L-BAND/FL07/PS05/T02/INF_hterra07L	
28	INF	21G	/mnt/esa/22HTERRA/F-SAR/INF/L-BAND/FL07/PS06/T02/INF_hterra07L	
29	INF	21G	/mnt/esa/22HTERRA/F-SAR/INF/L-BAND/FL07/PS07/T02/INF_hterra07L	
30	INF	21G	/mnt/esa/22HTERRA/F-SAR/INF/L-BAND/FL07/PS08/T02/INF_hterra07L	
31	INF	21G	/mnt/esa/22HTERRA/F-SAR/INF/L-BAND/FL07/PS09/T02/INF_hterra07L	
32	INF	21G	/mnt/esa/22HTERRA/F-SAR/INF/L-BAND/FL07/PS10/T02/INF_hterra07L	
33	INF	21G	/mnt/esa/22HTERRA/F-SAR/INF/L-BAND/FL07/PS11/T02/INF_hterra07L	
34	INF	21G	/mnt/esa/22HTERRA/F-SAR/INF/L-BAND/FL07/PS13/T02/INF_hterra07L	
35	INF	21G	/mnt/esa/22HTERRA/F-SAR/INF/L-BAND/FL07/PS14/T02/INF_hterra07L	
36	INF	21G	/mnt/esa/22HTERRA/F-SAR/INF/L-BAND/FL07/PS15/T02/INF_hterra07L	
37	INF	21G	/mnt/esa/22HTERRA/F-SAR/INF/L-BAND/FL07/PS16/T02/INF_hterra07L	
38	INF	156M	/mnt/esa/22HTERRA/F-SAR/INF/L-BAND/FL06/PS04/T02/INF_hterra08L	master
39	INF	11G	/mnt/esa/22HTERRA/F-SAR/INF/L-BAND/FL08/PS04/T02/INF_hterra08L	
40	INF	21G	/mnt/esa/22HTERRA/F-SAR/INF/L-BAND/FL08/PS05/T02/INF_hterra08L	
41	INF	21G	/mnt/esa/22HTERRA/F-SAR/INF/L-BAND/FL08/PS06/T02/INF_hterra08L	
42	INF	21G	/mnt/esa/22HTERRA/F-SAR/INF/L-BAND/FL08/PS09/T02/INF_hterra08L	

4.3.4 Summary of RGI, GTC and INF products delivered


In total, 180 standard F-SAR products (4.5 TB) have been delivered, listed in Table 4-13 and Table 4-14.

Table 4-13: Summary of delivered F-SAR data products – Mission 01.

F-SAR	Mission 01							total
Type	Master	Master	Master	Slave	Slave	Slave	Slave	Type
Product	RGI	GTC	INF					Product
Name	0204	0204	0204	FL01	FL02	FL03	FL04	Name
C-band	1	1	4	12	11	12	5	46
L-band	1	1	4	12	11	12	5	46
total	2	2	8	24	22	24	10	92

Table 4-14: Summary of delivered F-SAR data products – Mission 02.

F-SAR	Mission 02							total
Type	Master	Master	Master	Slave	Slave	Slave	Slave	Type
Product	RGI	GTC	INF					Product
Name	0604	0604	0604	FL05	FL06	FL07	FL08	Name
C-band	1	1	4	11	11	12	4	44
L-band	1	1	4	11	11	12	4	44
total	2	2	8	22	22	24	8	88

	<p>SARSimHT-NG – Simulation of Hydroterra SAR System Performance in the Mediterranean and the Alps Based on Experimental Airborne SAR Data</p> <p>D2: Data Acquisition Report of SSM Experiment</p>	<p>Doc.: DLR-HR-TR-SARSimHT-NG-02</p> <p>Issue: 1.7 (final)</p> <p>Date: 06.09.2023</p>
---	---	---

5 Simulation of Hydroterra Products

5.1 Overview

As part of 'WP240 – Hydroterra Product Simulation and Analysis – SSM Experiment', DLR has simulated Hydroterra products in C-band. Two kinds of simulation products have been generated:

1. Simulated Geosynchronous SAR products (GEO) with F-SAR resolution and interferograms, and
2. Simulated Hydroterra SAR products (HT) and interferograms.

The nominal zero-baseline passes out of the first three flights of each mission (FL01, ..., FL03 and FL05, ..., FL07) were used as input and six products were generated for each category.

To investigate primarily the impact of the long integration time of geosynchronous SAR on SSM retrieval, products with the resolution and NESZ of the F-SAR system have been simulated. With such high resolution it is easier to discriminate between different effects and compare geosynchronous SAR products to the ones of LEO SAR.

Hydroterra simulation products have been generated using the parameter settings listed in Table 5-5. Reference: Scenario 4 of the interferometric type (Glacier flow / Landslides) [7]. The goal of these products is to perform an assessment of the potential to retrieve SSM from realistic Hydroterra data.

In Section 5.2 the simulation procedure of geosynchronous SAR and Hydroterra products is described. This procedure was used to simulate the products which are then presented in Section 5.3. In Section 5.4 the simulation product data formats and data set structures are explained. Section 5.5 lists the products which have been delivered.

5.2 Simulation Procedure

The simulation procedure to generate Hydroterra image products is visualized in Figure 5-1. Each image of an image stack is filtered to the desired resolution in azimuth and slant range and normalized in terms of energy [4], [9]. As described above, all images are co-registered to the master geometry, i.e. all images have the same number of pixels in azimuth and range direction. Pixels with the same coordinate correspond to one another in the direction of depth in an image stack.

In our image stacks, we consider the first image as master and the following as slaves. The coregistration step can be skipped as the input INF products are already co-registered.

In the next step, an interferometric calibration is performed in order to coherently align the images in a proper way. This is performed for each slave image by subtracting the interferometric phase between this image and the master. After the phase calibration, each image is Fourier transformed to the azimuth frequency domain, where a different bandpass filter is applied to each image. This bandpass filter is needed to simulate the long integration time of the sensor in a geosynchronous orbit.

The bandwidth and centre frequency of each bandpass filter is calculated to ensure the desired final resolution of the Hydroterra product. An overlap of 50% between adjacent bands is performed by using a weighting function. An overlap is needed to eliminate phase jumps in the final product, which otherwise would degrade the final simulated Hydroterra product, something which is not occurring in a real Hydroterra product. Phase jumps occur because spectra from different images are combined; implying different phase offsets at the edges between the spectra. A weighting function ensures a smooth transition between bands. After bandpass filtering, all images are coherently combined in the azimuth frequency domain. Finally, an inverse Fourier transform in the azimuth domain is performed and the noise equivalent sigma zero (NESZ) of the product is adjusted to the one of a Hydroterra product, as described in [4]. The result of this simulation is a simulated Hydroterra single-look complex (SLC) product. The simulation procedure is described in more detail in [5], [9], [10].

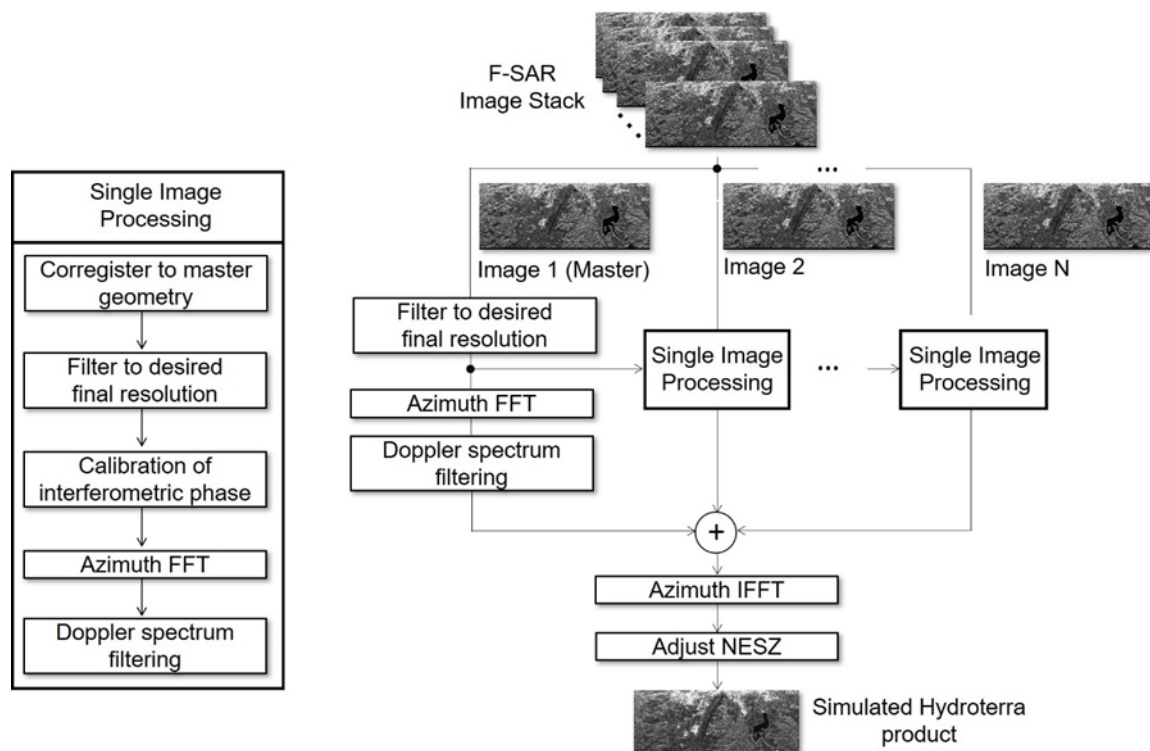


Figure 5-1: Simulation procedure to generate a simulated Hydroterra SLC product.

5.3 Simulation Results

5.3.1 Integration Times

The integration times in azimuth are the same for both kinds of simulation products, the geosynchronous SAR (GEO) and Hydroterra (HT). They are listed in Table 5-1 and Table 5-2 for the two missions.

Table 5-1: Integration Times for GEO and HT Products of Mission 01 (April).

Mission 01	GEO Product	HT Product	Start Time	Stop Time	Integration Time
hterra01C	GEO_FL01	HT_FL01	2022-04-28T07:42:56.65	2022-04-28T09:41:59.45	119.05 min
hterra02C	GEO_FL02	HT_FL02	2022-04-28T12:46:12.25	2022-04-28T14:39:53.58	113.70 min
hterra03C	GEO_FL03	HT_FL03	2022-04-29T07:50:07.25	2022-04-29T09:45:15.57	115.15 min

Table 5-2: Integration Times for GEO and HT Products in Mission 02 (June).

Mission 02	GEO Product	HT Product	Start Time	Stop Time	Integration Time
hterra05C	GEO_FL05	HT_FL05	2022-06-15T07:51:45.18	2022-06-15T09:44:07.00	112.36 min
hterra06C	GEO_FL06	HT_FL06	2022-06-15T12:48:16.21	2022-06-15T14:37:53.00	109.62 min
hterra07C	GEO_FL07	HT_FL07	2022-06-16T07:34:46.44	2022-06-16T09:28:24.39	113.64 min

The name of a simulation product is composed of a qualifier (GEO or HT) and the respective flight number.

5.3.2 Geosynchronous SAR Products (GEO)

In order to simulate the radar image product of a geostationary radar satellite featuring a very long integration time, we have fused azimuth bandwidths of master and slave passes available in a flight. In the following tables the GEO simulation products available from the first three flights of each mission are listed. They are also referred to as 'Hi-Res' product.

Three simulated GEO products allow to calculate three interferograms.

Table 5-3: GEO simulation products and interferograms formed in group "C1".

Mission 01	Product	Interferogram1	Interferogram2	Interferogram3
hterra01C	GEO-FL01			
hterra02C	GEO-FL02	GEO_FL01-FL02	GEO_FL01-FL03	GEO_FL02-FL03
hterra03C	GEO-FL03			

Table 5-4: GEO simulation products and interferograms formed in group "C2".

Mission 02	Product	Interferogram1	Interferogram2	Interferogram3
hterra05C	GEO-FL05			
hterra06C	GEO-FL06	GEO_FL05-FL06	GEO_FL05-FL07	GEO_FL06-FL07
hterra07C	GEO-FL07			

In the images below (Figure 5-2 - Figure 5-7) we exemplify the three GEO interferometric products available for mission 01 (coherence and phase). Similar interferograms are available for mission 02.



Figure 5-2: GEO-FL01 versus GEO-FL02 - coherence.



Figure 5-3: GEO-FL01 versus GEO-FL03 - coherence.



Figure 5-4: GEO-FL02 versus GEO-FL03 - coherence.

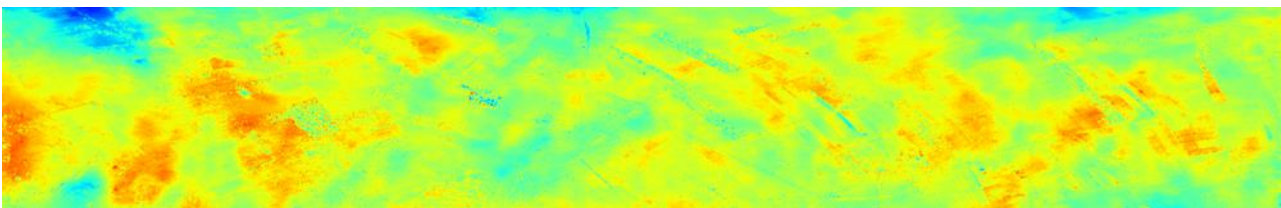


Figure 5-5: GEO-FL01 versus GEO-FL02 - interferometric phase.

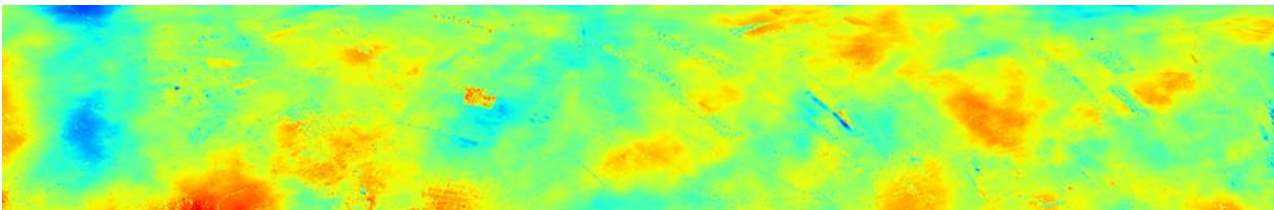


Figure 5-6: GEO-FL01 versus GEO-FL03 - interferometric phase.

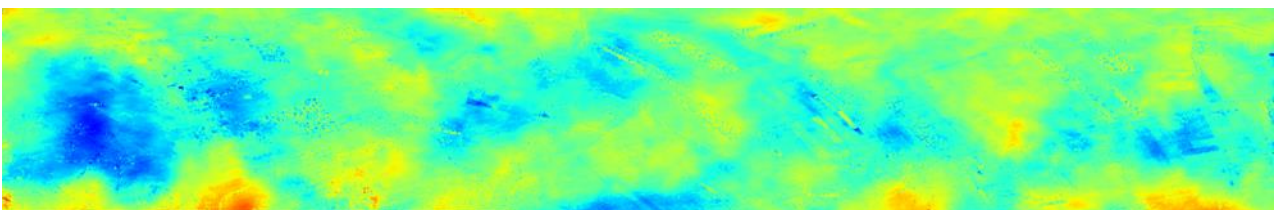


Figure 5-7: GEO-FL02 versus GEO-FL03 - interferometric phase.

These interferometric products may be compared with those obtained for the HT simulation shown in the next section in Figure 5-8 to Figure 5-13.

5.3.3 Hydroterra SAR Products (HT)

In this section we describe the generation of the Hydroterra (HT) SAR image products. Basically, this process follows the same steps as for the GEO products, with the difference that this time the parameters resolution, sampling, number of samples and NESZ are additionally adjusted to match those of the Hydroterra system. These parameters are listed in Table 5-5.

Table 5-5: Hydroterra product simulation parameters.

Parameter	Value
Single-look azimuth resolution	5 m
Multi-look azimuth resolution	50 m
Number of looks in azimuth	10
Range bandwidth	6 MHz
Single-look slant range resolution	22.2 m
Multi-look slant range resolution	22.2 m
Number of looks in range	1
Noise Equivalent Sigma Zero	-21.1 dB

Reference: Scenario 4 of the interferometric type (Glacier flow / Landslides) [7].

The following tables show the HT simulation products available from the first three flights of both missions 01 and 02. They are referred to as 'LowRes' product.

Three simulated HT products allow to calculate three interferograms.

Table 5-6: HT simulation products and interferograms formed in group "C1".

Mission 01	Product	Interferogram1	Interferogram2	Interferogram3
hterra01C	HT-FL01			
hterra02C	HT-FL02	HT_FL01-FL02	HT_FL01-FL03	HT_FL02-FL03
hterra03C	HT-FL03			

Table 5-7: HT simulation products and interferograms formed in group "C2".

Mission 02	Product	Interferogram1	Interferogram2	Interferogram3
hterra05C	HT-FL05			
hterra06C	HT-FL06	HT_FL05-FL06	HT_FL05-FL07	HT_FL06-FL07
hterra07C	HT-FL07			

In the images below (Figure 5-8 - Figure 5-13) we exemplify the three HT interferometric products available for mission 01 (coherence and phase). Similar interferograms are available for mission 02.

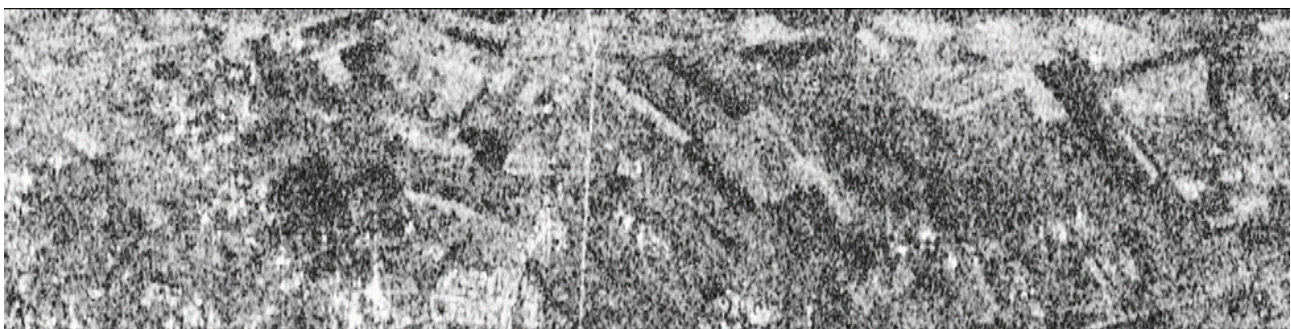


Figure 5-8: HT-FL01 versus HT-FL02 - coherence.



Figure 5-9: HT-FL01 versus HT-FL03 - coherence.



Figure 5-10: HT-FL02 versus HT-FL03 - coherence.

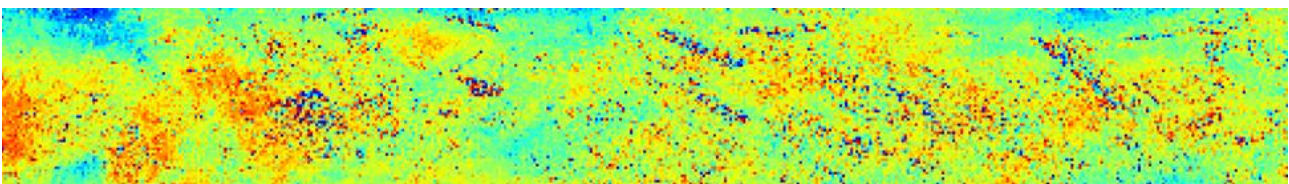


Figure 5-11: HT-FL01 versus HT-FL02 - interferometric phase.

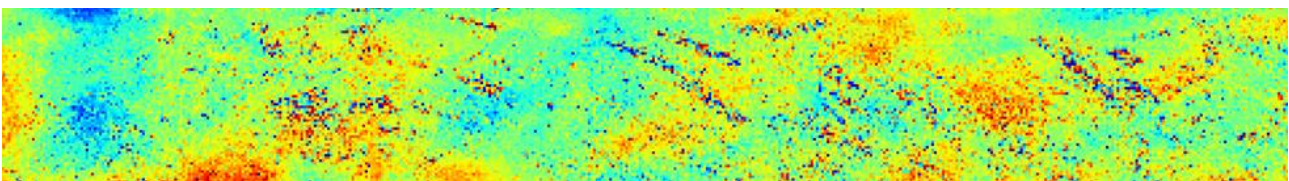


Figure 5-12: HT-FL01 versus HT-FL03 - interferometric phase.

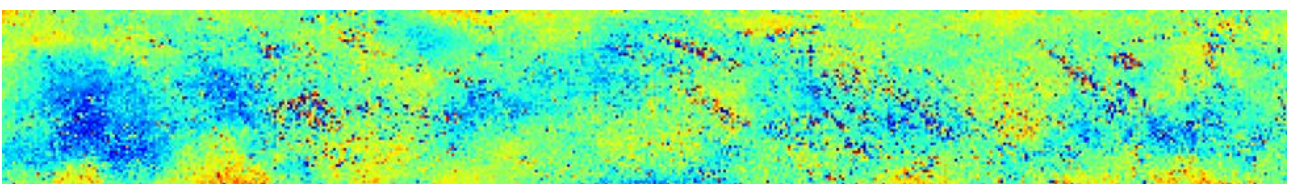


Figure 5-13: HT-FL02 versus HT-FL03 - interferometric phase.

5.4 Simulation Product Data Formats and Data Set Structure

In this section the product data formats are explained and the simulation data available from the 2022 SSM experiment are listed.

Quicklook images are stored in PNG format (Portable Network Graphics). Parameter text files are stored in XML format (eXtensible Markup Language). Complex or floating-point-valued data are stored in RAT format (RADarTools). A detailed description of the standard F-SAR data format RAT can be found at www.dlr.de/hr/f-sar/data-formats.


5.4.1 Geosynchronous SAR Product (GEO) Compilation

In the following we have exemplified the compilation of the data products “GEO-FL01” and “GEO-FL02” and their interferogram “GEO-FL01-FL02” including all files which belong to these products accompanied by an explanation (“Remark”). All other data sets follow the same scheme.


The two contrast files express an increase of contrast between single pass (F-SAR) only and multiple passes assembled within the simulation product. An explanation of these files can be found in Gracheva, EUSAR 2021, [9], Figure 6.

Table 5-8: Product “GEO-FL01” and “GEO-FL02” and their interferogram “GEO-FL01-FL02”.

Size	Folder Content	Remark
	interferogram_GEO_FL01-FL02/simGEO_FL01-HH:	FL01-HH
722K	contrast_ht_hh.png*	contrast of the SLC simulation product (all passes fused)
692K	contrast_slc_hh.png*	contrast of the SLC data product (first pass only)
7.4G	slc_0104_hh.rat*	SLC of the first pass only
7.4G	slc_ht_0104_hh.rat*	SLC of the simulation product
153K	slc_pp_ht_0104_hh.xml*	processing parameters of the SLC simulation product
	interferogram_GEO_FL01-FL02/simGEO_FL01-HV:	FL01-HV
733K	contrast_ht_hv.png*	contrast of the SLC simulation product (all passes fused)
683K	contrast_slc_hv.png*	contrast of the SLC data product (first pass only)
7.4G	slc_0104_hv.rat*	SLC of the first pass only
7.4G	slc_ht_0104_hv.rat*	SLC of the simulation product
153K	slc_pp_ht_0104_hv.xml*	processing parameters of the SLC simulation product
	interferogram_GEO_FL01-FL02/simGEO_FL01-VH:	FL01-VH
734K	contrast_ht_vh.png*	contrast of the SLC simulation product (all passes fused)
682K	contrast_slc_vh.png*	contrast of the SLC data product (first pass only)
7.4G	slc_0104_vh.rat*	SLC of the first pass only
7.4G	slc_ht_0104_vh.rat*	SLC of the simulation product
153K	slc_pp_ht_0104_vh.xml*	processing parameters of the SLC simulation product

	<p>SARSimHT-NG – Simulation of Hydroterra SAR System Performance in the Mediterranean and the Alps Based on Experimental Airborne SAR Data</p> <p>D2: Data Acquisition Report of SSM Experiment</p>	<p>Doc.: DLR-HR-TR-SARSimHT-NG-02</p> <p>Issue: 1.7 (final)</p> <p>Date: 06.09.2023</p>
---	---	---

	interferogram_GEO_FL01-FL02/simGEO_FL01-VV:	FL01-VV
715K	contrast_ht_vv.png*	contrast of the SLC simulation product (all passes fused)
674K	contrast_slc_vv.png*	contrast of the SLC data product (first pass only)
7.4G	slc_0104_vv.rat*	SLC of the first pass only
7.4G	slc_ht_0104_vv.rat*	SLC of the simulation product
153K	slc_pp_ht_0104_vv.xml*	processing parameters of the SLC simulation product
	interferogram_GEO_FL01-FL02/simGEO_FL02-HH:	FL02-HH
718K	contrast_ht_hh.png*	contrast of the SLC simulation product (all passes fused)
688K	contrast_slc_hh.png*	contrast of the SLC data product (first pass only)
7.4G	slc_0204_hh.rat*	SLC of the first pass only
7.4G	slc_ht_0204_hh.rat*	SLC of the simulation product
153K	slc_pp_ht_0204_hh.xml*	processing parameters of the SLC simulation product
546K	coh_ht_0202_hh.png*	coherency of the interferogram (quicklook)
3.7G	coh_ht_0202_hh.rat*	coherency of the interferogram (data, RAT format)
323K	ph_ht_0202_hh.png*	phase of interferogram (quicklook)
3.7G	ph_ht_0202_hh.rat*	phase of interferogram (data, RAT format)
8.0K	ppinsar_ht_fl_0202hh.xml*	processing parameters of the simulated interferogram
	interferogram_GEO_FL01-FL02/simGEO_FL02-HV:	FL02-HV
730K	contrast_ht_hv.png*	contrast of the SLC simulation product (all passes fused)
678K	contrast_slc_hv.png*	contrast of the SLC data product (first pass only)
7.4G	slc_0204_hv.rat*	SLC of the first pass only
7.4G	slc_ht_0204_hv.rat*	SLC of the simulation product
153K	slc_pp_ht_0204_hv.xml*	processing parameters of the SLC simulation product
547K	coh_ht_0202_hv.png*	coherency of the interferogram (quicklook)
3.7G	coh_ht_0202_hv.rat*	coherency of the interferogram (data, RAT format)
354K	ph_ht_0202_hv.png*	phase of interferogram (quicklook)
3.7G	ph_ht_0202_hv.rat*	phase of interferogram (data, RAT format)
8.0K	ppinsar_ht_fl_0202hv.xml*	processing parameters of the simulated interferogram
	interferogram_GEO_FL01-FL02/simGEO_FL02-VH:	FL02-VH
729K	contrast_ht_vh.png*	contrast of the SLC simulation product (all passes fused)
679K	contrast_slc_vh.png*	contrast of the SLC data product (first pass only)
7.4G	slc_0204_vh.rat*	SLC of the first pass only
7.4G	slc_ht_0204_vh.rat*	SLC of the simulation product
153K	slc_pp_ht_0204_vh.xml*	processing parameters of the SLC simulation product

	SARSimHT-NG – Simulation of Hydroterra SAR System Performance in the Mediterranean and the Alps Based on Experimental Airborne SAR Data D2: Data Acquisition Report of SSM Experiment	Doc.: DLR-HR-TR-SARSimHT-NG-02 Issue: 1.7 (final) Date: 06.09.2023
---	--	--

549K	coh_ht_0202_vh.png*	coherency of the interferogram (quicklook)
3.7G	coh_ht_0202_vh.rat*	coherency of the interferogram (data, RAT format)
354K	ph_ht_0202_vh.png*	phase of interferogram (quicklook)
3.7G	ph_ht_0202_vh.rat*	phase of interferogram (data, RAT format)
8.0K	ppinsar_ht_fl_0202vh.xml*	processing parameters of the simulated interferogram
	interferogram_GEO_FL01-FL02/simGEO_FL02-VV:	FL02-VV
716K	contrast_ht_vv.png*	contrast of the SLC simulation product (all passes fused)
669K	contrast_slc_vv.png*	contrast of the SLC data product (first pass only)
7.4G	slc_0204_vv.rat*	SLC of the first pass only
7.4G	slc_ht_0204_vv.rat*	SLC of the simulation product
153K	slc_pp_ht_0204_vv.xml*	processing parameters of the SLC simulation product
551K	coh_ht_0202_vv.png*	coherency of the interferogram (quicklook)
3.7G	coh_ht_0202_vv.rat*	coherency of the interferogram (data, RAT format)
377K	ph_ht_0202_vv.png*	phase of interferogram (quicklook)
3.7G	ph_ht_0202_vv.rat*	phase of interferogram (data, RAT format)
8.0K	ppinsar_ht_fl_0202vv.xml*	processing parameters of the simulated interferogram


Note: Fields coloured dark blue in Table 5-8 indicate files which belong to interferogram “GEO-FL01-FL02”. Files of the respective interferogram can always be found where the files of the second pass (here “GEO-FL02”) are stored.

5.4.2 Hydroterra SAR Product (HT) Compilation


In the following we have exemplified the compilation of the data products “HT-FL01” and “HT-FL02” and their interferogram “HT-FL01-FL02” including all files which belong to these products accompanied by an explanation (“Remark”). All other data sets follow the same scheme.

Table 5-9: Product “HT-FL01” and “HT-FL02” and their interferogram “HT-FL01-FL02”.

Size	Folder Content	Remark
	interferogram_HT_FL01-FL02/simHT_FL01:	HT-FL01
22M	contrast_ht_hh.png*	contrast of the SLC simulation product (all passes fused), HH
22M	contrast_ht_hv.png*	contrast of the SLC simulation product (all passes fused), HV
22M	contrast_ht_vh.png*	contrast of the SLC simulation product (all passes fused), VH
22M	contrast_ht_vv.png*	contrast of the SLC simulation product (all passes fused), VV
22M	contrast_slc_hh.png*	contrast of the SLC data product (first pass only), HH
22M	contrast_slc_hv.png*	contrast of the SLC data product (first pass only), HV
22M	contrast_slc_vh.png*	contrast of the SLC data product (first pass only), VH
22M	contrast_slc_vv.png*	contrast of the SLC data product (first pass only), VV


	SARSimHT-NG – Simulation of Hydroterra SAR System Performance in the Mediterranean and the Alps Based on Experimental Airborne SAR Data D2: Data Acquisition Report of SSM Experiment	Doc.: DLR-HR-TR-SARSimHT-NG-02 Issue: 1.7 (final) Date: 06.09.2023
---	--	--

425K	ml_ht_0104_hh.png*	multilook simulation product quicklook (PNG), HH
452K	ml_ht_0104_hv.png*	multilook simulation product quicklook (PNG), HV
450K	ml_ht_0104_vh.png*	multilook simulation product quicklook (PNG), VH
429K	ml_ht_0104_vv.png*	multilook simulation product quicklook (PNG), VV
3.4M	ml_ht_0104_hh.rat*	multilook simulation product data (RAT), HH
3.4M	ml_ht_0104_hv.rat*	multilook simulation product data (RAT), HV
3.4M	ml_ht_0104_vh.rat*	multilook simulation product data (RAT), VH
3.4M	ml_ht_0104_vv.rat*	multilook simulation product data (RAT), VV
28K	ml_pp_ht_0104_hh.xml*	multilook simulation product processing parameters (XML), HH
28K	ml_pp_ht_0104_hv.xml*	multilook simulation product processing parameters (XML), HV
28K	ml_pp_ht_0104_vh.xml*	multilook simulation product processing parameters (XML), VH
28K	ml_pp_ht_0104_vv.xml*	multilook simulation product processing parameters (XML), VV
8.4M	slc_0104_hh.rat*	SLC of the first pass only, HH
8.4M	slc_0104_hv.rat*	SLC of the first pass only, HV
8.4M	slc_0104_vh.rat*	SLC of the first pass only, VH
8.4M	slc_0104_vv.rat*	SLC of the first pass only, VV
8.4M	slc_ht_0104_hh.rat*	SLC of the simulation product, HH
8.4M	slc_ht_0104_hv.rat*	SLC of the simulation product, HV
8.4M	slc_ht_0104_vh.rat*	SLC of the simulation product, VH
8.4M	slc_ht_0104_vv.rat*	SLC of the simulation product, VV
28K	slc_pp_ht_0104_hh.xml*	processing parameters of the SLC simulation product, HH
28K	slc_pp_ht_0104_hv.xml*	processing parameters of the SLC simulation product, HV
28K	slc_pp_ht_0104_vh.xml*	processing parameters of the SLC simulation product, VH
28K	slc_pp_ht_0104_vv.xml*	processing parameters of the SLC simulation product, VV
	interferogram_HT_FL01-FL02/simHT_FL02:	HT-FL02
22M	contrast_ht_hh.png*	contrast of the SLC simulation product (all passes fused), HH
22M	contrast_ht_hv.png*	contrast of the SLC simulation product (all passes fused), HV
22M	contrast_ht_vh.png*	contrast of the SLC simulation product (all passes fused), VH
22M	contrast_ht_vv.png*	contrast of the SLC simulation product (all passes fused), VV
22M	contrast_slc_hh.png*	contrast of the SLC data product (first pass only), HH
22M	contrast_slc_hv.png*	contrast of the SLC data product (first pass only), HV
22M	contrast_slc_vh.png*	contrast of the SLC data product (first pass only), VH
22M	contrast_slc_vv.png*	contrast of the SLC data product (first pass only), VV
427K	ml_ht_0204_hh.png*	multilook simulation product quicklook (PNG), HH
454K	ml_ht_0204_hv.png*	multilook simulation product quicklook (PNG), HV
451K	ml_ht_0204_vh.png*	multilook simulation product quicklook (PNG), VH
429K	ml_ht_0204_vv.png*	multilook simulation product quicklook (PNG), VV
3.4M	ml_ht_0204_hh.rat*	multilook simulation product data (RAT), HH
3.4M	ml_ht_0204_hv.rat*	multilook simulation product data (RAT), HV
3.4M	ml_ht_0204_vh.rat*	multilook simulation product data (RAT), VH

	SARSimHT-NG – Simulation of Hydroterra SAR System Performance in the Mediterranean and the Alps Based on Experimental Airborne SAR Data D2: Data Acquisition Report of SSM Experiment	Doc.: DLR-HR-TR-SARSimHT-NG-02 Issue: 1.7 (final) Date: 06.09.2023
---	--	--

3.4M	ml_ht_0204_vv.rat*	multilook simulation product data (RAT), VV
28K	ml_pp_ht_0204_hh.xml*	multilook simulation product processing parameters (XML), HH
28K	ml_pp_ht_0204_hv.xml*	multilook simulation product processing parameters (XML), HV
28K	ml_pp_ht_0204_vh.xml*	multilook simulation product processing parameters (XML), VH
28K	ml_pp_ht_0204_vv.xml*	multilook simulation product processing parameters (XML), VV
8.4M	slc_0204_hh.rat*	SLC of the first pass only, HH
8.4M	slc_0204_hv.rat*	SLC of the first pass only, HV
8.4M	slc_0204_vh.rat*	SLC of the first pass only, VH
8.4M	slc_0204_vv.rat*	SLC of the first pass only, VV
8.4M	slc_ht_0204_hh.rat*	SLC of the simulation product, HH
8.4M	slc_ht_0204_hv.rat*	SLC of the simulation product, HV
8.4M	slc_ht_0204_vh.rat*	SLC of the simulation product, VH
8.4M	slc_ht_0204_vv.rat*	SLC of the simulation product, VV
28K	slc_pp_ht_0204_hh.xml*	processing parameters of the SLC simulation product, HH
28K	slc_pp_ht_0204_hv.xml*	processing parameters of the SLC simulation product, HV
28K	slc_pp_ht_0204_vh.xml*	processing parameters of the SLC simulation product, VH
28K	slc_pp_ht_0204_vv.xml*	processing parameters of the SLC simulation product, VV
15M	coh_ht_0202_hh.png*	coherency of the interferogram (quicklook), HH
15M	coh_ht_0202_hv.png*	coherency of the interferogram (quicklook), HV
15M	coh_ht_0202_vh.png*	coherency of the interferogram (quicklook), VH
15M	coh_ht_0202_vv.png*	coherency of the interferogram (quicklook), VV
4.2M	coh_ht_0202_hh.rat*	coherency of the interferogram (data, RAT format), HH
4.2M	coh_ht_0202_hv.rat*	coherency of the interferogram (data, RAT format), HV
4.2M	coh_ht_0202_vh.rat*	coherency of the interferogram (data, RAT format), VH
4.2M	coh_ht_0202_vv.rat*	coherency of the interferogram (data, RAT format), VV
435K	ph_ht_0202_hh.png*	phase of interferogram (quicklook), HH
442K	ph_ht_0202_hv.png*	phase of interferogram (quicklook), HV
442K	ph_ht_0202_vh.png*	phase of interferogram (quicklook), VH
440K	ph_ht_0202_vv.png*	phase of interferogram (quicklook), VV
4.2M	ph_ht_0202_hh.rat*	phase of interferogram (data, RAT format), HH
4.2M	ph_ht_0202_hv.rat*	phase of interferogram (data, RAT format), HV
4.2M	ph_ht_0202_vh.rat*	phase of interferogram (data, RAT format), VH
4.2M	ph_ht_0202_vv.rat*	phase of interferogram (data, RAT format), VV
8.0K	ppinsar_ht_fl_0202hh.xml*	processing parameters of the simulated interferogram, HH
8.0K	ppinsar_ht_fl_0202hv.xml*	processing parameters of the simulated interferogram, HV
8.0K	ppinsar_ht_fl_0202vh.xml*	processing parameters of the simulated interferogram, VH
8.0K	ppinsar_ht_fl_0202vv.xml*	processing parameters of the simulated interferogram, VV

Note: Fields coloured dark blue in Table 5-9 indicate files which belong to interferogram “HT-FL01-FL02”. Files of the respective interferogram can always be found where the files of the second pass (here “HT-FL02”) are stored.

	SARSimHT-NG – Simulation of Hydroterra SAR System Performance in the Mediterranean and the Alps Based on Experimental Airborne SAR Data D2: Data Acquisition Report of SSM Experiment	Doc.: DLR-HR-TR-SARSimHT-NG-02 Issue: 1.7 (final) Date: 06.09.2023
---	--	--

5.5 Inventory of Delivered Simulation Products

The following simulation product data sets have been delivered on January 27, 2023 to CNR-IREA and to ESA-ESTEC. The total size of the simulation products on hard disc was 880 GB.

Table 5-10: Delivered simulated geosynchronous SAR products (GEO).


Pass1	Pass2	Interferogram	Size	Location	Mission
GEO-FL01	GEO-FL02	GEO-FL01-FL02	147G	/mnt/esa/22HTERRA/SIMULATION/interferogram_GEO_FL01-FL02	April
GEO-FL01	GEO-FL03	GEO-FL01-FL03	147G	/mnt/esa/22HTERRA/SIMULATION/interferogram_GEO_FL01-FL03	April
GEO-FL02	GEO-FL03	GEO-FL02-FL03	147G	/mnt/esa/22HTERRA/SIMULATION/interferogram_GEO_FL02-FL03	April
GEO-FL05	GEO-FL06	GEO-FL05-FL06	147G	/mnt/esa/22HTERRA/SIMULATION/interferogram_GEO_FL05-FL06	June
GEO-FL05	GEO-FL07	GEO-FL05-FL07	147G	/mnt/esa/22HTERRA/SIMULATION/interferogram_GEO_FL05-FL07	June
GEO-FL06	GEO-FL07	GEO-FL06-FL07	147G	/mnt/esa/22HTERRA/SIMULATION/interferogram_GEO_FL06-FL07	June

Table 5-11: Delivered simulated Hydroterra SAR products (HT).

Pass1	Pass2	Interferogram	Size	Location	Mission
HT-FL01	HT-FL02	HT-FL01-FL02	602M	/mnt/esa/22HTERRA/SIMULATION/interferogram_HT_FL01-FL02	April
HT-FL01	HT-FL03	HT-FL01-FL03	603M	/mnt/esa/22HTERRA/SIMULATION/interferogram_HT_FL01-FL03	April
HT-FL02	HT-FL03	HT-FL02-FL03	602M	/mnt/esa/22HTERRA/SIMULATION/interferogram_HT_FL02-FL03	April
HT-FL05	HT-FL06	HT-FL05-FL06	602M	/mnt/esa/22HTERRA/SIMULATION/interferogram_HT_FL05-FL06	June
HT-FL05	HT-FL07	HT-FL05-FL07	602M	/mnt/esa/22HTERRA/SIMULATION/interferogram_HT_FL05-FL07	June
HT-FL06	HT-FL07	HT-FL06-FL07	602M	/mnt/esa/22HTERRA/SIMULATION/interferogram_HT_FL06-FL07	June

Table 5-12: Summary of delivered simulation products.

Simulation	Mission 01		Mission 02		total
	Passes	Interferograms	Passes	Interferograms	Products
GEO products	3	3	3	3	12
HT products	3	3	3	3	12
total	6	6	6	6	24

	<p>SARSimHT-NG – Simulation of Hydroterra SAR System Performance in the Mediterranean and the Alps Based on Experimental Airborne SAR Data</p> <p>D2: Data Acquisition Report of SSM Experiment</p>	<p>Doc.: DLR-HR-TR-SARSimHT-NG-02</p> <p>Issue: 1.7 (final)</p> <p>Date: 06.09.2023</p>
---	---	---

6 Summary

In this Data Acquisition Report the field work performed as part of the surface soil moisture (SSM) chapter of the SARSimHT-NG study is described. This includes the 22HTERRA airborne SAR measurements executed at the Apulian Tavoliere test site at Foggia (Italy) in April and June 2022 and the ground truth measurements carried out simultaneously with the F-SAR flights.

The report details the volume of ground measurements collected by CNR-IREA and CREA in Chapter 3. The structure of the associated data base is described in Sect. 3.6.

In Chapter 4 the available F-SAR RGI, GTC and INF data products generated by DLR are listed. Information about all available SAR simulation products is given in Chapter 5.

The described ground-truth data, the processed airborne SAR data and the SAR simulation data products have been delivered to ESA and to the project partner CNR-IREA.

7 Appendix A: Portable Sensor Calibration

HydraGO and Field scout TDR 300 sensors were calibrated applying the thermo-gravimetric method. Kopecky ring samples were collected and brought immediately after in the lab, weighted and re-weighted after oven-drying at 105°C for 48h and the gravimetric soil moisture content was calculated. The volumetric water content (ϑ_{KR}) was determined by multiplying the gravimetric water content by the soil bulk density.

For the HydraGO sensors, 137 Kopecky ring samples were collected in April and June over the monitored fields. The calibration equation was developed by relating the real dielectric constant (ϵ_r) from HydraGO at the time of Kopecky ring sampling to the volumetric soil moisture content calculated in the lab:

$$\vartheta_{KR} = A\sqrt{\epsilon_r} + B, \quad \text{where} \quad A = 0.06635 \quad B = -0.03382$$

The coefficients A and B were determined empirically as shown in Figure 7-1. The overall site-specific calibration has $rmse = 0.034 \text{ m}^3/\text{m}^3$ and Pearson correlation $R = 0.92$ (9 outliers were excluded). A and B coefficients were applied to the real dielectric constant values measured by HydraGO sensors to obtain calibrated soil moisture values.

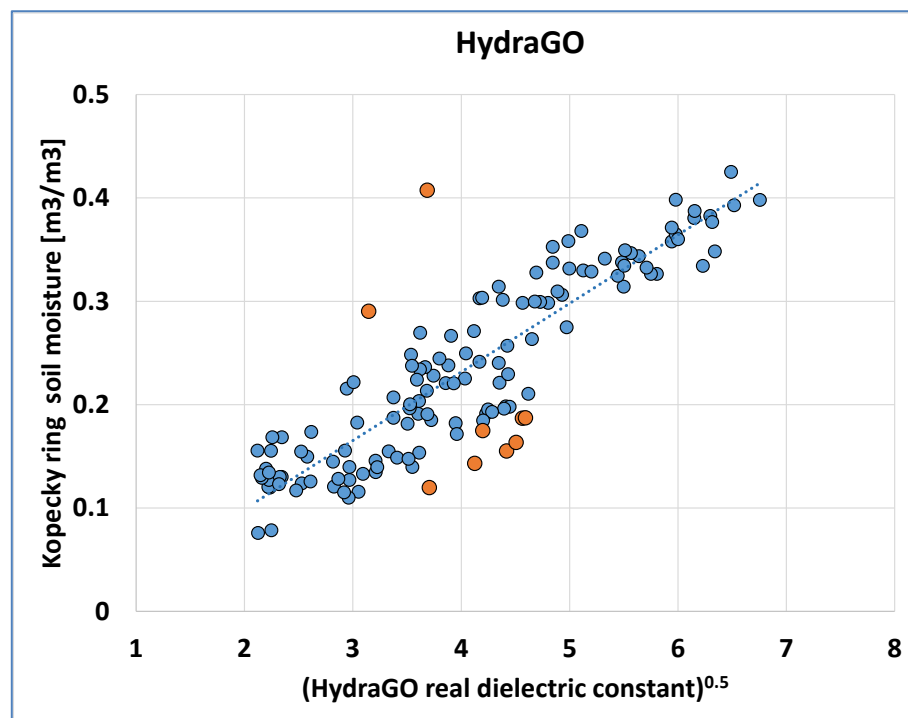


Figure 7-1: Volumetric soil moisture values from Kopecky ring sampling versus the square root of the real dielectric constant from HydraGO sensors. Total number of points is 137. In orange the 9 outliers (2.5 sigma). The blue dotted line is the linear fit.

For the Field Scout TDR 300, 104 Kopecky ring samples were collected in April and June over the selected fields. The calibration equation was developed by relating the volumetric soil moisture content (ϑ_{FS}) from Field Scout at the time of Kopecky ring sampling to the volumetric soil moisture content calculated in the lab (ϑ_{KR}):

$$\vartheta_{KR} = A\vartheta_{FS} + B, \quad \text{where} \quad A = 0.40697 \quad B = 0.11256$$

The coefficients A and B were determined empirically as shown in Figure 7-2. The overall site-specific calibration has $rmse = 0.032 \text{ m}^3/\text{m}^3$ and Pearson correlation $R = 0.91$. A and B coefficients were applied to the volumetric soil moisture content values measured by the Field Scout to obtain calibrated soil moisture values.

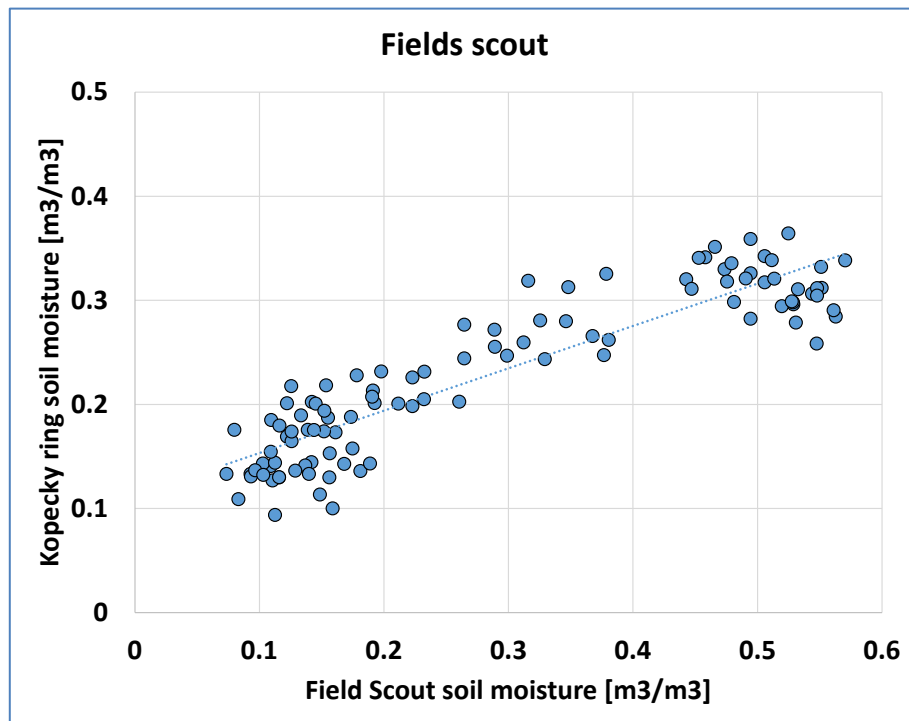


Figure 7-2: Volumetric soil moisture values from Kopecky ring sampling versus volumetric soil moisture values from Field Scout TDR 300. Total number of points is 104.